An Investigation Of Viscous Fluid Flow Between External Surfaces Of Pairsof Rotating Cylinders.

TAYLOR, Jr., James Howard. AN INVESTIGATION OF VISCOUS FLUID FLOW BETWEEN EXTERNAL SURFACES OF PAIRS OF ROTATING CYLINDERS.

Lehigh University, Ph.D., 1959
Engineering, chemical

University Microfilms, Inc., Ann Arbor, Michigan

AN INVESTIGATION OF VISCOUS FLUID FLOW BETWEEN EXTERNAL SURFACES OF PAIRS OF ROTATING CYLINDERS

By

James H. Taylor

A DISSERTATION

Presented to the Graduate Faculty

of Lehigh University

in Candidacy for the Degree of

Doctor of Philosophy

Lehigh University

1959

Approved and recommended for acceptance as a dissertation in partial fulfillment of the requirements for the degree of Doctor of Philosophy.

May 3, 1954
Date

A. C. Zettlemoyer
Professor in Charge

Accepted _____
Date

_____ Chairman
A. S. Foust

A. C. Zettlemoyer
A. C. Zettlemoyer

C. A. Shook
C. A. Shook

L. Maus
L. Maus

L. A. Wenzel
L. A. Wenzel

ABSTRACT

A theoretical study was made of the pressure distribution, rate-of-flow, and stream patterns in the flow of viscous liquids through the nip region between the surfaces of two external rotating cylinders. Application of viscous flow theory to the roll nip problem led to the prediction that pressure in the bank should be proportional to the cube of the reciprocal of the distance from the point of roll tangency. This relationship provided, for the first time, a rational basis for specification of the nip inlet boundary condition necessary for solution of the flow rate problem by hydrodynamic lubrication theory. A second boundary condition was provided by knowledge that real liquids, not specially purified, can withstand only moderate levels of tension without failure by cavitation. The hydrodynamic problem was solved for the case of constant viscosity flow between cylinders rotating at differential speeds, and a method for the rapid computation of numerical results was developed and programmed for digital computer solution.

An experimental investigation was conducted to test the validity of the theory, and to determine the limitations of its applicability. Eleven viscous liquids with viscosities in the range from 17 to 240 poise were tested on pairs of four-inch and six-inch diameter rolls, with roll speeds ranging from 35 to 300 rpm and speed ratios of 1, 2, and 3. The theory was found to agree with experimental data for fluids with viscosities below 90 poise and total roll surface velocities of 10 feet per second or less. Under these conditions, 95 percent of the data fell within limits of -25 to +35 percent deviation from the theoretical flow rates. Greater deviations were observed for higher viscosity fluids,

but 95 percent of all measured flow rates fell within limits of -52 to +110 percent deviation from the predicted values. Deviations are attributed to uncertainty of the actual fluid viscosity in the nip region, and to viscosity variations induced by temperature and pressure gradients within the nip. With high viscosity fluids and with high roll surface speeds, these factors cause the experimental system to deviate from the constant viscosity assumptions employed in derivation of the flow theory.

A theoretical solution for the relative transfer of fluid to the faster roll was obtained. Experimental observations indicated that the theoretical transfer fraction is a limiting value which is attained under ideal constant viscosity conditions. Greater than theoretical transfer is obtained when the liquid viscosity is subject to variation during nip passage.

When the fluid between the rolls contained a low concentration of small glass beads, the size of the largest bead passed without fracture was proportional to, but not equal to, the theoretical nip clearance. Differences between bead size and calculated clearances are attributed to viscosity variations due, in part, to the presence of the beads themselves. In accordance with theoretical predictions, beads are not captured and fractured by the the rolls until the nip clearance is opened to some critical value dependent on the bead size and the roll speed ratio.

ACKNOWLEDGEMENTS

The author expresses his grateful acknowledgement to the following groups and individuals whose assistance and advice materially aided in the completion of this investigation.

The National Printing Ink Research Institute provided financial support for the work as well as an introduction to the problem of viscous flow between rotating cylinders. The Research Committee of NPIRI provided numerous practical suggestions which were incorporated in the experimental program. Dr. Edward C. Haines of Superior Varnish and Drier Co. supplied many of the viscous liquids used in the experimental investigation.

Members of the author's special committee provided advice and direction which pointed the way over and around theoretical and experimental snags and pitfalls. The constant encouragement and technical assistance of Dr. A. S. Foust of the Lehigh Chemical Engineering Department and Dr. A. C. Zettlemoyer of the Lehigh Chemistry Department are especially acknowledged. As professor in charge of the project, Dr. Zettlemoyer brought untiring enthusiasm and technical suggestions to the assistance of the author. The work of Mr. Richard Whetzel, whose care and attention to detail in obtaining part of the experimental data made possible an extension of the range of conditions investigated, is highly appreciated.

The devotion and encouragement of my wife, Jo, must be cited as one of the major factors making progress in this undertaking possible.

TABLE OF CONTENTS

LIST OF FIGURES

LIST OF TABLES

NOMENCLATURE

Symbol	Meaning	Where Used
A	Factor in equation 39	p. 29
A	Factor in equation A II 40	p.p. 127 - 133
A_1	Constant in equation A II 29	p.p. 125 - 127
B	Factor in equation 39	p. 29
B_1	Constant in equation A II 29	p.p. 125 - 127
C	Factor in equation 39	p. 29
C	Factor in equation A II 40	p.p. 127 - 132
C	Factor in equation A II 29	p.p. 125 - 127
C	Square root of sum of squares of deviations from mean removed by regression line	p.p. 162 - 172
C_o	Factor in defining constants of equation A II 29	p. 126
C_1	Constant of integration	p.p. 21, 30, 135
C_2	Constant of integration	p.p. 21, 135
C_3	Constant of integration, pressure at nip center	p.p. 24, 25
C_p	Heat capacity of liquid	p. 81
D	Factor in equation 39	p. 29
D	Distance between roll centers in bipolar coordinate system	p.p. 122 - 127
D_b	Diameter of glass bead	p.p. 93, 95
E	Logarithm of experimental flow rate + 5	
F	Force exerted on rolls	
F	Factor in equation A II 40	p.p. 127 - 132
F	Ratio of variances in statistics	p.p. 166 - 176
G	Factor in equation A II 40	p.p. 127 - 134

Symbol	Meaning	Where Used
K	Constant in bipolar coordinate system	p.p. 122 - 127
K	Function of roll speed ratio	p.p. 129 - 130
L	Length of cylinder	
L	Dimension used in derivation of relationship between nip clearance and location in nip	p.p. 22, 23
M	Slope of log viscosity vs. reciprocal temperature curve	
N_1	Slow roll rpm	
N_2	Fast roll rpm	
O_a	Angular velocity of fast roll	
O_b	Angular velocity of slow roll	
P	Fluid pressure	
P_1	Pressure at entrance to nip zone	
P^*	Minimum nip pressure, i.e. cavitation threshold pressure	
P_o	Nip power consumption	
Q	Rate of fluid flow through nip per unit roll length	
Q_f	Rate of fluid flow associated with fast roll	
R	Roll radius	
R	Total three-roll mill flow rate per unit roll length	p. 119
S	Integers from 1 - ∞, used in series terms of equation A II 29	p.p. 125 - 127
S	Standard deviation	p.p. 162 - 172
T	Absolute temperature	p.p. 41, 42, 85
T	Logarithm of theoretical flow rate + 5	p.p. 161 - 177

Symbol	Meaning	Where Used
U_1	Slow roll surface velocity	
U_2	Fast roll surface velocity	
U_t	$U_1 + U_2$	
W	Rate of flow to apron nip per unit roll length	p.p. 118 - 119
X	Component of body force in x direction	
Y	Component of body force in y direction	
Z	Component of body force in z direction	
a	Apron nip transfer fraction	p.p. 13, 118, 119
a	Exponent in empirical power equation	p. 6
a	Radius of fast roll	p.p. 122, 123
a	Intercept of regression line of coded logarithm of experimental vs. theoretical nip flow rate	p.p. 161 - 163
a_c	Intercept of regression line of actual logarithm of experimental vs. theoretical nip flow rate	p.p. 161 - 163
a_o, a_1, a_s	Constants in equation A II 29	p.p. 125, 126
b	Exponent in empirical power equation	p. 6
b	Radius of slow roll	p.p. 122, 123
b	Intercept of log viscosity vs. reciprocal temperature curve	p.p. 41, 42, 85
b_o, b_1, b_s	Constants in equation A II 29	p.p. 125, 126
b_m	Coefficient of viscosity change with pressure	p.p. 86, 87

Symbol	Meaning	Where Used
f	Feed nip transfer fraction	
h	Distance between roll surfaces	
h_o	Distance between roll surfaces at point of closest approach	
h_1	Distance between roll surfaces at nip inlet	
h^*	Distance between roll surfaces at point of minimum pressure	
h_s	Distance between roll surfaces at stagnation point	
k	Thermal conductivity	
n	Number of points in a data set	
q	Rate of heat generation due to viscous shear in nip	
r	Roll speed ratio	
r	Correlation coefficient	p.p. 72, 162 - 164
r_1, r_2	In bipolar coordinate system, distances from a given point to focii	p. 124
t	Take-off-knife factor	p.p. 13, 118, 119
t	Time	p. 14
t	Temperature	
t	In statistics, ratio of a difference to a standard deviation	p.p. 166 - 175
u	Velocity component in x direction	
v	Velocity component in y direction	
w	Velocity component in z direction	
x	Rectangular coordinate in direction of nip flow	
x_1	Point of nip entrance	

Symbol	Meaning	Where Used
x^*	Location of point of minimum pressure	
x_s	Location of stagnation point	
y	Rectangular coordinate across direction of nip flow	
y_s	y coordinate of stagnation point	
z	Rectangular coordinate parallel with roll axis	

Greek

α	Function of roll speed ratio defined by equation 45, p. 32	
α_o	Constant in equation A II 29	p.p. 125, 127
β	Function of roll speed ratio defined by equation 46, p. 32	
γ	In bipolar coordinate system, the distance from nip midpoint to focii of system	
δ	In development of nip geometry, $\delta = \frac{1}{2}(h - h_o)$	p.p. 22, 23
δ	Constant in bipolar coordinate system	p. 123
δ_1	Thickness of non-rejected liquid near slow roll surface	p.p. 92, 93
δ_2	Thickness of non-rejected liquid film near fast roll surface	p.p. 92, 93
ζ	Dimensionless coordinate, x/R	
η	Dimensionless coordinate, y/R	
λ	Complex coordinate, x + iy	
μ	Complex coordinate, x - iy	p. 122
μ	Coefficient of viscosity	
ν	Coefficient of kinematic viscosity	

Symbol	Meaning	Where Used
ρ	Coordinate in bipolar coordinate system	p.p. 122 - 126
ρ	Density of fluid	
σ	Coordinate in bipolar coordinate system	
τ	Shear stress	
ϕ	Volume fraction of solids in suspension	p. 96
ϕ	Dimensionless stream function	p. 129
$\phi(x)$	Sum of terms in equation A IV 1	p.p. 141 - 152
ψ	Stream function	

Symbols employed in the floating point computer code are summarized on pages 158 through 160.

I. INTRODUCTION

Fluid flow between the surfaces of mutually external, rotating cylinders is of practical importance in a number of instances. Although this investigation is directed primarily at the flow between cylinders such as those used in the printing ink and paint manufacturing industries for dispersion mills, similar phenomena are encountered in the flow between calendering rolls for plastics, coating rolls for films and paper, and distribution rolls in printing presses. The flow of viscous liquids between moving surfaces separated by small clearances has been investigated extensively for the geometrical systems encountered in bearing design, and the theory involved in this type of flow serves as a basis for modern lubrication theory. However, very little experimental work has been reported for the geometrical system represented by two external cylinders separated by a thin film of viscous liquid, and previous theoretical papers in this field have failed to specify adaquate boundary conditions for solution of the problem. Extension of the previous theory, specification of boundary conditions, and experimental determination of the range of applicability of the theory has been undertaken in order to provide an improved basis for the design and operation of three-roll dispersion mills and to extend the general fund of knowledge of the high shear-rate flow behavior of viscous fluids.

Roll mills of two, three, and five roll design are in common use. Heavy duty two-roll batch operation mills are generally used for compounding rubber and plastics, but continuous or semi-continuous three-roll

mills enjoy wide popularity in the manufacture of printing inks. The wide application of roll mills to pigment dispersion in viscous fluids is due to several factors; among these are ability to process materials with a wide range of rheological properties, ease of cleaning, ability to segregate and reject large, undispersable pigment agglomerates or trash, and high ratio of heat transfer area to volume of material being sheared. The latter feature permits high levels of dispersion energy input without undue temperature rise in the product, and permits dispersion of heat sensitive organic pigments in viscous media without deterioration of pigment properties. On the other hand, roll mills have relatively high initial costs and, unless care is taken to obtain maximum efficiency, have high operating costs.

A three-roll mill, such as that shown schematically in Fig. 1, consists of three hardened steel cylinders with parallel axes which may, or may not, lie in the same plane. The two end rolls rotate in the same angular direction while the center roll turns in the opposite direction. The speed of rotation is increased progressively from the first or feed roll to the take-off or apron roll. The largest present day mills have rolls sixteen inches in diameter by forty inches long, with apron roll speeds as high as 400 rpm. Roll speed ratios of 2:1 and 3:1 are commonly employed. Mills with independently driven, variable speed feed rolls are also available. In operation, a mixture of incompletely dispersed pigment and vehicle is fed to the bank region above the nip between feed and center rolls. As the rolls turn, the mixture is drawn into the nip where it is subjected to shear and pressure which disperses the agglomerated solid particles and wets them with liquid.

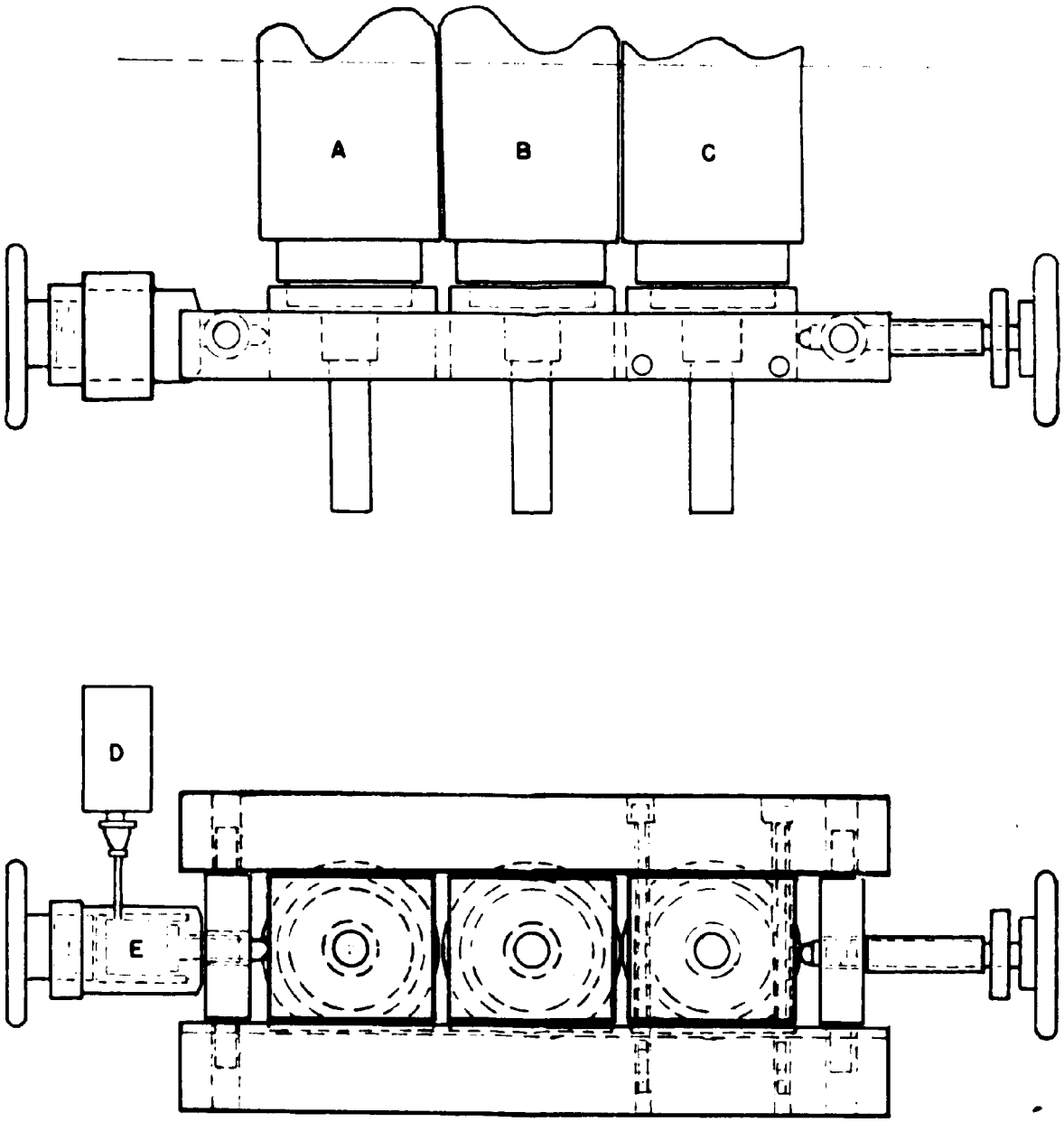

A. FEED ROLL
B. CENTER ROLL
C. APRON ROLL
D. PRESSURE GAGE
E. HYDRAULIC INSERT
F. SCREWJACK

DEPARTMENT OF CHEMICAL ENGINEERING
LEHIGH UNIVERSITY

EXPERIMENTAL THREE ROLL MILL

FIGURE 1. | SCALE: 1 = 4

Some of the larger particles are crushed by the rolls as they enter the nip. The film of fluid splits after passage through the nip. Part remains on the slow roll and returns to the feed bank. The remainder travels forward to the apron nip, where it is subjected to shear and pressure gradients even more severe than encountered in the feed nip. The film splits again after the apron nip passage, and again, part returns to the feed bank. The portion of fluid transferred to the apron roll moves forward to the take-off knife, where it passes from the roll to the apron as product.

Production rate through the mill depends on three factors:

1. The rate of fluid flow through the feed nip between the first and second rolls;

2. The relative split of the fluid between slower and faster rolls at the feed and apron nip outlets;

3. The effectiveness of the take-off knife in removing product from the apron roll.

In turn, these factors depend on fluid and mechanical variables associated with the mill and with the material being processed.

The degree of dispersion produced during passage through the mill depends on the nature of the solid and liquid as well as upon the operating conditions of the mill. It is obvious that no solid particles larger than the minimum clearance between center and fast roll surfaces can appear in the product. Most of the material processed through the mill is dispersed to a particle size much smaller than this maximum limiting value.

Modern roll mills have rolls ground to tolerances measured by the wave length of light. They are equipped with gages and controls that permit accurate and reproducible determination of operating conditions. Yet the relationship between these operating conditions and mill performance remains poorly understood. If the full potentialities of these precision machines are to be realized, a better understanding of the basic principles governing their operation must be obtained. A quantitative understanding of the behavior of viscous fluids passing between rotating cylinders can also serve as a basis for rational design of improved milling equipment. Outside of the field of dispersion equipment, knowledge of the behavior of fluids during passage between rolls can aid in understanding the operation of coating machines and ink distribution systems.

The purpose of the research reported in this dissertation was to develop a mathematical method of predicting the rate of fluid flow through the feed nip of a mill as a function of measurable and controllable variables. A further objective was to determine experimentally the accuracy of the theory and to evaluate the limitations of its applicability. The final objective of this work was the determination of the relationship between the velocity ratio of two rotating cylinders and the relative transfer of a Newtonian fluid flowing between them.

II. LITERATURE

The literature pertinent to the present investigation may be divided conveniently into experimental and semi-empirical investigations of roll mill behavior, mathematical investigations of the fluid dynamics of viscous flow between rotating cylinders, and studies of the mechanism of film split between separating surfaces.

Studies of Roll Mill Operation

Data on production performance of commercial and laboratory size roll mills have been published by a number of investigators. Notable among these have been the reports of the New York Paint and Varnish Production Club on techniques of roll mill dispersion of titanium dioxide, toluidine red, and phthalocyanine blue pigments (1,2,3,4). Fisher (5) measured the throughput rate of laboratory mills and presented an empirical equation for production rate as a function of mill speed, clearance setting, and fluid viscosity. Maus (6) correlated mill power consumption with operating variables by a semi-empirical equation of the form,

$$(\text{Power Number}) = \text{Const}\ (\text{Reynolds Number})^{a}\ (\text{Froude Number})^{b}\ .$$

The analysis of Maus was applied to the case of two nips in a Floating Center Roll type of three-roll mill by Taylor (7). Gamble and Sparta (8,9) employed electrical plug stopping to halt mill rolls for the measurement of film thickness on the roll surfaces. These latter workers employed fluids containing a dye which could be measured colorimetrically after extraction from a cotton pad onto which the fluid from a known area of roll surface had been wiped.

Viscous Flow Theory

The fundamental equations of viscous fluid flow theory were first developed by Navier (10) and Poisson (11); and independently, by St. Venant (12) and Stokes (13). The Navier-Stokes differential equations express the general motion of a Newtonian viscous fluid as a function of the forces acting upon it. Solutions for these equations have been found only for certain special cases, and usually with a number of simplifying assumptions. The two-dimensional theory of viscous flow between an inclined block and a moving plane surface was treated by Osborne Reynolds in 1886 (14) and was confirmed experimentally in connection with lubrication problems by Lord Rayleigh (15) and others (16). The method of Reynolds involved solution of the equation,

$$dP/dx = \mu\, d^2u/dy^2 ,$$

together with the equation of continuity,

$$Q = \mu\, dy .$$

For the case of cylinders rotating in a viscous fluid, Frazer (17) obtained analytical solutions to the more gereral equations,

$$dP/dx = \mu\,(d^2u/dy^2 + d^2u/dx^2)$$

$$dP/dy = \mu\,(d^2v/dy^2 + d^2v/dx^2) .$$

Although Frazer's work was quite extensive, his equations have received little application to the roll mill problem because of computational difficulties associated with their solution when the cylinders in question are separated by only a thin film of fluid.

Less complicated analyses of the pressure distribution in the nip between rotating rolls were presented by Ardichvili in 1938 (18),

Eley in 1946 (19), and by Gatcombe in 1945 (20). Eley assumed that the material passing between the rolls acted as a plastic solid, and based his calculation on the rate of compression in the nip. It was shown by Bergen and Scott (21) that Eley's results differed from those of Ardichvili only by a constant factor, $R/2\sqrt{2}$. Gatcombe applied the lubrication theory of Reynolds to the roll geometry with the boundary conditions of vanishing pressure at points infinitely far from the nip center. Gatcombe extended his theory to consider the effect of fluid viscosity change caused by pressure increase in the nip. Gatcombe's results, like those of Ardichvili, Eley, and Frazer, predicted that the pressure on the inlet side of the nip would increase to a maximum and then drop to zero at the center or point of minimum clearance.

In 1949, Gaskell (22) employed an approach similar to that of Gatcombe to calculate the pressure distribution in the calendering of plastic materials. The boundary conditions employed by Gaskell were that both the pressure and the pressure gradient vanish at the point where the calendered sheet leaves the rolls. To use these conditions, the roll speed and thickness of the calendered sheet must be known. These boundary conditions involve the assumption that the sheet separates from the rolls when the pressure becomes zero, i.e. there is no adhesion between calendered product and roll. Gaskell extended his theory to the case of a material with Bingham plastic flow properties having a stress, shear-rate relationship of the form,

$$\tau = \tau_0 + \mu_p \, (du/dy) \quad .$$

Gaskell's results differed from those of previous investigators in

that his theory predicted a finite, positive pressure at the nip center, and the point of exit from the nip was recognized as being downstream from the center.

Thermal effects involved in calendering a viscous fluid were studied in a theoretical investigation by Finston in 1950 (23), and the theory of calendering a viscoelastic fluid was treated by Paslay in 1957 (24). Experimental measurements of the pressure distribution in the nip between calendering rolls were reported by Bergen and Scott (21). It was observed by the latter that their results were in qualitative agreement with the predictions of Gaskell, but differed considerably from those of Ardichvili and Eley. The greatest deviations from Gaskell's theory were found in the region of the nip entrance, and it was stated that these deviations were probably due to the fact that the Gaskell equation presents no rational physical method of defining the true point of nip entrance. Hummel (25) derived equations for the pressure distribution in a roll mill nip with differential roll speed, using the same basic theory as Gaskell and Gatcombe. Like previous investigators, Hummel did not specify a method of defining the points of inlet and outlet to the nip.

Film Split and Cavitation

The theories of both Frazer and Gatcombe predict that, in a complete-immersed system, the pressure on the outlet side of a nip will fall to negative values equal in magnitude to the positive pressures encountered on the inlet side. Since real liquids, containing even trace amounts of impurities to serve as nuclei, are incapable of withstanding large tensile

stresses, Banks and Mill (26) hypothesized that cavitation would occur in a liquid film contained between two rapidly separating surfaces. By using a glass roll system, these authors (27) were able to observe and photograph the cavities or bubbles formed in the outlet region of the nip. Miller and Myers (28,29) made a systematic study of the formation of cavities in the nip of an apparatus consisting of a steel cone held against a rotating glass plate. It was observed that the split of film between the separating surfaces was preceeded by cavitation whenever the product of fluid viscosity times surface velocity exceeded a critical value, characteristic of the material being sheared. At lower than critical values of the viscosity x viscosity product, the film split smoothly at the air-liquid interface with out cavitation. At higher than critical values, the number of bubbles observed was proportional to the viscosity-velocity product.

The relative quantity of fluid remaining on each of two surfaces after shearing and separation was investigated experimentally by Sparta (8) for the case of roll mills, and by Fetsko and Walker (30), Scarr (31), Hammel (32) and Lin (33) for the case of ink transfer in printing. Sparta demonstrated that the relative transfer depends on the rheological properties of the fluid and on the relative speeds of the two surfaces. The largest quantity of fluid was always transferred to the faster moving surface. Fetsko and Walker developed an equation which permits separation of the total quantity of ink transferred from the printing plate to stock into two portions: that initially immobilized by the printing stock during impression; and that portion of the remaining ink film which splits toward the paper as the surfaces separate. Scarr found a correlation

between the position of film split and the ink "shortness", or ratio of ink yield value to plastic viscosity. High shortness values were associated with inks that split close to the surface of the stock. Hammel found that the position of film split was affected by the nature of the pigment and vehicle as well as by the shortness of the ink. It was also observed that, when unpigmented vehicles were "printed", the position of split moved closer to the stock as the vehicle viscosity increased. Lin measured the variation of transfer with changing printing speed and pressure. Increasing printing speed appeared to decrease the quantity of the free ink film split to the stock when printing on aluminum laminated paper board, but to increase the split to stock when printing on polyethylene film. Changing printing pressure did not affect the results with polyethylene, but with the aluminum laminated board, increased printing pressure appeared to increase the transfer split.

III. THEORY OF VISCOUS FLOW IN NIP BETWEEN ROTATING CYLINDERS

The theory of roll mill operation may be simplified by subdividing the question of overall throughput rate into two phases and by considering each in turn. This subdivision is accomplished through a material balance which permits separate analysis of:

1. Rate of fluid flow between rotating cylinders as a function of mechanical and fluid variables;

2. Relative position of split in a fluid film between separating surfaces moving at different speeds.

Approximate solutions of the Navier-Stokes equations for viscous fluids serve as the basis for the analysis of the fluid flow rate through the nip between feed and center rolls. A solution to the lubrication theory problem for the nip geometry is used to establish the shape of the nip pressure gradient. Appropriate boundary conditions are established by consideration of the bank pressure distribution derived from Frazer's solution for the rolls-in-contact problem and by recognition of the existance of a minimum nip outlet pressure at which real liquids cavitate. From the basic nip flow theory, equations are derived for calculation of the nip pressure distribution, shear-rates, flow rate, minimum nip clearance, power consumption, location of point of flow stagnation, and relative quantities of flow associated with the slow and fast rolls. The location of the stagnation point, that point beyond which all fluid travels in the forward direction through the nip, is related to the ability of the nip to accept or reject particles of a given size that may be suspended in the fluid. This

point is also related to the relative quantity of fluid associated with the two rolls, since under constant viscosity conditions, the same stream line passes through the stagnation point and the point of division between the separating fluid surfaces at the nip outlet.

Roll Mill Material Balance

The total rate of fluid flow through three-roll mills is related to the flow rate through the feed nip, Q, the fraction of fluid transferred to the faster roll at the feed nip, f, and the apron nip, a, and to the fraction, t, of fluid removed from the apron roll by the take-off knife. A material balance, given in detail in Appendix I, leads to the following equation.

$$\text{Mill throughput rate} = \left(\frac{t\,a\,f}{1 - a + at}\right) Q \quad , \qquad (1)$$

This equation reduces the problem of predicting roll mill production rate to that of determining the relationship between fluid properties, mechanical variables, and the transfer fractions and rate of flow between feed and center roll.

Basic Viscous Flow Theory

The Navier-Stokes equations serve as the starting point for derivation of the nip flow hydrodynamic theory. Using the nomenclature of Schlichting (34), these equations, for a constant viscosity, non compressible fluid, are written as follows.

$$\frac{\partial u}{\partial t} + u\frac{\partial u}{\partial x} + v\frac{\partial u}{\partial y} + w\frac{\partial u}{\partial z} = -\frac{1}{\rho}\frac{\partial P}{\partial x} + \nu\left(\frac{\partial^2 u}{\partial x^2} + \frac{\partial^2 u}{\partial y^2} + \frac{\partial^2 u}{\partial z^2}\right) + X \quad . \qquad (2)$$

$$\frac{\partial v}{\partial t} + u\frac{\partial v}{\partial x} + v\frac{\partial v}{\partial y} + w\frac{\partial v}{\partial z} = -\frac{1}{\rho}\frac{\partial P}{\partial y} + \nu\left(\frac{\partial^2 v}{\partial x^2} + \frac{\partial^2 v}{\partial y^2} + \frac{\partial^2 v}{\partial z^2}\right) + Y \quad . \qquad (3)$$

$$\frac{\partial w}{\partial t} + u\frac{\partial w}{\partial x} + v\frac{\partial w}{\partial y} + w\frac{\partial w}{\partial z} = -\frac{1}{\rho}\frac{\partial P}{\partial x} + \nu\left(\frac{\partial^2 w}{\partial x^2} + \frac{\partial^2 w}{\partial y^2} + \frac{\partial^2 w}{\partial z^2}\right) + Z \quad . \qquad (4)$$

Another condition is supplied by the equation of continuity, which for a non-compressible fluid is,

$$\frac{\partial u}{\partial x} + \frac{\partial v}{\partial y} + \frac{\partial w}{\partial z} = 0 \quad . \qquad (5)$$

Symbols used in these equations have the following significance:

x, y, z,	rectangular orthogonal coordinates ,
u, v, w,	velocity components in x, y, z, directions, respectively,
X, Y, Z,	components of body forces in x, y, z, directions, respectively ,
P	hydrostatic pressure ,
μ	coefficient of viscosity ,
ρ	fluid density ,
ν	kinematic viscosity = μ/ρ ,
t	time.

Although the arrangement of rolls in a mill is normally in a horizontal plane with flow in the vertical direction as shown in Fig.2, the geometry and coordinate system shown in Fig. 3 will be used in the following derivations to maintain conformity with the nomenclature used in previous investigations in this and related fields. Where gravity is a factor, it is assumed to produce an acceleration in the positive x direction.

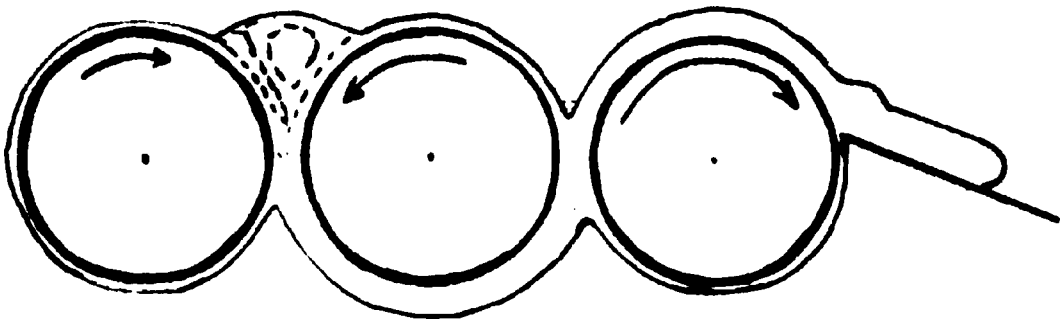

Figure 2. Flow of Material Through Roll Mill

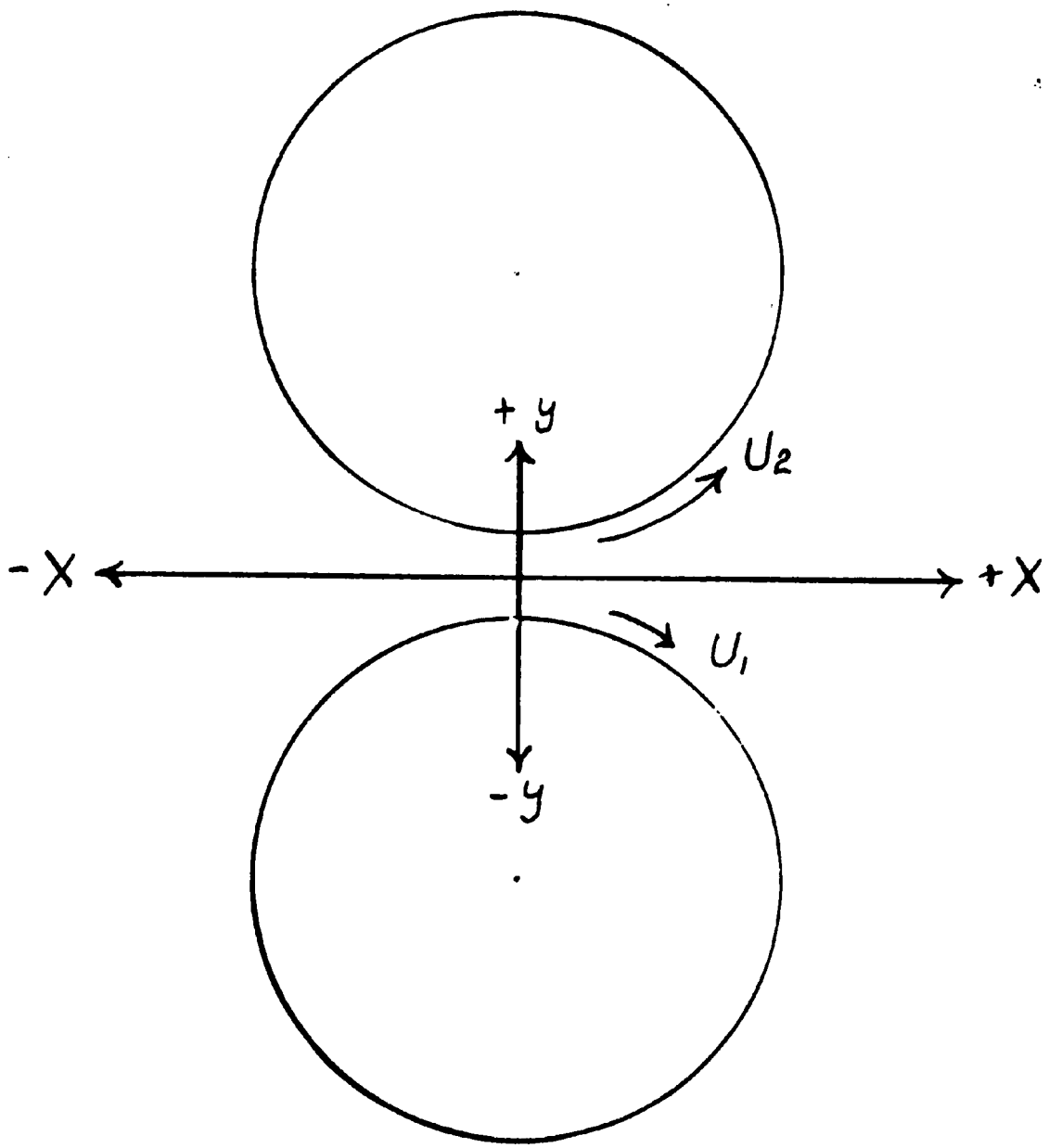

Figure 3. Coordinate System Used in Nip Flow Theory

Application to Region Distant from Nip. By making certain simplifying assumptions, it is possible to reduce the Navier-Stokes equations to a linear form amenable to solution. The approximations made in the present case are those which apply to conditions of very low Reynolds number where the forces due to viscosity greatly exceed those due to inertia. Where these assumptions are valid, the terms to the left of the equality sign in equations 2 , 3 , and 4 may be neglected in comparison with those on the right. If flow in the z direction is absent, further simplification is possible, since all of equation 4 and the terms involving z in equations 2 and 3 drop out. The latter approximation applies when the cylinders are so long compared with their diameter that flow in the axial direction may be neglected. In actual roll systems, the conditions of this approximation are not completely satisfied; however the presence of end-plates at the cylinder ends does restrict axial flow to a small component of the total motion. The conditions taken and assumptions made in reducing the Navier-Stokes equations to the case of two-dimensional, purely viscous flow are summarized here.

1. Forces due to inertia are negligible compared with viscous forces. This implies relatively high viscosity and low speeds.

2. Body forces are negligible compared with viscous forces.

3. The flow is in a steady state.

4. The cylinders are long compared with their diameter, and flow in the z direction, parallel with the roll axis, is negligible.

5. As with the full set of Navier-Stokes equations, the boundary condition of no slip at the walls is assumed.

When these conditions apply, the Navier-Stokes equations reduce to the

form given in equations 6 and 7 .

$$\frac{\partial P}{\partial x} = \mu \left(\frac{\partial^2 u}{\partial x^2} + \frac{\partial^2 u}{\partial y^2} \right) . \qquad (6)$$

$$\frac{\partial P}{\partial y} = \mu \left(\frac{\partial^2 v}{\partial x^2} + \frac{\partial^2 v}{\partial y^2} \right) . \qquad (7)$$

The equation of continuity becomes,

$$\frac{\partial u}{\partial x} + \frac{\partial v}{\partial y} = 0 \qquad . \qquad (8)$$

A general solution of these equations for viscous flow associated with two rotating cylinders was treated extensively by Frazer (17). Frazer's results, as applied to the roll mill problem, are described in Appendix II. It is unfortunate that these results become very inconvenient to apply when the distance of separation between cylinder surfaces is small compared with the cylinder radii. This inconvenience originates from the presence in the stream function of slowly converging series and hyperbolic functions of arguments of very small magnitude. One of the special cases considered by Frazer does lead to a relatively simple expression for the stream function in the bank region distant from the vicinity of the nip. This special case is that of two rolls in actual contact. The results of this theory do not apply in the vicinity of the nip, but should be valid in the bank region where the influence of the small nip clearance is negligible. As shown in Appendix II, this special stream function can be differentiated to give an expression for the pressure gradient along the x axis. Assuming that the free fluid surface is located at a distance of one roll radius from the nip center, and including the effect of fluid head, the bank pressure distribution

is given by equation (9);

$$P = R\rho\left[\zeta + 1\right] - \frac{7}{15}(N_1 + N_2)\mu\left[1 + \left(\frac{1}{\zeta}\right)^3\right] , \qquad (9)$$

where:

P = pressure at point ζ ,

R = roll radius ,

N_1 = rpm of slow roll ,

N_2 = rpm of fast roll ,

μ = fluid viscosity ,

$\zeta = x/R$.

The first group of terms on the right of equation 9 expresses the pressure contribution of the hydrostatic head of fluid, while the second group is due to the motion of the rolls.

Application of Viscous Flow Theory to Nip Region. Equation 9 is indeterminate at the nip center where x is zero. Approaching this point from negative values of x, the pressure approaches ∞ ; while approaching zero from positive values of x, the pressure approaches $-\infty$. The application of equation 9 is therefore restricted to negative values of x, out of the nip zone. In order to treat flow through the nip itself, additional simplifying assumptions are made, and the Navier-Stokes equations are reduced to an even more simple form than given by 6 and 7 . The additional assumptions and conditions are:

1. In the narrow passage comprising the nip, the vertical pressure gradient, $\partial P/\partial y$, vanishes, and flow in the y direction may be neglected.

2. In this same region, the second derivative of u with respect

to y is so much larger than the second derivative of u with respect to x that the latter may be neglected. Gatcombe (20) presented an order of magnitude analysis showing the conditions under which these approximations are justified, and concluded that they are reasonable so long as there are regions in the nip where the distance, x, from the nip center is much larger than the corresponding value of h, the separation between surfaces. When these assumptions and conditions are applied, the Navier-Stokes equations are reduced to the single expression;

$$\frac{\partial P}{\partial x} = \mu \frac{\partial^2 u}{\partial y^2} \quad . \tag{10}$$

Since $\partial P/\partial y$ is negligible compared with $\partial P/\partial x$, the pressure may be considered a function of x alone, in which case 10 is written;

$$\frac{dP}{dx} = \mu \frac{d^2 u}{dy^2} \tag{11}$$

The condition of continuity is satisfied by an equation which expresses the fact that the total quantity of fluid passing each point in the nip is a constant. This condition is satisfied by,

$$Q = \int_{-h/2}^{h/2} u \, dy \tag{12}$$

Derivation of Nip Flow Equations

Equations 11 and 12 and their underlying assumptions are the basis of the lubrication theory of Reynolds (14), and the nip pressure theories of Gatcombe (20), Gaskell (22), and Hummel (25). Since these equations, and the results obtained from them, serve as a basis for the

present work as well, the derivations will be shown here in detail.

Equation 11 is integrated twice, giving:

$$\frac{du}{dy} = \int \frac{1}{\mu} \left(\frac{dP}{dx}\right) dy \quad , \tag{13}$$

$$\frac{du}{dy} = \frac{1}{\mu} \left(\frac{dP}{dx}\right) y + C_1 \quad , \tag{14}$$

$$u = \int \left(\frac{1}{\mu} \frac{dP}{dx} y + C_1\right) dy \quad , \tag{15}$$

$$u = \frac{1}{\mu} \frac{dP}{dx} \frac{y^2}{2} + C_1 y + C_2 \quad . \tag{16}$$

The constants, C_1, and C_2, are evaluated from the conditions that at the surface of the slow roll ($y = -h/2$) the velocity is U_1, and at the surface of the fast roll ($y = h/2$) the velocity is U_2. It follows that:

$$U_1 = \frac{1}{\mu} \frac{dP}{dx} \frac{h^2}{8} - C_1 \frac{h}{2} + C_2 \quad , \tag{17}$$

$$C_2 = U_1 + C_1 \frac{h}{2} - \frac{1}{\mu} \frac{dP}{dx} \frac{h^2}{8} \quad , \tag{18}$$

$$U_2 = \frac{1}{\mu} \frac{dP}{dx} \frac{h^2}{8} + C_1 \frac{h}{2} + U_1 + C_1 \frac{h}{2} - \frac{1}{\mu} \frac{dP}{dx} \frac{h^2}{8} \quad , \tag{19}$$

$$C_1 = (U_2 - U_1) / h \quad . \tag{20}$$

Inserting the values for the constants into equation 16 gives the expression for fluid velocity as a function of position and pressure gradient in the nip. This is,

$$u = U_1 + \frac{1}{2\mu} \frac{dP}{dx} \left[y^2 - \left(\frac{h}{2}\right)^2 \right] + (U_2 - U_1)\left(\frac{y}{h} + \frac{1}{2}\right) \quad . \tag{21}$$

Geometrical Approximation for Nip Region. The separation between the roll surfaces, h, can be related to position in the nip, x, by consideration of the geometry of the system as shown in Figure 4. If the minimum nip clearance is h_o, the total clearance at any point is $h_o + 2\delta$, where,

$$\delta = R - L \quad , \tag{22}$$

$$L = \sqrt{R^2 - x^2} \quad , \tag{23}$$

$$\delta = R - (R^2 - x^2)^{\frac{1}{2}} \quad , \tag{24}$$

$$h = h_o + 2R - 2\,(R^2 - x^2)^{\frac{1}{2}} \quad . \tag{25}$$

Equation 25 may be simplified by expanding $(R^2 - x^2)^{\frac{1}{2}}$ in a binomial expansion and neglecting terms of small magnitude. This expansion is;

$$(R^2 - x^2)^{\frac{1}{2}} = R - \frac{x^2}{2R} - \frac{1}{8}\frac{x^4}{R^3} + \cdots \quad , \tag{26}$$

$$(R^2 - x^2)^{\frac{1}{2}} \approx R - \frac{x^2}{2R} \quad , \tag{27}$$

$$\delta \approx \frac{x^2}{2R} \quad , \tag{28}$$

$$h \approx h_o + \frac{x^2}{R} \quad . \tag{29}$$

The approximation given by equation 28 differs from the correct value of δ by only one percent at a value of x of 0.2R, and is much closer at smaller values of x. The relationship between local nip clearance and x coordinate given by equation 29 is employed in the following derivations.

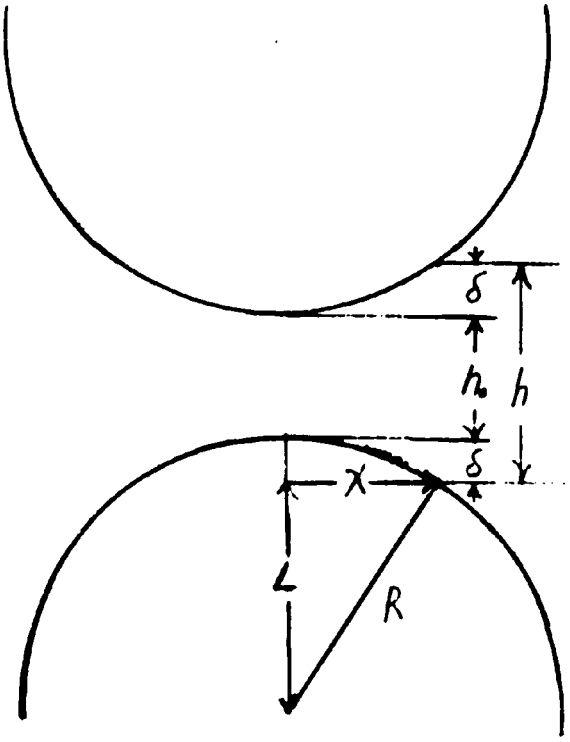

Figure 4. Geometrical Relationship Between Nip Clearance and Location

Pressure Distribution. The expression for velocity, 21 , may be substituted into the continuity equation, 12 , giving;

$$Q = \int_{-h/2}^{h/2} \left\{ U_1 + \left[U_2 - U_1 \right] \left[\frac{y}{h} + \frac{1}{2} \right] + \frac{1}{2} \mu \left(\frac{dP}{dx} \right) \left[y^2 - \left(\frac{h}{2} \right)^2 \right] \right\} dy \quad . \tag{30}$$

Integration of 30 gives,

$$Q = \left(\frac{U_t}{2} \right) h - \frac{h^3}{12 \mu} \left(\frac{dP}{dx} \right) \quad , \tag{31}$$

where U_t is defined as $(U_1 + U_2)$.

Solving 31 for the pressure gradient gives,

$$\frac{dP}{dx} = 12 \mu / h^3 \left[\frac{U_t}{2} h - Q \right] \quad . \tag{32}$$

Integration of equation 32 gives pressure as a function of location in the nip. In performing this integration, x is related to h through equation 29 . The result is;

$$P = \int \left(\frac{dP}{dx} \right) dx = \frac{3 \mu}{h_o} \left[U_t - 1.5 \frac{Q}{h_o} \right] \left[\frac{x}{h} + \sqrt{R/h_o} \tan^{-1} \left(\frac{x}{\sqrt{R\, h_o}} \right) \right]$$

$$- \frac{3 \mu Q}{h_o} \frac{x}{h^2} + C_3 \quad . \tag{33}$$

In equation 33 , C_3 is the pressure at nip center, and is usually unknown. If the pressure, P_1, at some point, x_1, is known, equation 32 may be integrated from limits x_1 to x, giving;

$$P = P_1 + \frac{3 \mu}{h_o} \left[U_t - 1.5 \frac{Q}{h_o} \right] \left[\frac{x}{h} - \frac{x_1}{h_1} + \sqrt{R/h_o} \left(\tan^{-1} \frac{x}{\sqrt{R\, h_o}} - \tan^{-1} \frac{x_1}{\sqrt{R\, h_o}} \right) \right]$$

$$- \frac{3 \mu Q}{h_o} \left(\frac{x}{h^2} - \frac{x_1}{h_1^2} \right) \quad . \tag{33-a}$$

Boundary Conditions. Equation 33 contains two unknown factors, Q, and C_3; or, Q and P_1, as in 33-a . Evaluation of these constants requires two appropriate boundary conditions. One boundary condition is supplied by the fact that at some point on the outlet side of the nip, the pressure passes through a minimum value, P*, which will be determined by the cohesive or adhesive properties of the fluid. At the point of minimum pressure, designated x*, the clearance is h*, and the pressure gradient, dP/dx, is zero. The velocity gradient between roll surfaces is therefore linear at x*, and the rate of flow, Q, can be expressed as,

$$Q = \frac{U_t}{2} h^* \quad . \tag{34}$$

If the value of P^* is known, or can be estimated, only one further condition is needed to solve equation 33-a at a given value of h_o.

Gaskell assumed that Q was known and evaluated h^* and x^* from equations analagous to 34 and 29 . Gatcombe employed different boundary conditions, assuming that pressure was zero at what amounted to $x = \pm\infty$. These conditions gave the result that P = 0 at x = 0. By solving for the point at which dP/dx = 0, Gatcombe calculated Q from equation 34 . This analysis led to the result,

$$h^* = 4/3\ h_o \quad , \tag{35}$$

and

$$Q = 2/3\ U_t\ h_o \quad . \tag{36}$$

The boundary conditions chosen by Gatcombe are subject to question on the following grounds.

1. For the pressure to equal zero at x = 0 and at $x = \pm\infty$, the fluid would have to withstand large tensile stresses. Gatcombe realized that real fluids would not withstand such stresses, but instead of

modifying the entire pressure profile, he assumed that pressure was atmospheric where the equation predicted negative values.

2. The geometrical approximation, $x = h_o + x^2/R$, breaks down at large values of x, and the equation based upon it is not valid at the points where the boundary conditions were invoked.

While Gatcombe's pressure distribution involves the assumption that the fluid is capable of resisting tensile stresses of any magnitude that might be developed, Gaskell assumed that the fluid would sustain no tensile stress and that the pressure, P*, would be zero at x*. Neither assumption can be strictly correct, because real liquids can actually withstand some moderate amount of tensile stress. Where special precautions have been taken to remove disturbing influences, tensile stresses of several hundred atmospheres have been observed before fluid rupture occurs. Vincent and Simmonds (36) reported rupture in a mineral oil at -119 atm., and Trevenna (37) observed a stress of -300 atm. in water. Ordinary fluids, not subjected to special purification procedures, contain impurities which serve as nuclei for cavitation, and are unable to withstand appreciable tension before rupture. Banks and Mill (26) were able to account for the force and time required to separate two smooth-ended brass cylinders originally stuck together with a viscous liquid, by assuming that cavitation occurred when the absolute pressure in the liquid reached zero. On the basis of these data, the assumption of $P^* = 0$ employed by Gaskell appears to be a reasonable approximation of the cavitation pressure. The assumption that P* is zero will also be employed in the present investigation.

In order to solve equation 33 without the boundary conditions of Gatcombe or the independent knowledge of Q used by Gaskell, a new

condition or relationship must be employed. This relationship is provided by equation 9 . It is assumed that there is a point, x_1, near the entrance to the nip region where both equations 33-a and 9 are applicable. Equation 9 , based on the assumption that h_o is zero, is used to calculate the pressure at point x_1. This pressure is then taken as a boundary condition for equation 33-a . The second boundary condition, $P = 0$ at x^* where $dP/dx = 0$, is the same as that employed by Gaskell. If more exact knowledge of the pressure at which cavitation occurs were available, this cavitation pressure could be taken as the boundary value at x^*.

The point, x_1, was chosen as, $x_1 = -0.1\ R$. At this point, $h_1 = h_o + 0.01\ R$ from equation 29 . Under most operating conditions, h_o is a small rfaction of h_1, and the assumptions leading to equation 9 are not seriously violated. Further, at $x = 0.1\ R$, the approximation given by equation 29 is 99.75 percent of the actual value of h.

Features of Nip Flow Theory and Method of Calculation

The solution of equation 33-a for the nip pressure distribution, and equation 34 for the nip flow rate, permits additional features of flow through the nip to be derived. The procedure followed in solving 33-a , and the additional derived results will be presented here.

Location of Coordinate of Film Split, x^*. Equation 33-a was solved by a trial-and-error procedure which is outlined below.

1. Equation 9 is solved for the value of P_1 at $\zeta_1 = -0.1$

2. A trial value of x^* is assumed from the relationship, $x^* \approx 0.474 \sqrt{R\ h_o}$.

3. A value of h* is calculated from equation 29 .

4. A trial value of Q is calculated from equation 34 .

5. P_1, x_1, h_1, x*, h*, and Q are substituted into equation 33-a in order to evaluate P*.

6. If P* calculated in step 5 is not zero, a new value of x* is selected, and steps 3 through 5 are repeated.

7. The value of x giving P* equal to zero is the correct x*.

Flow Rate. The value of x* found by the procedure outlined above is subetituted into equation 34 to calculate the throughput rate, Q.

Force between Rolls. The force acting on the rolls is found by integrating the pressure - area product between the bank entrance and the point of film split. In terms of force per unit roll length, this integral is,

$$F/L = \int_{-R}^{x^*} P \, dx \quad . \tag{37}$$

The integral is conveniently divided in two parts; the force due to the bank and the force due to the nip. The bank pressure is taken from equation 9 , and the nip pressure from equation 33-a . Combining these equations gives,

$$F/L = \int_{-1}^{-0.1} R^2 \rho \left[\zeta + 1\right] d\zeta - \int_{-1}^{-0.1} \frac{\pi}{15} R \, (N_1 + N_2) \, \mu \left[\frac{1}{\zeta^3} + 1\right] d\zeta$$

$$+ \int_{-0.1R}^{x^*} \left\{ P_1 + \frac{3\mu}{h_o} \left[U_t - 1.5 \frac{Q}{h_o}\right] \left[\frac{x}{h} - \frac{x_1}{h_1} + \sqrt{\frac{R}{h_o}} \left(\tan^{-1} \frac{x}{\sqrt{R\, h_o}} - \tan^{-1} \frac{x_1}{\sqrt{R\, h_o}}\right)\right] \right.$$

$$\left. - \frac{3\mu Q}{h_o} \left(\frac{x}{h^2} - \frac{x_1}{h_1^2}\right) \right\} dx \quad . \tag{38}$$

Integration of equation 38 gives,

$$F/L = C.405\, R^2\rho - \frac{197.1}{15}\pi (N_1 + N_2)\, R\, \mu + A\,\frac{R}{2}\log_e\left(\frac{h^*}{h_1}\right) + B\,\frac{R}{2}\left[\frac{1}{h^*} - \frac{1}{h_1}\right]$$

$$+ D\left[x^* \tan^{-1}\frac{x^*}{\sqrt{R\,h_o}} - x_1 \tan^{-1}\frac{x_1}{\sqrt{R\,h_o}} + \frac{\sqrt{R\,h_o}}{2}\log_e\left(\frac{R\,h_o + x_1^2}{R\,h_o + x^{*2}}\right)\right] + C\,(x^* - x_1), \tag{39}$$

where:

$$A = \frac{3\,\mu}{h_o}\left(U_t - 1.5\,\frac{c}{h_o}\right) ,$$

$$B = 3\,\frac{\mu\, Q}{h_o} ,$$

$$D = A\sqrt{R/h_o} ,$$

$$C = P_1 - A\,\frac{x_1}{h_1} + B\,\frac{x_1}{h_1^2} - D\tan^{-1}\left(\frac{x_1}{\sqrt{R\,h_o}}\right) .$$

The terms of equation 39 are calculated in a straightforward manner after x* has been evaluated. For given conditions of roll speed and size, and fluid viscosity and density, the equations developed here permit calculation of total roll force and throughput rate for given values of nip clearance. A curve of production rate versus roll force can be constructed by repeating the calculations for a series of values of clearance. The calculation of x* from equation 33-a and the subsequent calculation of throughput rate and force were programmed for solution on a Royal-McBee LGP-30, stored program digital computer in order to facilitate comparison of theory with experiment. Details of the computer program are given in Appendix IV.

Maximum Pressure. The maximum pressure in the nip is located on the inlet side of the nip at the point, $-x^*$. The points of maximum and minimum pressure are equidistant from the center, because at these points the pressure gradient vanishes, the velocity profiles are linear and equal, and the clearances must be equal in order to provide a constant flow rate. To calculate the maximum pressure, a value of $-x^*$ is substituted for x in equation 33-a , once the flow rate and x^* have been evaluated.

Maximum Shear Rate. In its passage through the nip, the fluid is subjected to shear rates which range from zero to more than 10^5 sec^{-1} in some cases. The maximum rate of shear is found at the slow roll surface at the point, $x = 0$. The value of this maximum shear rate can be calculated by substituting values of C_1 from equation 20 and dP/dx from 32 into equation 14 , and setting h equal to h_o and y equal to $-h_o/2$. This gives,

$$\left(\frac{du}{dy}\right)_{max} = 3\left(\frac{U_t}{h_o}\right)\left(\frac{h^*}{h_o} - 1\right) + \frac{U_2 - U_1}{h_o} \quad . \tag{40}$$

Power Dissipation. Power supplied to turn the rolls is dissipated as heat due to viscous shear in both the bank and nip regions. Only power dissipation in the nip is considered here. The rate of energy dissipation per unit volume in a fluid subjected to simple shear is the product of the viscosity and the square of the shear rate. Thus the power consumed per unit length of roll is given by,

$$\frac{P_o}{L} = \mu \int_{x_1}^{x^*} \int_{-h/2}^{h/2} \left(\frac{du}{dy}\right)^2 \, dy \, dx \quad . \tag{41}$$

Carrying out the integration indicated in equation 41 yields the following expression for nip power consumption;

$$\frac{P_o}{L\mu} = \sqrt{\frac{R}{h_o}}\left[4\,(U_t)^2 - \frac{6\,Q(U_t)}{h_o} + \frac{9}{2}\left(\frac{Q}{h_o}\right)^2\right]\left[\tan^{-1}\frac{x^*}{\sqrt{R\,h_o}} - \tan^{-1}\frac{x_1}{\sqrt{R\,h_o}}\right]$$
$$+ \left[\frac{9}{2}\left(\frac{Q}{h_o}\right)^2 - \frac{6\,Q\,U_t}{h_o}\right]\left[\frac{x^*}{h^*} - \frac{x_1}{h_1}\right] + \left[\frac{3\,Q^2}{h_o}\right]\left[\frac{x^*}{h^{*2}} - \frac{x_1}{h_1^2}\right] . \qquad (42)$$

Equation 42 may be further reduced, giving,

$$\frac{P_o}{L\,\mu\,U_t^2} = \sqrt{\frac{R}{h_o}}\left[4 - 3\,\frac{h^*}{h_o} + \frac{9}{8}\left(\frac{h^*}{h_o}\right)^2\right]\left[\tan^{-1}\frac{x^*}{\sqrt{R\,h_o}} - \tan^{-1}\frac{x_1}{\sqrt{R\,h_o}}\right]$$
$$+ \left[\frac{9}{8}\left(\frac{h^*}{h_o}\right)^2 - 3\,\frac{h^*}{h_o}\right]\left[\frac{x^*}{h^*} - \frac{x_1}{h_1}\right] + \frac{3}{4}\,\frac{h^{*2}}{h_o}\left[\frac{x^*}{h^{*2}} - \frac{x_1}{h_1^2}\right] . \qquad (42\text{-a})$$

Stagnation Point. In the bank region of the mill, fluid near the roll surfaces is carried toward the nip while fluid distant from the surfaces flows away from the nip. The stream lines obtained from Frazer's solution, equation (A II 40) of Appendix II, show the general features of this flow in regions remote from the immediate vicinity of the nip. Since this equation is based on the assumption of no clearance between the rolls, it breaks down in the immediate vicinity of the nip, and is unable to predict the point of ultimate flow reversal, or stagnation point, beyond which all fluid moves forward through the nip. On the other hand, the equations based on equation 10 do apply in the nip region, and provide a method of estimating the location of the stagnation point.

By requiring du/dy and u from equations 14 and 16 to vanish simultaneously, the coordinates of the stagnation point may be determined.

From this derivation, shown in detail in Appendix III, coordinates of the stagnation point are given by:

$$x_s = - \sqrt{R\,(\alpha h^* - h_o)} \quad , \tag{43}$$

$$y_s = \beta h^* \quad . \tag{44}$$

The values of α and β are functions of the roll speed ratio, r, and are given by:

$$\alpha = 3/2 \quad 1 + r \, \frac{1 + r + \sqrt{r}}{1 + r + r^2} \quad , \tag{45}$$

$$\beta = \frac{\alpha^2 (1 - r)}{6(\alpha - 1)(1 + r)} \quad . \tag{46}$$

The clearance between the rolls at the stagnation point is,

$$h_s = \alpha h^* \quad . \tag{47}$$

For six-inch diameter rolls at equal roll speeds and a minimum nip clearance of 100 microns, the h^*/h_o ratio is equal to 1.229, and the point of flow reversal given by equation 43 is -0.0146 ft., or 4450 microns. This corresponds to a value of -0.0885 R. For the same roll diameter and roll speed ratio, the theoretical point of flow reversal moves to -0.1 R when the minimum nip clearance increases to 280 microns. Since a clearance of 280 microns corresponds to an unusually wide operating clearance, the point of flow reversal usually falls between the nip center and the the assumed boundary of the nip flow equations.

Fraction of Flow Associated with Fast Roll. A portion of the total flow passing through the nip comes from a layer of fluid near the surface of the fast roll, and the remainder comes from a layer near the slow roll. The fraction of the total flow in each of these layers can be calculated

if the velocity distribution and thickness of these layers is known. The quantity of flow associated with the fast roll is given by

$$Q_f = \int_{y_s}^{h_s/2} u \, dy \quad , \tag{48}$$

where y_s is the point of division between slow and fast roll streams, and $h_s/2$ is the surface of the fast roll at x_s. Substituting the expression for u from equation 21 into 48 , and integrating between the limits, $y_s = \beta h^*$, 44 , and $h_s/2 = \alpha h^*/2$, 47 , gives,

$$Q_f = U_1\left[\frac{\alpha h^*}{2} - \beta h^*\right] + \left[U_2 - U_1\right]\left[\frac{1}{2\alpha h^*}\left(\frac{\alpha^2 h^{*2}}{4} - \beta^2 h^{*2}\right) + \tfrac{1}{2}\left(\frac{h^*}{2}\alpha - \beta h^*\right)\right]$$

$$+ \frac{1}{2\mu}\left(\frac{dP}{dx}\right)_s\left[\frac{1}{3}\left(\frac{\alpha^3 h^{*3}}{8} - \beta^3 h^{*3}\right) - \frac{\alpha^2 h^{*2}}{4}\left(\frac{\alpha h^*}{2} - \beta h^*\right)\right]. \tag{49}$$

Equation 49 may be reduced to,

$$Q_f = U_1 h^*\left\{\left(\frac{\alpha}{2} - \beta\right) + (r-1)\left(\frac{3\alpha}{8} - \frac{\beta}{2} - \frac{\beta^2}{2\alpha}\right)\right.$$

$$\left. + (r+1)\left(1 - \frac{1}{\alpha}\right)\left(\frac{3\beta}{4} - \frac{\beta^3}{\alpha} - \frac{\alpha}{4}\right)\right. . \tag{50}$$

The total flow, Q, from equation 34 is,

$$Q = U_t h^*/2 = U_1 h^* (1 + r)/2.$$

The ratio $Q_f/Q = f$ is therefore,

$$f = \left(\frac{2}{r+1}\right)\left(\frac{\alpha}{2} - \beta\right) + 2\left(\frac{r-1}{r+1}\right)\left(\frac{3\alpha}{8} - \frac{\beta}{2} - \frac{\beta^2}{2\alpha}\right) + 2\left(1 - \frac{1}{\alpha}\right)\left(\frac{3\beta}{4} - \frac{\beta^3}{\alpha} - \frac{\alpha}{4}\right). \tag{51}$$

Values of f calculated from equation 51 for common roll speed ratios are listed in Table I.

Table I. Estimates of Relative Flow Fractions Associated with Fast Roll

Roll Speed Ratio r	Fraction of Flow Associated with Fast Roll, f
1	0.5
2	0.744
3	0.851
4	0.907

Relative Point of Flow Division. The coordinates of the point at which the forward-flowing layer from the fast roll joins the forward-flowing layer from the slow roll were given by equations 43 and 44 . The distance from the fast roll surface to this point is $h_s/2 - y_s$, and the ratio of this distance to the total clearance is $(0.5 - y_s/h_s)$, or $(0.5 - \beta/\alpha)$, a function of roll speed ratio alone.

IV. EXPERIMENTAL INVESTIGATION

The experimental program was designed to test the validity and range of applicability of the nip flow theory based on the hydrodynamic theory of flow of a constant viscosity liquid. The greater portion of the experimental work was directed at evaluation of the relationship between force applied to the rolls and the total quantity of flow through the nip. The maximum size of spherical glass beads passed through the nip without fracture, and the relative transfer of fluid to the faster roll were also investigated.

Apparatus

The principle experimental apparatus consisted of pairs of rotating cylinders. Auxiliary equipment consisted of pressure measuring gages, a temperature measuring pyrometer, a balance, a viscometer, and a microscope.

Roll System. The roll system was mounted on a Kent laboratory three-roll mill frame. During part of the investigation, the roll system consisted of three, 4-inch diameter rolls, eight inches in length. No take-off knife was employed, and the rate of flow through the feed nip was determined from the quantity of fluid carried on the surfaces of the slow and center rolls. To extend the studies to larger size rolls, the 4-inch diameter rolls were replaced with two, 6-inch rolls, five inches in length. All rolls were of hollow, hardened steel construction. Plates at the ends of the rolls were employed to maintain a bank of fluid between the rolls. Temperature control was provided by

circulation of cooling water through the interior of the rolls. Roll speed ratios of 1-1, 2-1, and 3-1 were obtained by changing the ratio of the driving gears. Total roll speed was varied by use of different ratios of chain sprocket sizes between the mill motor and the driven roll. A photograph of the system with 4-inch rolls in place is shown in Fig. 5.

The mill motor was equipped with General Electric Plug Stopping Controls for quick stopping. When the plug-stop switch is depressed, the phase relationship of the current to the two-horsepower, three-phase, 220 volt motor is reversed. The reversing relay is held closed by an electromagnet deriving its power from a plugging generator driven by the mill motor. When the motor stops, the reversing relay is spring opened, and all power to the motor is shut off. The sequence of events from depression of the plug-stop switch to complete mill stop is, for practical purposes, instantaneous. Since the rolls are stopped without coasting, the film thickness on the stopped rolls is the same as that on the rotating rolls. A diagram of the plug-stopping controls is shown in Fig. 6.

Pressure Gages. Force was applied to the rolls through two oil filled pistons equipped with pressure gages. The gages were calibrated in pounds force and could be read with a precision of $\pm$ five pounds. The total force applied to the rolls was the sum of the two gage readings. The range of each gage was 0 - 1000 pounds force. The gages were calibrated on a Tinius Olsen testing machine and were found accurate within 4 percent. A calibration chart was used in converting gage reading to true force values.

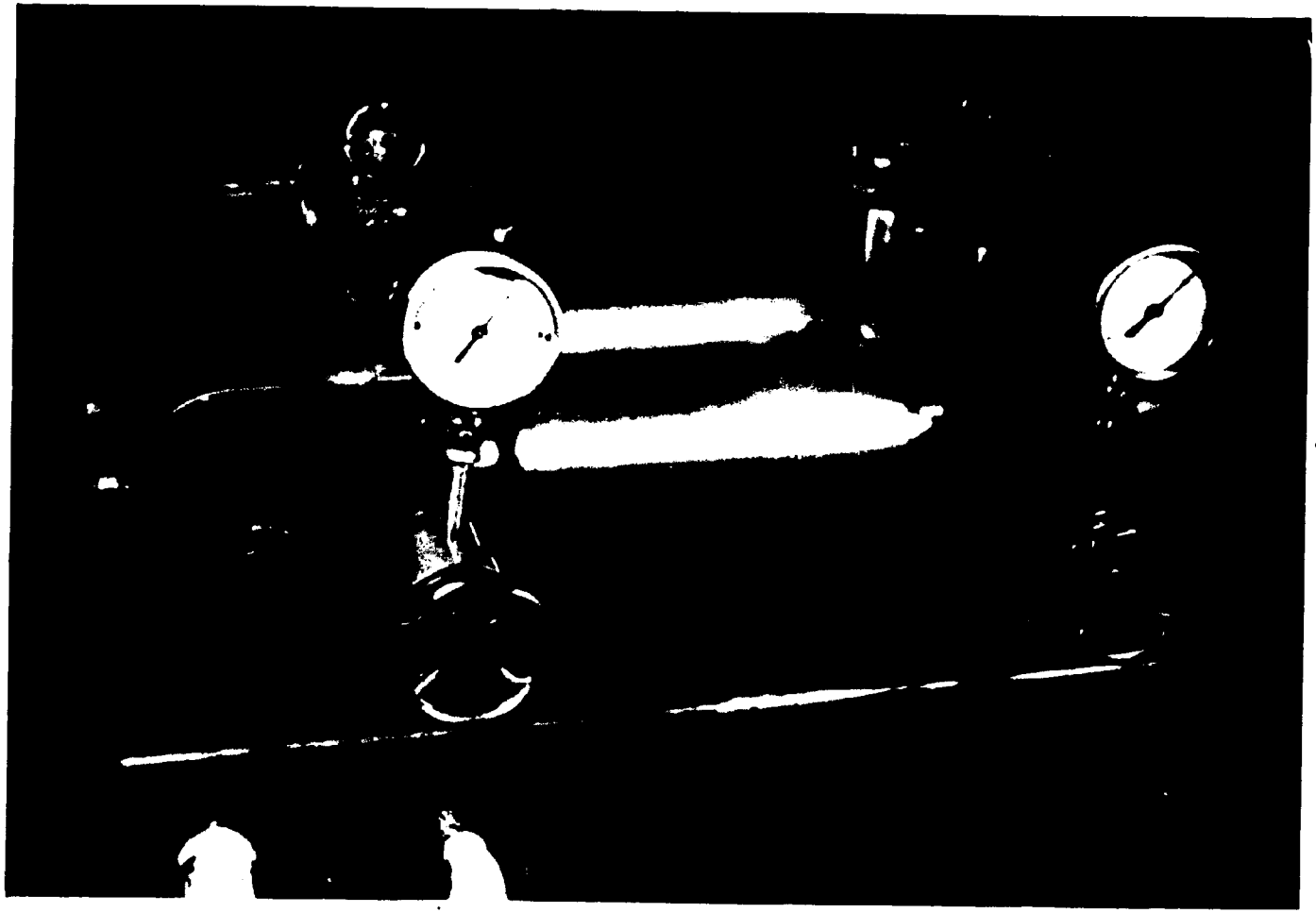

Figure 5. Photograph of Roll Mill with Four Inch Rolls in Place

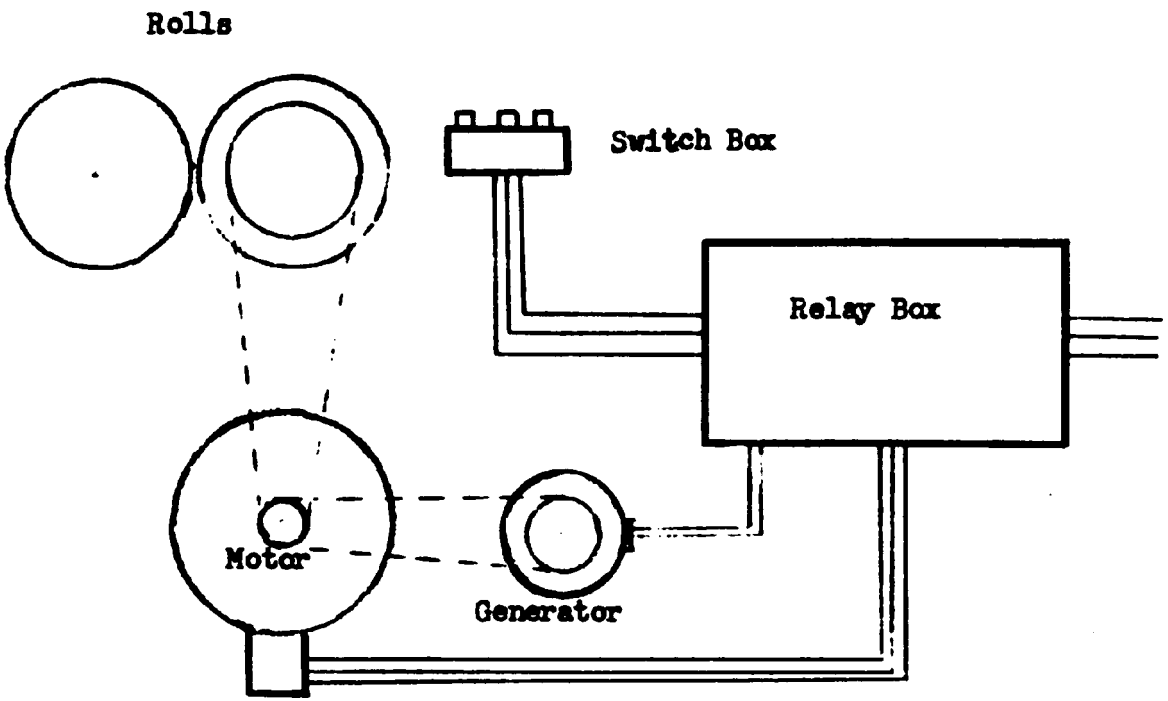

Figure 6. Schematic Diagram of Plug Stopping Controls

Surface Pyrometer. The temperature of the fluid on the surface of the rolls was measured with a type 4200 portable pyrometer manufactured by Illinois Testing Laboratories, using a type 4090 sensing head. The sensing element is a $\frac{1}{4}$-inch wide bimetalic junction in a strip $3\frac{7}{8}$ inches long. The temperature was measured by holding this strip against the rotating roll with a force of approximately one pound. In one series of tests the temperature was also measured by inserting a copper-constantan thermocouple into the fluid bank until it nearly entered the nip. The potential of the bank thermocouple was measured with a Leeds and Northrup potentiometer, using a water-ice bath for reference junction.

Balance. In the flow rate studies, cotton pads containing fluid scraped from measured areas of roll were weighed on a Christian Becker Chainomatic analytical balance. Weighings were estimated to be accurate within $\pm$ 0.2 milligrams, with sample weights ranging from a low of 0.02 grams to 1 gram of fluid scraped from the roll.

Viscometer. A precision rotational viscometer manufactured by Sun Chemical Co. was used to measure the viscosity of the fluids used in this study. A complete discription of this instrument and its theory of operation was given by Lower (30). The viscometer has a rotating outer cup with 2.53 cm radius and a fixed inner bob of 2.50 cm radius. The torque imparted to the bob through the fluid by rotation of the cup is measured by the deflection of a calibrated spring. The cup is surrounded by a thermostated water bath permitting operation at controlled, elevated temperatures. The measurement of viscosity in this instrument was limited to rates-of-shear below 200 sec^{-1}.

Microscope. Glass beads passed through the nip between rolls were observed and photographed with a Bausch and Lomb microscope mounted on an optical bench. The eyepiece used was a 5 x Hyperplane. Two objectives were used, a Bausch and Lomb 10 x with 0.25 N. A., and a 40 x Carl Zeiss lens with 0.65 N. A. Together with the magnification given at the photographic plate, these lenses gave magnifications of 74 x and 296 x respectively. Photographs were taken on Ansco type 282 panchromatic film. Measurement of bead size was performed by projecting the photographic negatives on a screen and measuring the particles with a scale calibrated from a stage micrometer photographed under the same maginification.

Materials

The materials used in this study were viscous liquids and glass beads.

Viscous Liquids. The fluids on which the force-throughput studies were performed are listed in Table II, along with their viscosities at 30 °C and the constants of their temperature - viscosity relationships. Lithographic varnishes are refined, heat bodied linseed oils of the type commonly employed in printing ink manufacture. The copolymer H-2185 ink vehicle is an alkyd resin type ink vehicle. Polybutenes are synthetic polymers obtained by the catalytic polymerization of normal and branched chain butenes. Acroloid HF 825 is a solution of butyl methacrylate polymer in di-2-ethylhexyl sebacate. Sucrose acetate isobutyrate, SAIB, is produced by the controlled esterification of sucrose with acetic and isobutyric anhydrides. It is notable for its unusually high viscosity-temperature coefficient.

Table II

Viscosity of Fluids Employed in Throughput Rate Studies

Material	Source	Viscosity at 30°C Poise	M(1)	b(1)	SpG
1. No 1 Pale Litho Varnish	Superior(a)	16.86	4707.3	10.0531	0.957
2. No 2 Pale Litho Varnish	Superior	27.20	4660.4	9.7728	0.960
3. No 3 Pale Litho Varnish	Superior	39.40	4660.3	9.6283	0.962
4. No 4 Pale Litho Varnish	Superior	61.2	4199.4	8.5600	0.964
5. No 5 Pale Litho Varnish		103.4	4856.0	9.5326	0.966
6. No 8 Pale Litho Varnish	Superior	294	4335.1	8.1515	0.966
7. 33 Poise Dark Litho Varnish	Braden(b)	26.1	3974.0	8.5561	0.961
8. H2185 Copolymer Ink Vehicle	Superior	235.1	6661.1	12.4896	1.002
9. Polybutene Mixture (c)	Indoil(d)	122	5823.0	11.2413	0.871
10. Acroloid (e)	R-H (f)	101.6	5171.6	10.13589	0.978
11. SAIB* (g)	Eastman(h)	972.2(J)	12269	21.4454	1.146
12. White Ink (k)	(k)	48	3997	8.3072	1.559

a. Superior Varnish and Drier Co., Merchantville, N. J.
b. Braden Sutphin Ink Co., Cleveland, Ohio
c. Mixture of Polybutene H-35 and 128
d. H-35 from Indoil Chemical Co., Chicago 5, Ill.
and 128 Polybutene from Oronite Chemical Co., San Francisco 4, Calif.
e. 40% Acroloid HF 825 in Plexol Solvent
f. Rohm and Haas Co., Philadelphia, Pa.
g. Sucrose Acetate Isobutyrate
h. Eastman Chemical Products, Inc., Kingsport, Tennessee.
j. Viscosity at 40° C
k. 50% by Weight Unitane OR342 Rutile TiO_2 (American Cyanamid Co.) in No 1 Pale Litho Varnish (Superior).

(1) Constants in Equation

$$\log_{10}\mu = M/T - b$$

μ = viscosity, lb-sec/ft²
T = temperature, degrees Rankine

* Range 40-50° C.

The viscosity of each of the fluids was measured at 20, 30, 40, and 50 °C on a rotational viscometer. An empirical equation of the form,

$$\log \mu = \frac{M}{T} - b \ , \qquad (52)$$

was fitted to the viscosity data for interpolation purposes. All of the systems studied, including the 50 percent dispersion of TiO_2 in varnish, exhibited Newtonian viscosity behavior at low rates of shear. At higher shear rates, the more viscous systems gave non-linear curves of stress versus rate-of-shear, but this curvature was of the order of magnitude that could be explained by the temperature rise in the rotational viscometer. Where curvature was evident, the slope of the stress-shear rate curve at low shear rates was used for determination of the viscosity.

Glass Beads. The glass beads used in determination of the minimum nip clearance were type 140 standard reflective beads obtained from the Flex-O-Lite Corporation. A photograph of a sample of the beads at a magnification of 74 x is shown in Fig. 7. Many of the beads appeared to be hollow, or at least, to have numerous air bubbles in their interiors.

Experimental Procedure

The experimental procedure followed involved measurement of the flow rate between the rolls, evaluation of the fraction transferred to the faster roll, and measurement of the size of glass beads passed through the rolls.

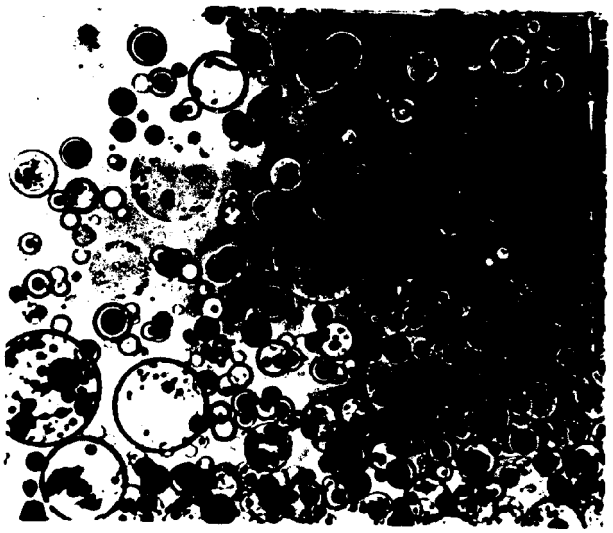

Figure 7. Unmilled Dispersion of Glass Beads

74 X Magnification

Measurement of Flow Rate. Rate of fluid flow through the mill nip was measured, after equilibrium operating conditions had been established, by plug stopping the rolls, scraping the fluid from a measured area of each roll with a razor blade, wiping the blade on tared cotton pads (a separate pad for each roll), and reweighing the pads. The weight of fluid divided by the scraped area and fluid density, amd multiplied by the surface velocity of the roll gave the flow rate on that roll in volume per unit time per unit roll length. The sum of flow rates on the two rolls gave the total nip flow rate. It was necessary to weigh control cotton pads when the sample pads were tared and reweighed, since the pads sometimes gained or lost moisture between weighings. The weight change of the control pads, which differed in handling from the sample pads only in that no fluid was wiped on them, was used to correct the sample pads for any change due to moisture gain or loss.

Dimensions of the scraped area on the rolls were measured with dividers and rule to within ± 0.05 cm. The chord of the width of the scraped area was actually measured, but was corrected to the arc length for the calculation of area. Weighings were carried out on an analytical balance with an estimated accuracy of ± 0.2 milligrams. The minimum fluid sample weight was 0.02 grams, and ranged up to one gram. Sample areas scraped from the roll ranged from 40 to 70 sq-cm, and were usually near 60 sq-cm.

When three rolls were employed, the flow rate on each was measured, although only feed roll and center roll flows were used in the calculations reported here. No take-off-knife was employed, and the thickness of fluid on the fast roll established an equilibrium with that on the other two rolls. Fluid which accumulated at the ends of the fast roll

was periodically removed and returned to the feed bank to keep the total quantity of fluid in the system constant during each series of measurements.

In establishing operating conditions for each series of tests, the cooling water flow rate to the rolls was regulated to give equal surface temperatures on each roll. Although water rate was not measured, it was observed that higher rates were required for the faster rolls in order to maintain equal roll surface temperatures. In general, it was not possible to keep roll temperatures constant as pressure was increased in any given series of measurements. For this reason the temperatures were recorded, and the viscosities at operating temperature were calculated from the viscosity-temperature equations of the fluids.

Nip Clearance Evaluation with Glass Beads. In order to obtain an independent measure of the clearance between rolls for comparison with the calculated values, experiments were made with fluids containing 5 percent by weight of spherical glass beads of the type used in reflecterized paint. The beads ranged in diameter from less than one, to over 200 microns. Operating procedure for the glass bead experiments was similar to that used in the flow rate studies with simple liquids, except that samples of the bead containing fluid were removed while the rolls were in operation. Samples of the fluid scraped from the moving rolls with a razor blade were placed in tared crucibles, weighed, and ignited at 900 °C. The weight of glass residue in the crucible was used to calculate the concentration of beads in the fluid passed by the nip. A second sample was placed in a flat, one-ounce can and allowed to stand overnight while the beads settled. The sediment, containing a concentrated sample of beads was examined microscopically to

determine the size of the largest particles that passed through the roll nip unbroken. Photomicrographs were taken of the bead samples using the equipment and procedure described under "Microscope".

Each set of experiments was performed in the order of decreasing roll force. A fresh sample of fluid and beads was placed in the bank at the start of each series, and the rolls were started at high roll force. When temperature equilibrium was established, operating samples were taken, and the rolls were plug-stopped. Samples were scraped from the rolls for flow rate measurement, and the rolls were restarted and adjusted to the next lower force level in the series. Each series consisted of runs at forces of 4320, 3360, 2880, 2400, 1920, and 1440 pounds per foot of roll length.

The effect of glass content, at the measured glass concentration, was taken into consideration in the fluid density used for calculation of the volumetric flow rate from the gravimetric flow rate measurements.

Experimental Conditions. The ranges of principal variables used in the force -throughput rate studies were:

1. Fluid viscosity, 17 - 240 poise;
2. Roll diameter, 4-inch and 6-inch;
3. Roll speed ratio, 1-1, 2-1, and 3-1;
4. Speed of fast roll, 155, 198, 245, and 300 rpm;
5. Force on rolls, 255 - 4320 lb/ft.

Although all possible combinations of these variables were not employed, force vs. throughput rate curves were obtained under 61 different combinations of conditions, which embraced a total of 404 experimental runs. Six conditions were explored with fluids containing glass beads in 41 experimental runs. A list of the different experimental

conditions employed is given in Table III, along with the notebook and page number where the original data were recorded. Fluid numbers in Table III correspond to the list of fluids given in Table II.

Table III Experimental Conditions Tested

4-in Roll Diameter

Fast Roll RPM 155			Fast Roll RPM 245		
Ratio 3-1	Ratio 2-1	Ratio 1-1	Ratio 3-1	Ratio 2-1	Ratio 1-1
1-222-124	1-222-90	1-222-112	1-222-130	1-222-104	1-222-118
3-222-126	2-222-94	3-222-132	3-222-114	3-222-106	3-222-120
10-222-142	3-222-96	10-228-8	10-222-148	3-222-140	10-228-6
11-231-34*	9-222-102	12-222-116	11-231-34	10-222-146	12-222-122
12-222-128	10-222-144		12-222-134	12-222-108	
	11-231-36				
	12-222-110				
	12-222-138				

6-in Roll Diameter

Fast Roll RPM 198			Fast Roll RPM 300		
Ratio 3-1	Ratio 2-1	Ratio 1-1	Ratio 3-1	Ratio 2-1	Ratio 1-1
1-228-28	1-228-34	1-228-44	1-228-22	1-228-18	1-228-14
5-228-30	1-228-102	5-228-42	1-228-74	3-228-80	6-228-16
6-228-32	3-228-104	6-228-40	1-228-144	6-228-20	
11-231-30	4-228-110	1g-231-22	3-228-76	1-228-78	
1g-231-16	5-228-36	6g-231-24	4-228-146		
6g-231-20	6-228-38		5-228-26		
	6-228-106		6-228-24		
	7-228-108		6-228-148		
	8-228-112		6g-231-10		
	11-231-32		6g-231-20		
	1g-228-122				
	1g-228-138				
	8g-228-124				

Numbers in table are given in order, Fluid, - Notebook Number - Page.

* Fast Roll RPM 104

V. RESULTS

Experimental and theoretical results of the flow rate studies are listed in Appendix VI, Table XXI. Glass bead study results are listed in Appendix VII, Table XXII. A graphical presentation of results is given in Figs. 8 through 23.

Relationship of Roll Force to Throughput Rate

The rate of flow through the roll nip was calculated from the measured fluid film weight per unit area and the known surface speed of the rolls. The force per unit length of roll was calculated by summing the corrected gage force readings and dividing by the roll length. The fluid viscosity at the measured film surface temperature was calculated from the appropriate viscosity-temperature equation. The theoretical force-flow rate relationship was computed for a series of values of minimum nip clearance for each condition of roll diameter, roll speed, roll speed ratio, and average fluid viscosity. Since it was not always possible to maintain the roll temperature constant as roll pressure was changed in one experimental series, the computer calculations were carried out at the average of the experimental fluid viscosity. In order to provide a valid comparison between the experimental and calculated results, it was necessary to correct for the resulting viscosity difference. The experimental results and the theoretical equations both indicated that the throughput rate was nearly proportional to viscosity when other conditions were equal. Advantage was taken of this relationship to correct for viscosity differences within a single

experimental series. In Figs. 8 - 19, the experimental flow rates, corrected to the average viscosity of the series, are plotted versus the reciprocal force per unit roll length on log-log coordinates. The machine computed curves at the same average viscosity values are plotted in these figures for direct comparison with the experimental values. The theoretical curves are identified by circled symbols of the same kind as used for the corresponding experimental points. The fluids are identified in Figs. 8 - 19 by numbers corresponding to those found in Table II, and the average fluid viscosity for each curve is given in poise units. Experimental values are tabulated in Appendix VI together with theoretical flow rate values. The theoretical values were corrected to the experimental viscosities by interpolation between theoretical curves. The experimental flow rate values for all the tests are plotted versus the corresponding theoretical flow rates in Fig. 20. Since the behavior of the No. 8 varnish and the SAIB differed somewhat from that of the other materials, the data points for these materials are identified separately in Fig 20. The theoretical line with unit slope is indicated together with dotted lines representing the 95 percent confidence limits of the best line through all of the points.

Transfer Fraction

Values of the fraction, f, of fluid transferred to the faster roll are listed in Tables XXI and XXII with each experimental run. This fraction is the ratio of the flow rate on the faster roll to the total nip flow rate. In the 1-1 roll speed ratio tests, the driven or front roll was considered the faster roll in calculation of f.

FIGURE 8 · NIP FORCE AND FLOW RATE

4 INCH ROLLS, 3-1 SPEED RATIO, 155 RPM FAST ROLL

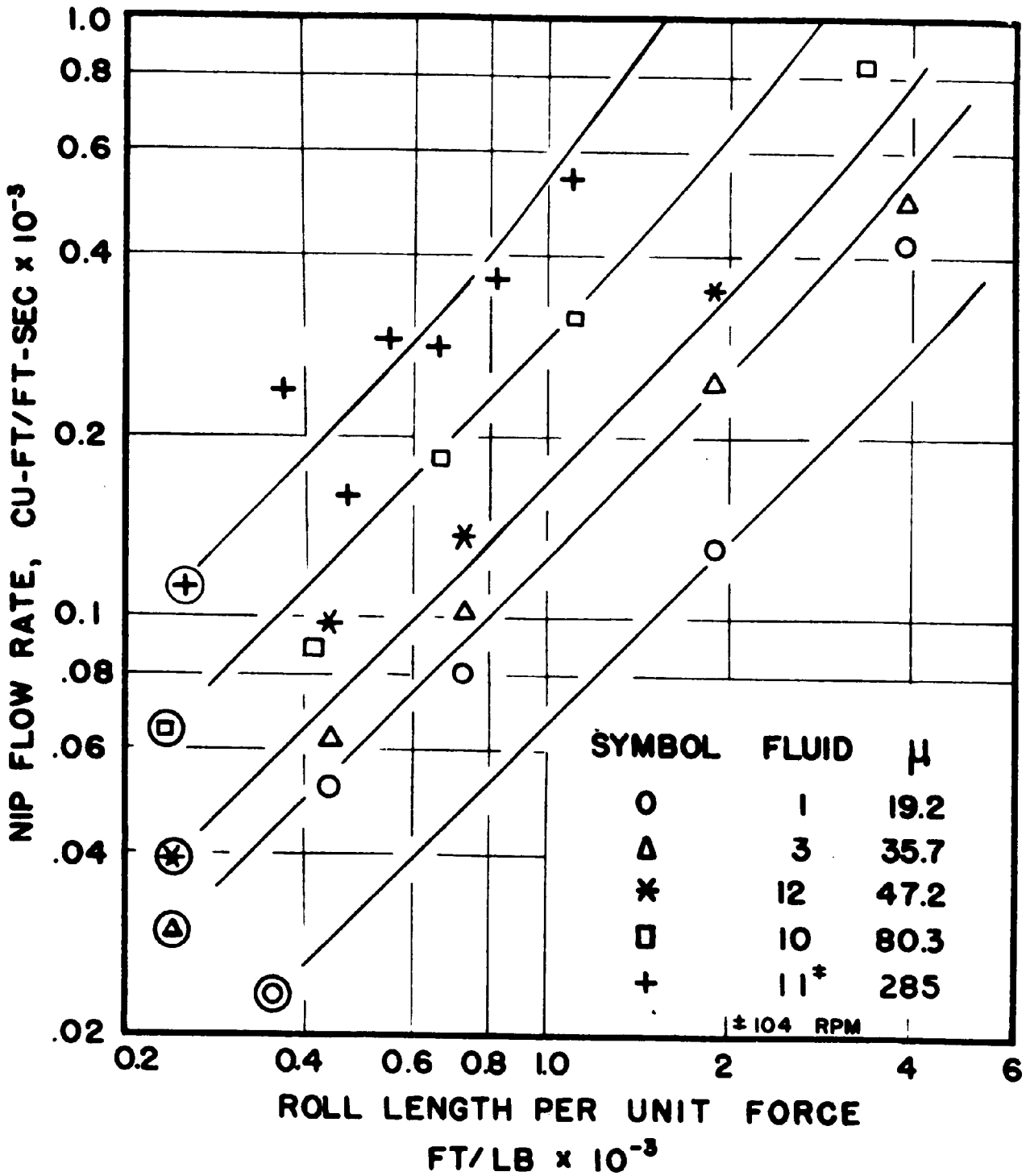

FIGURE 9. NIP FORCE AND FLOW RATE

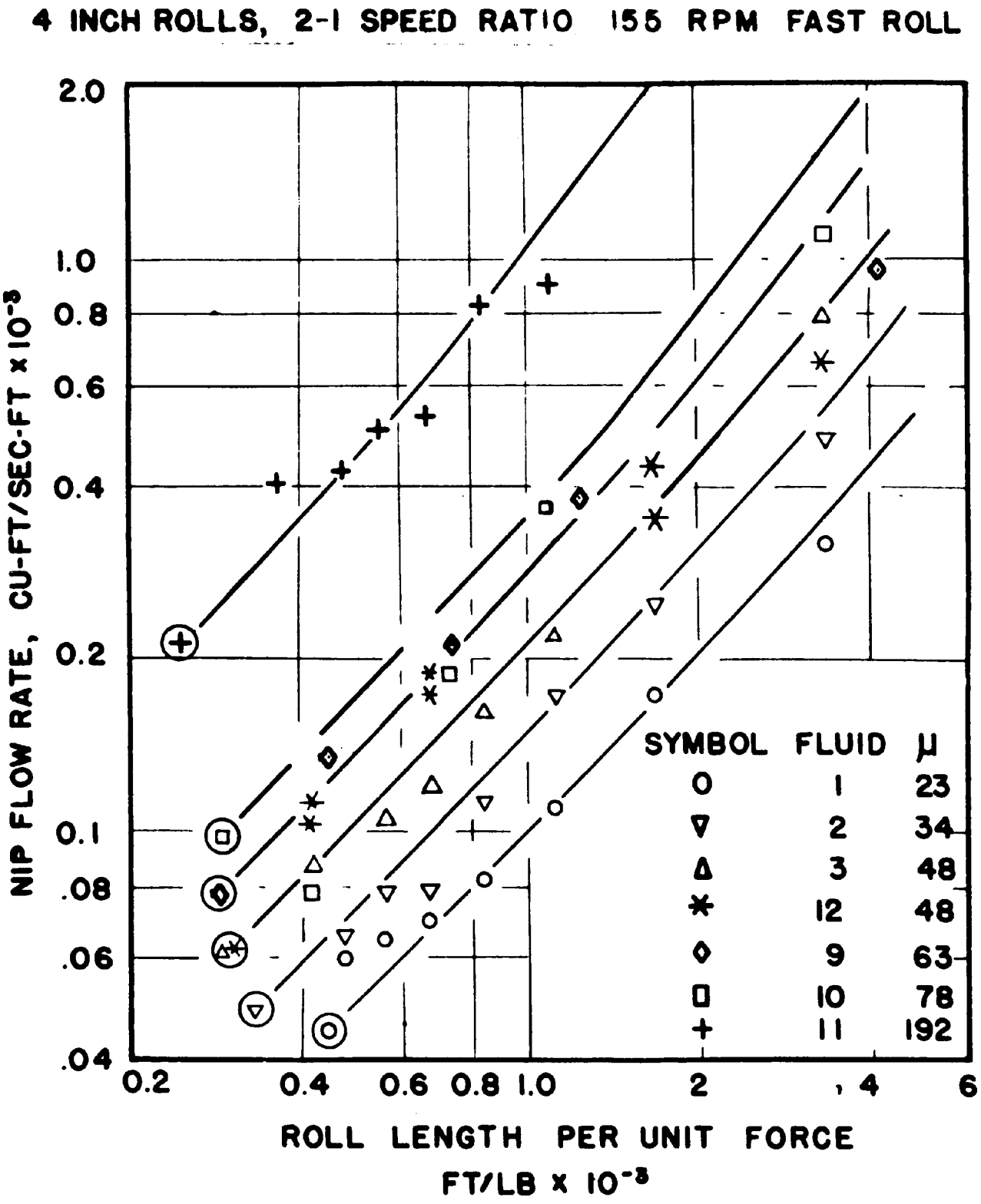

FIGURE 10. NIP FORCE AND FLOW RATE

4 INCH ROLLS, 1-1 SPEED RATIO, 155 RPM EACH ROLL

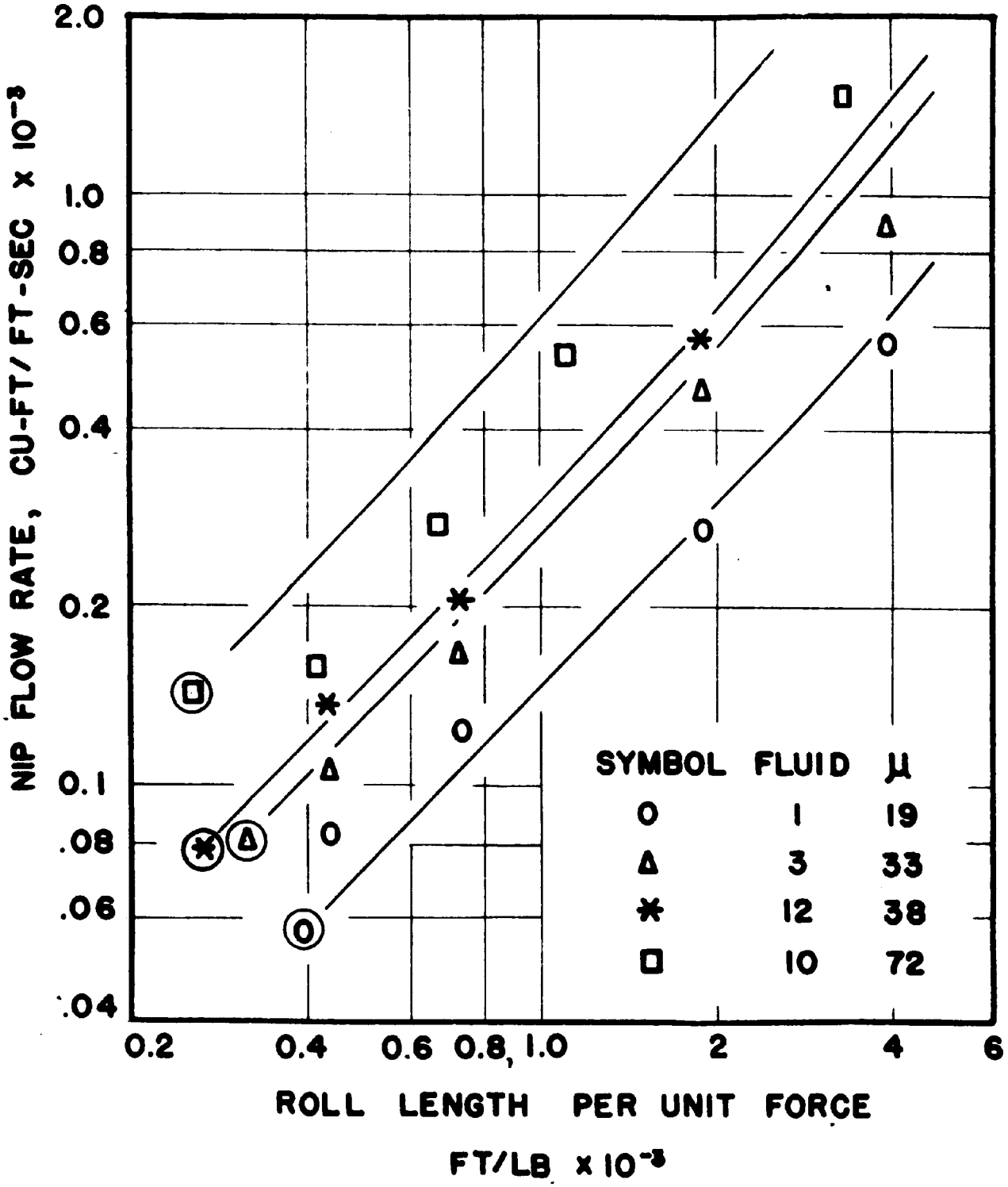

FIGURE 11. NIP FORCE AND FLOW RATE

4-INCH ROLLS, 3-1 SPEED RATIO 245 RPM FAST ROLL

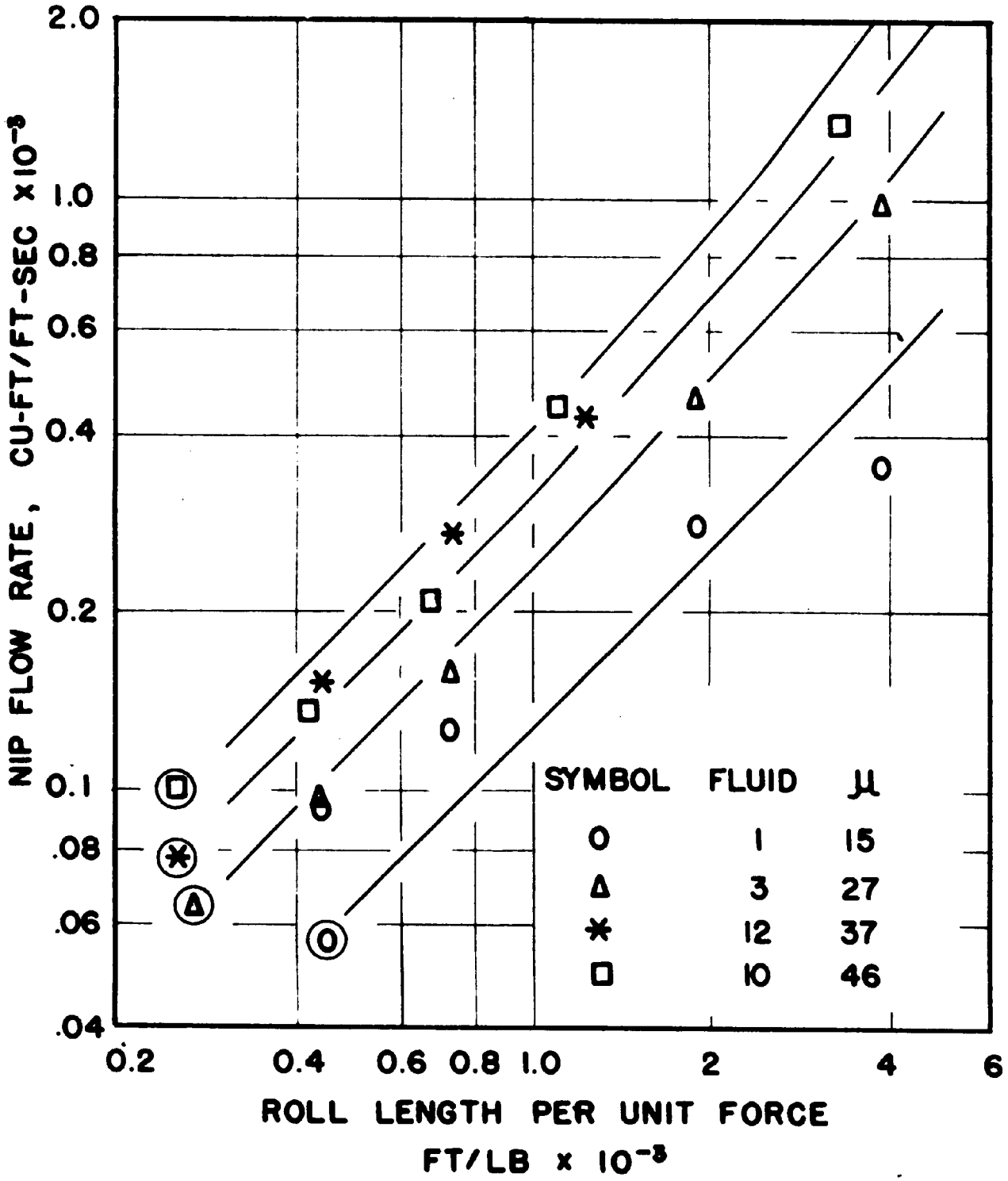

FIGURE 12. NIP FORCE AND FLOW RATE

4-INCH ROLLS, 2-1 SPEED RATIO, 245 RPM FAST ROLL

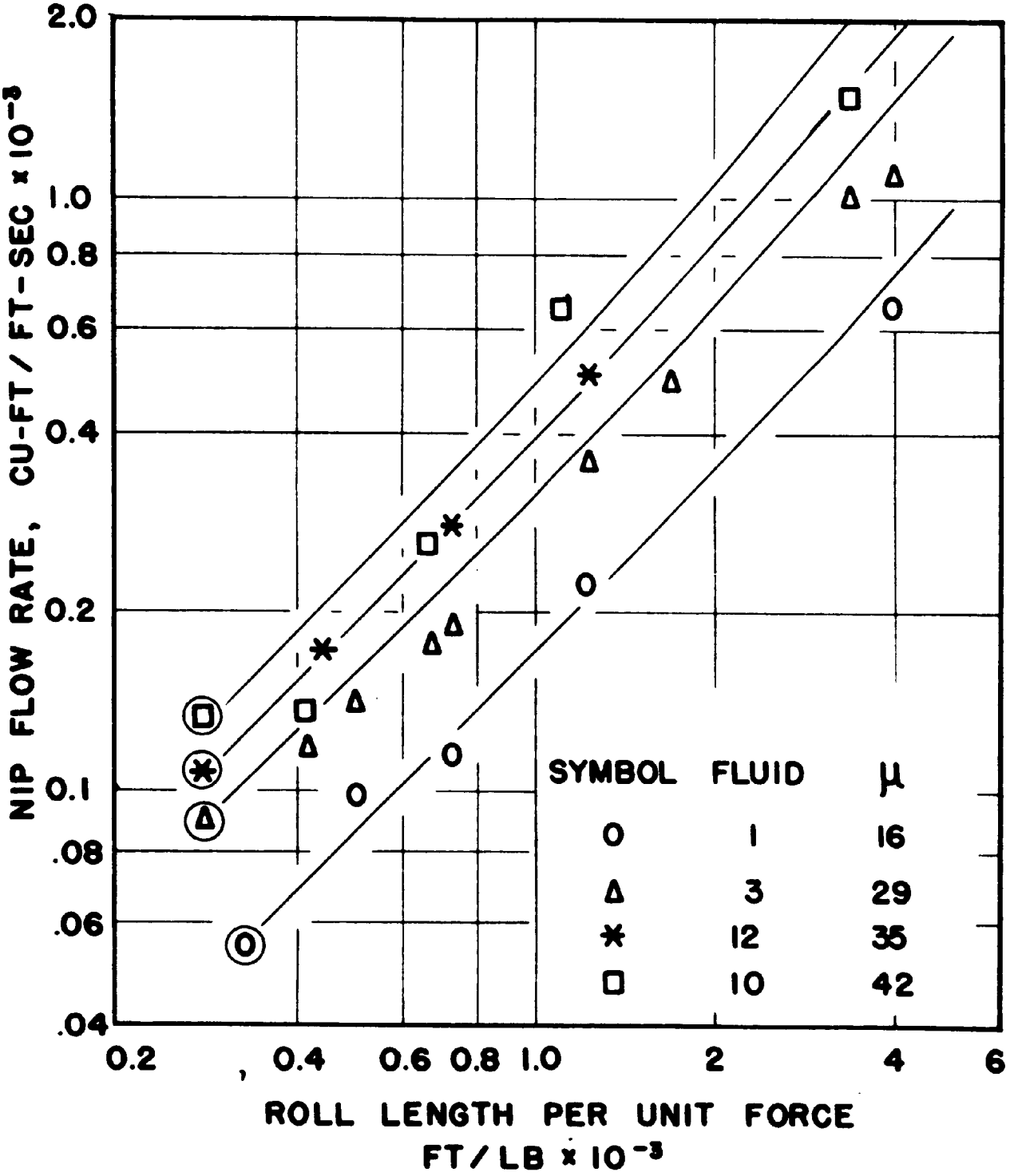

FIGURE 13. NIP FORCE AND FLOW RATE

4- INCH ROLLS, 1-1 SPEED RATIO, 245 RPM EACH ROLL

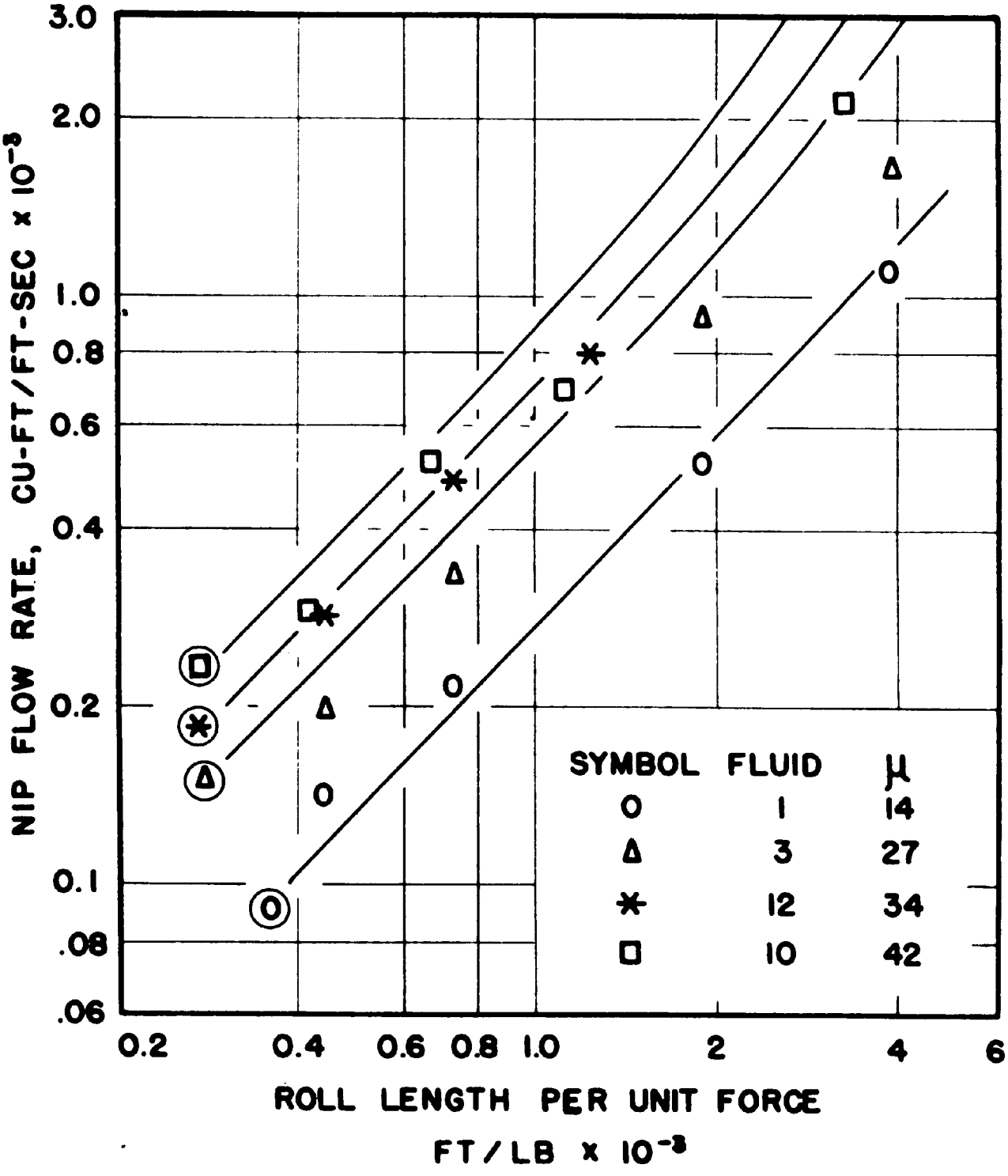

FIGURE 14. NIP FORCE AND FLOW RATE

6-INCH ROLLS, 3-1 SPEED RATIO, 200 RPM FAST ROLL

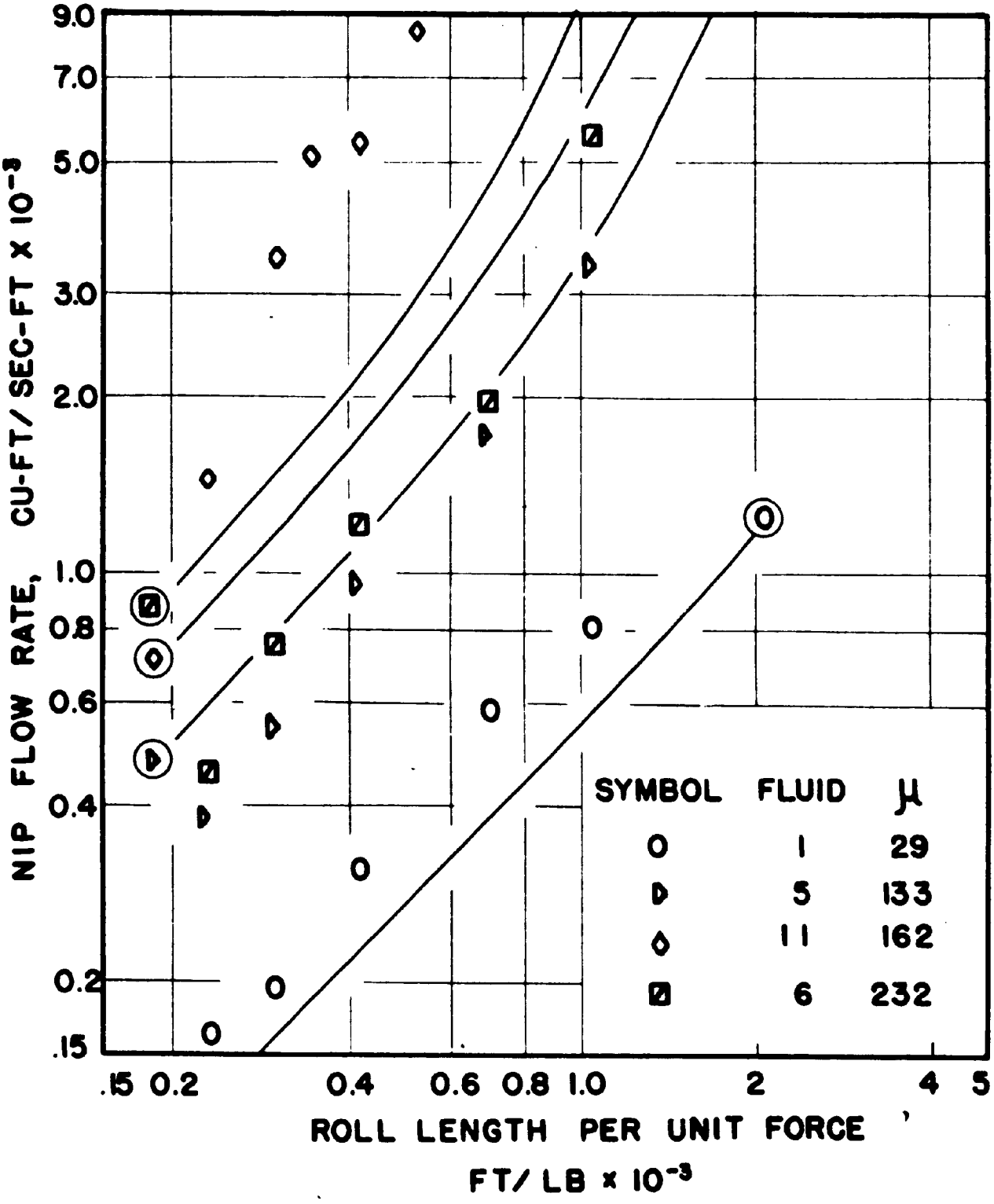

FIGURE 15. NIP FORCE AND FLOW RATE

6-INCH ROLLS, 2-1 SPEED RATIO, 200 RPM FAST ROLL

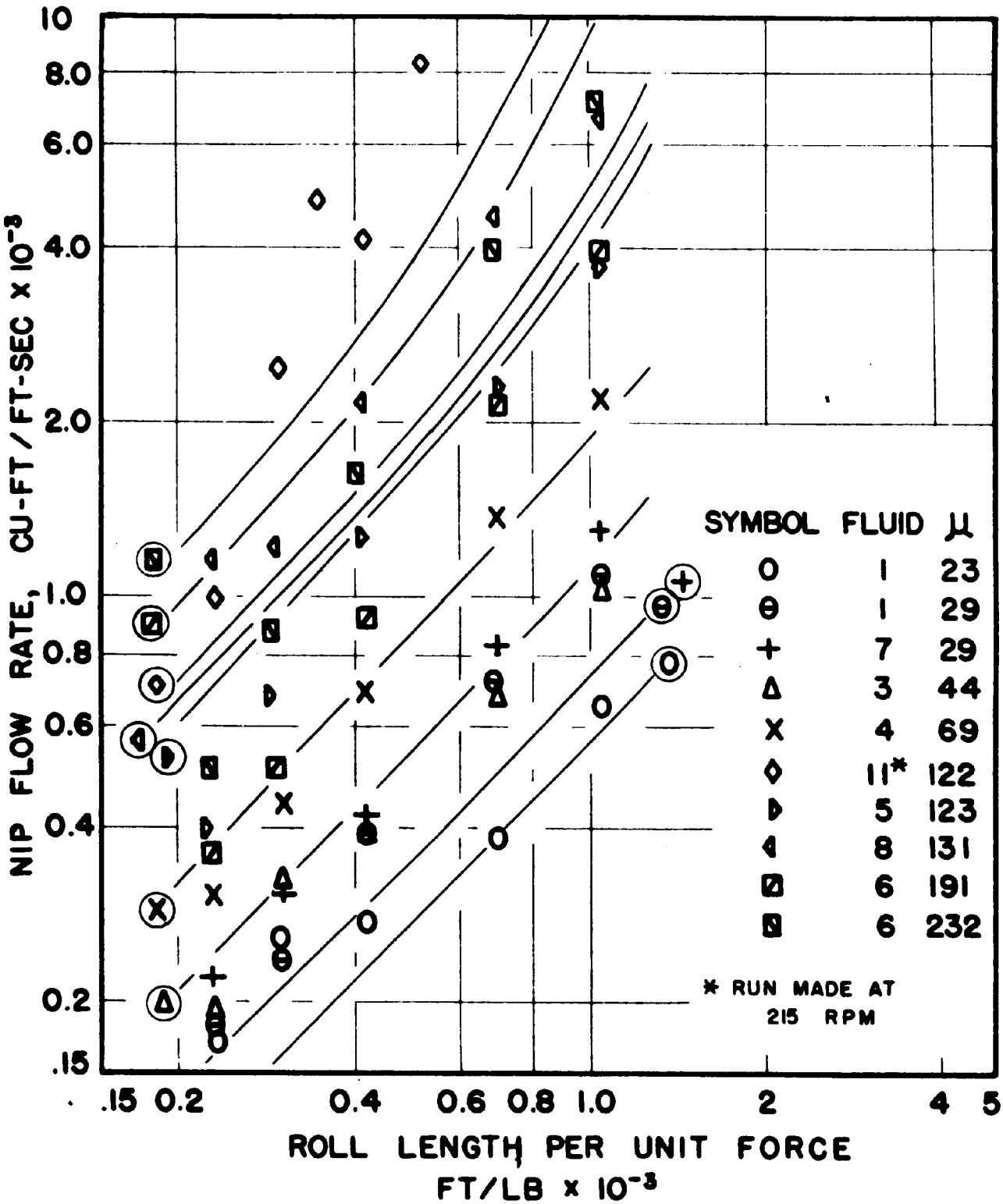

FIGURE 16. NIP FORCE AND FLOW RATE

6-INCH ROLLS, 1-1 SPEED RATIO, 200 RPM EACH ROLL

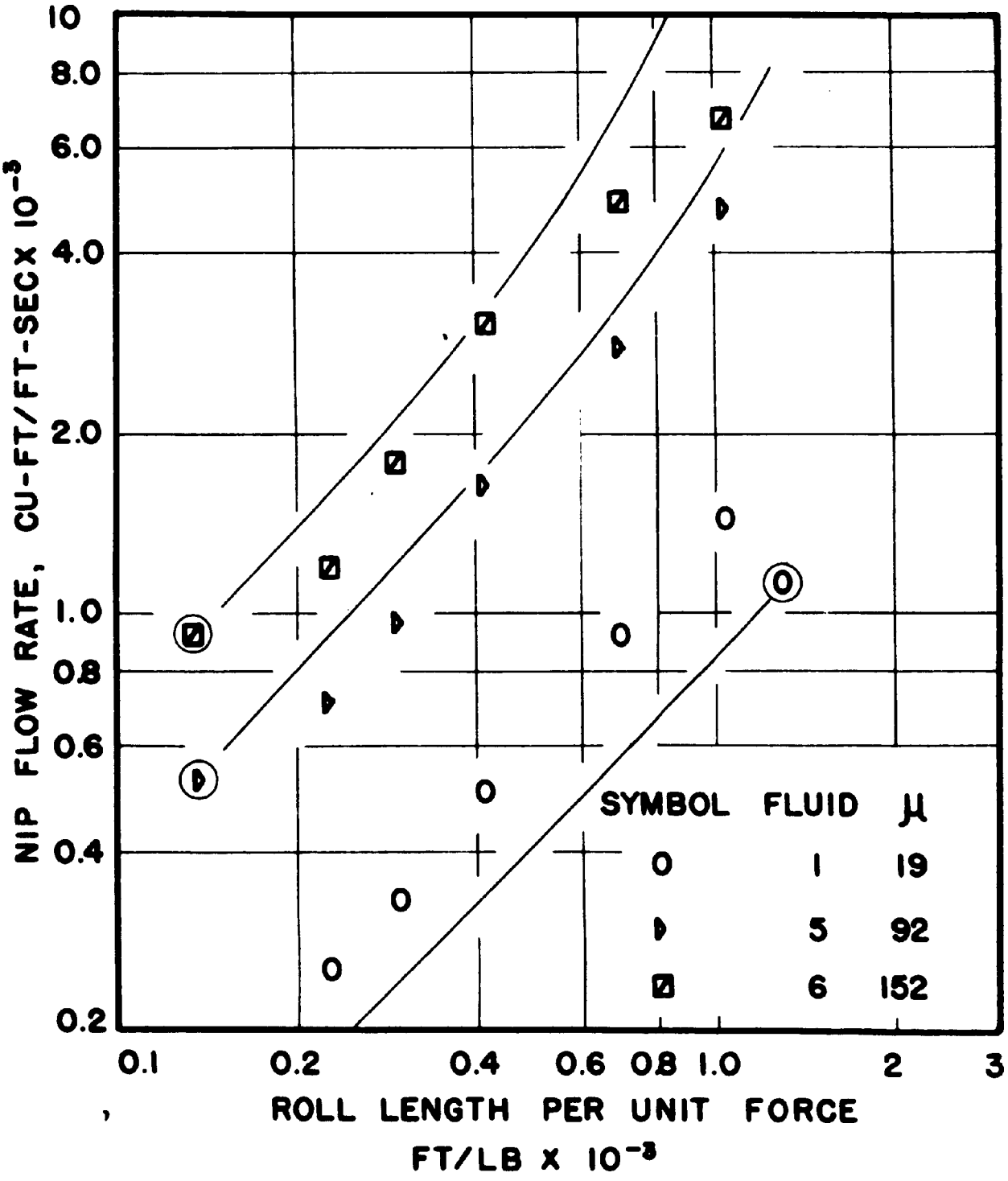

FIGURE 17. NIP FORCE AND FLOW RATE

6-INCH ROLLS, 3-1 SPEED RATIO, 300 RPM FAST ROLL

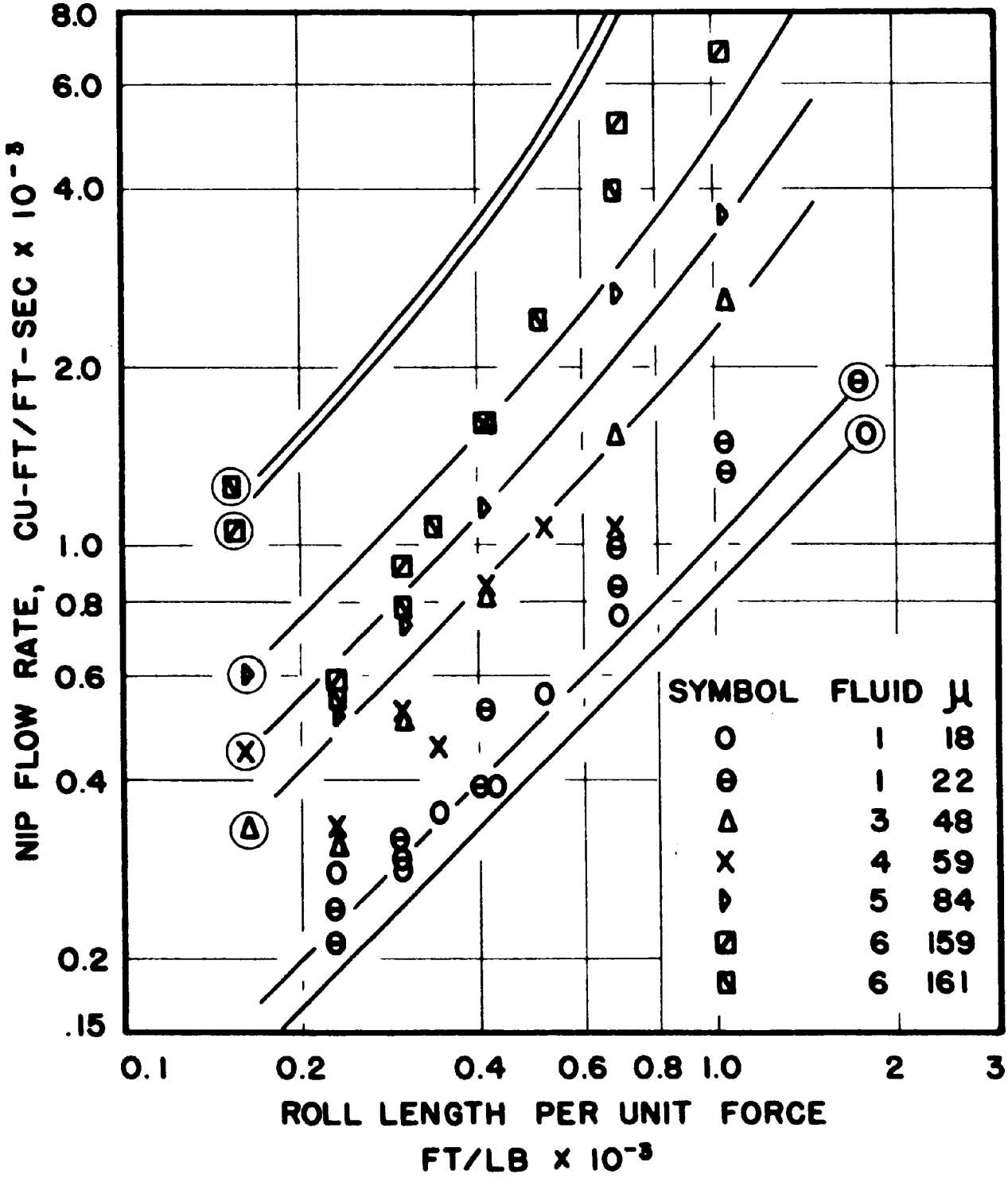

FIGURE 18. NIP FORCE AND FLOW RATE

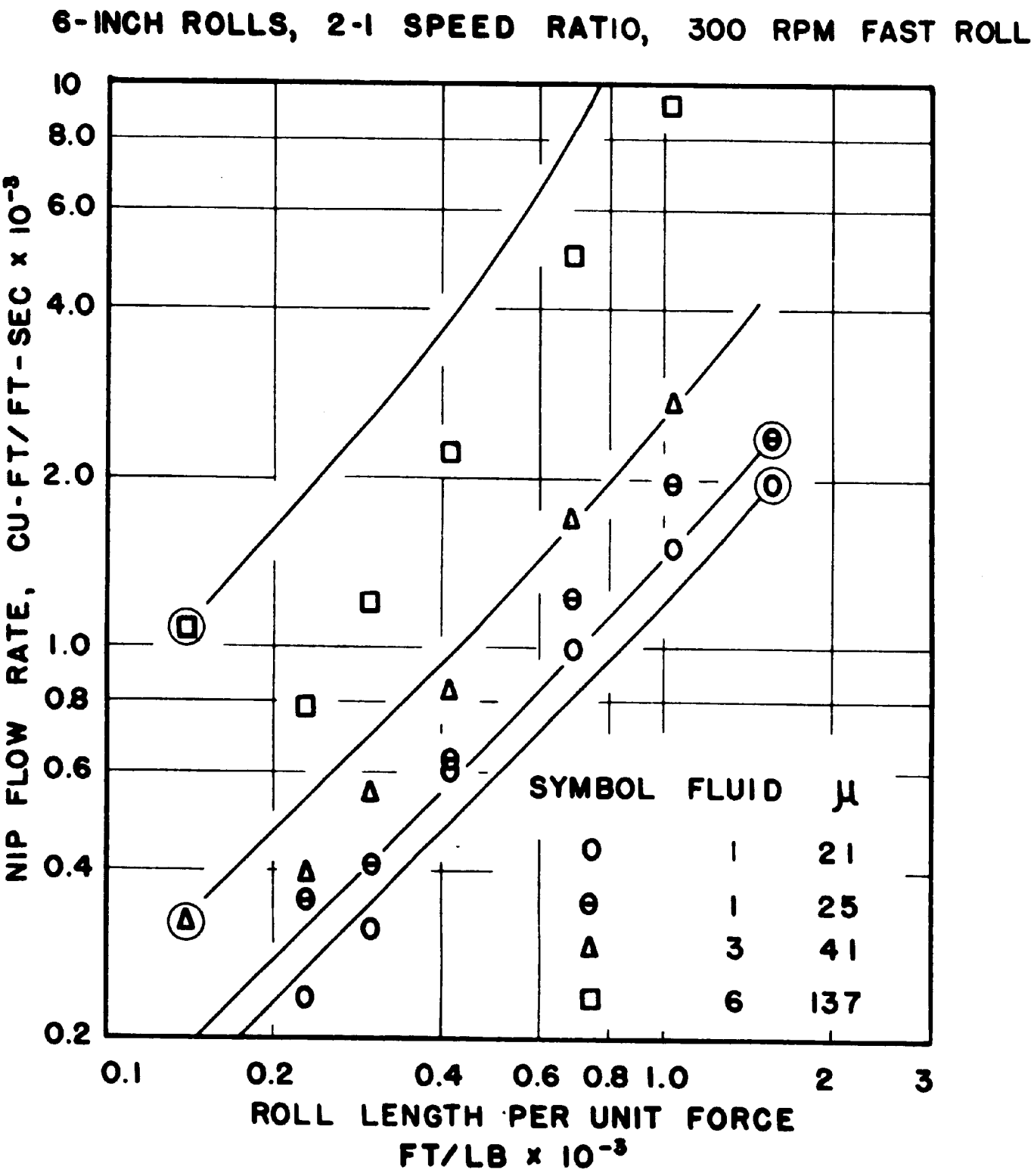

FIGURE 19. NIP FORCE AND FLOW RATE

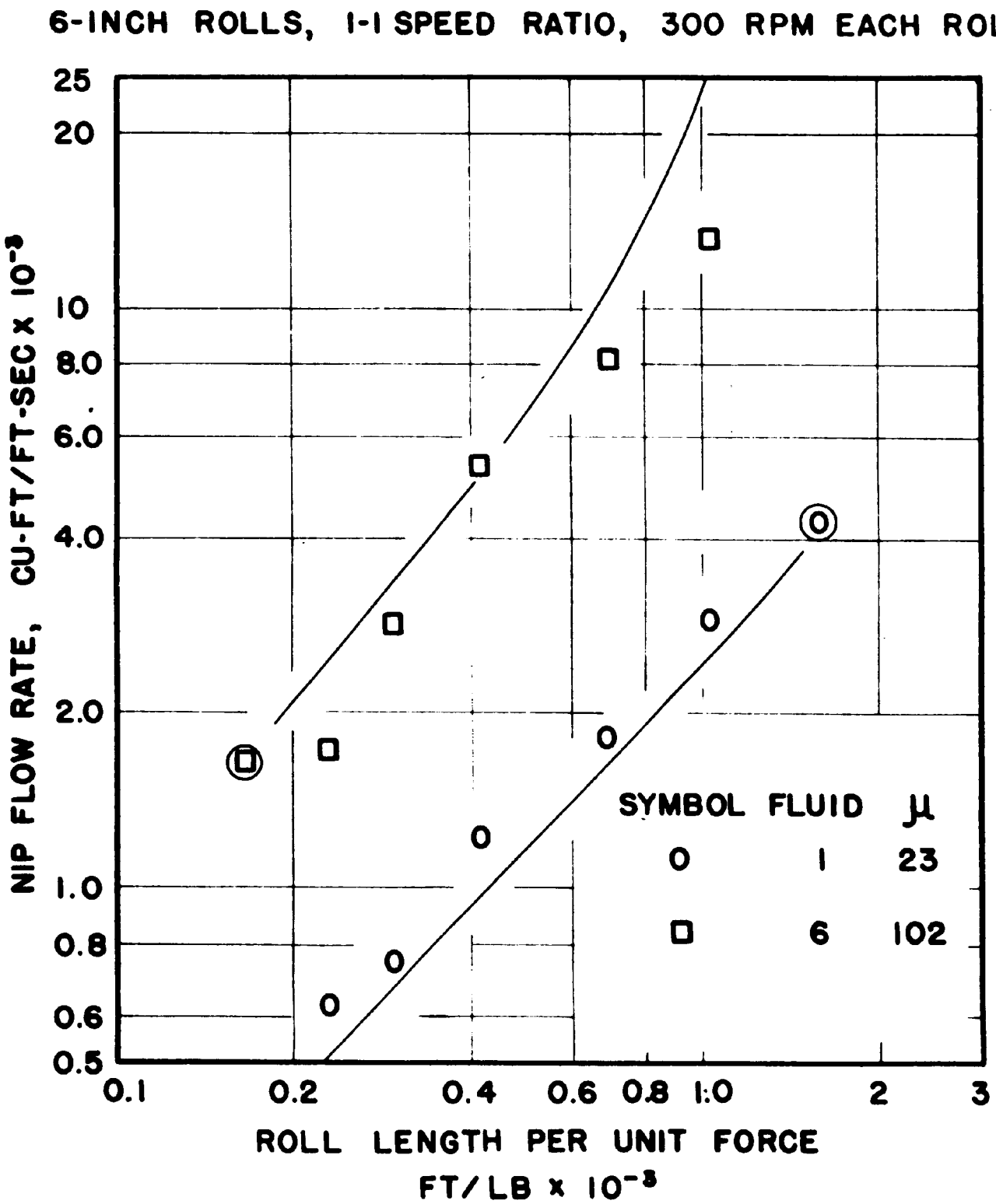

FIGURE 20. COMPARISON OF NIP FLOW RATE THEORY WITH EXPERIMENT

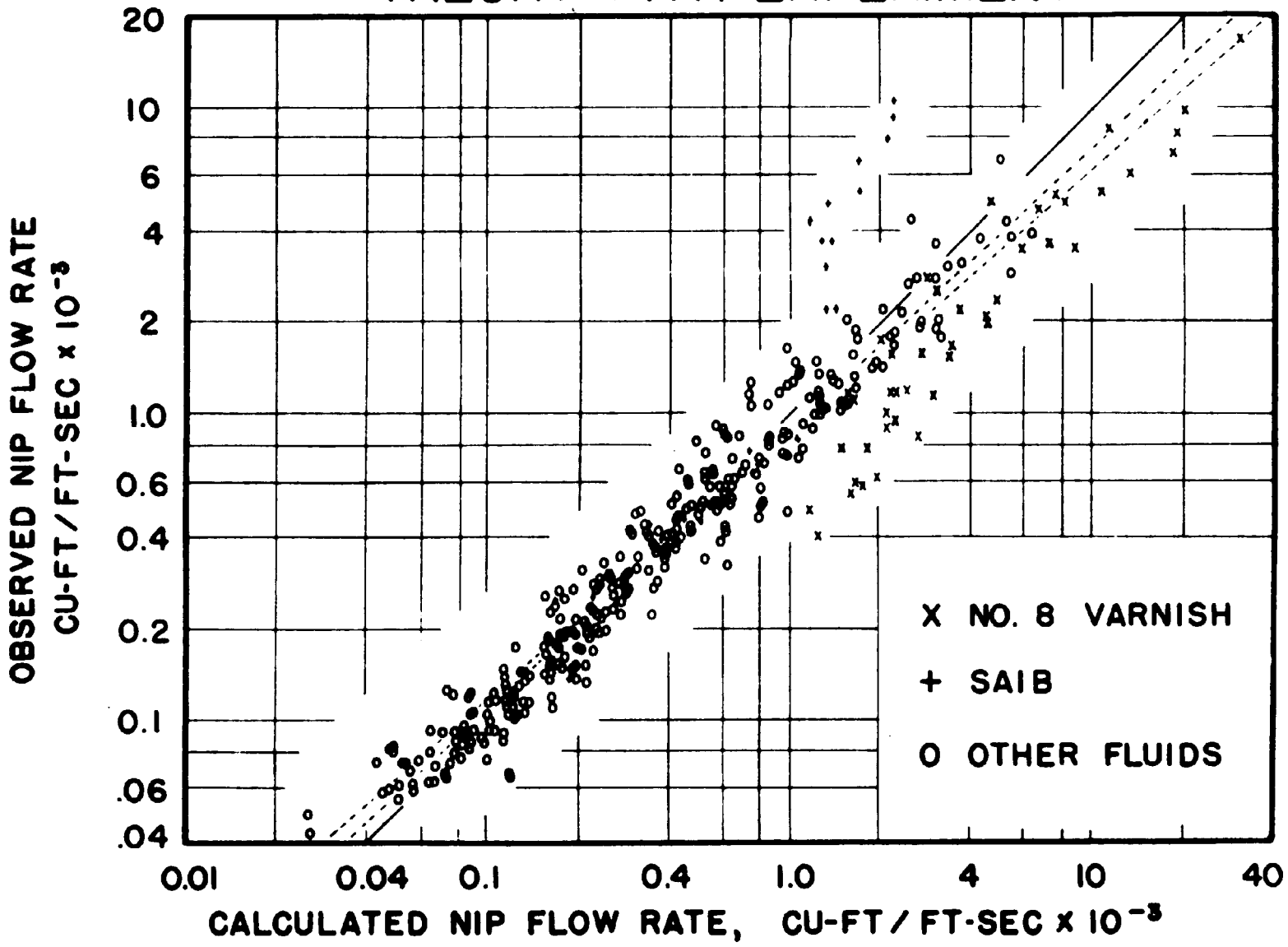

Passage of Glass Beads Through Nip

Data obtained from experiments made with glass beads are listed in Table XXII, Appendix VII, and are plotted in Figs. 21, 22, and 23. The observed maximum bead diameter passed by the nip is compared with the calculated minimum nip clearance in Fig. 21, the observed flow rates with calculated flow rates in Fig. 22; and the observed flow rate is plotted versus maximum bead diameter in Fig. 23. The theoretical flow rate-clearance curves are shown in the latter figure for comparison with the experimental values. Run conditions and data point symbol nomenclature for the three figures are given in Fig. 21.

FIGURE 21. OBSERVED MAXIMUM BEAD SIZE COMPARED WITH CALCULATED MINIMUM NIP CLEARANCE

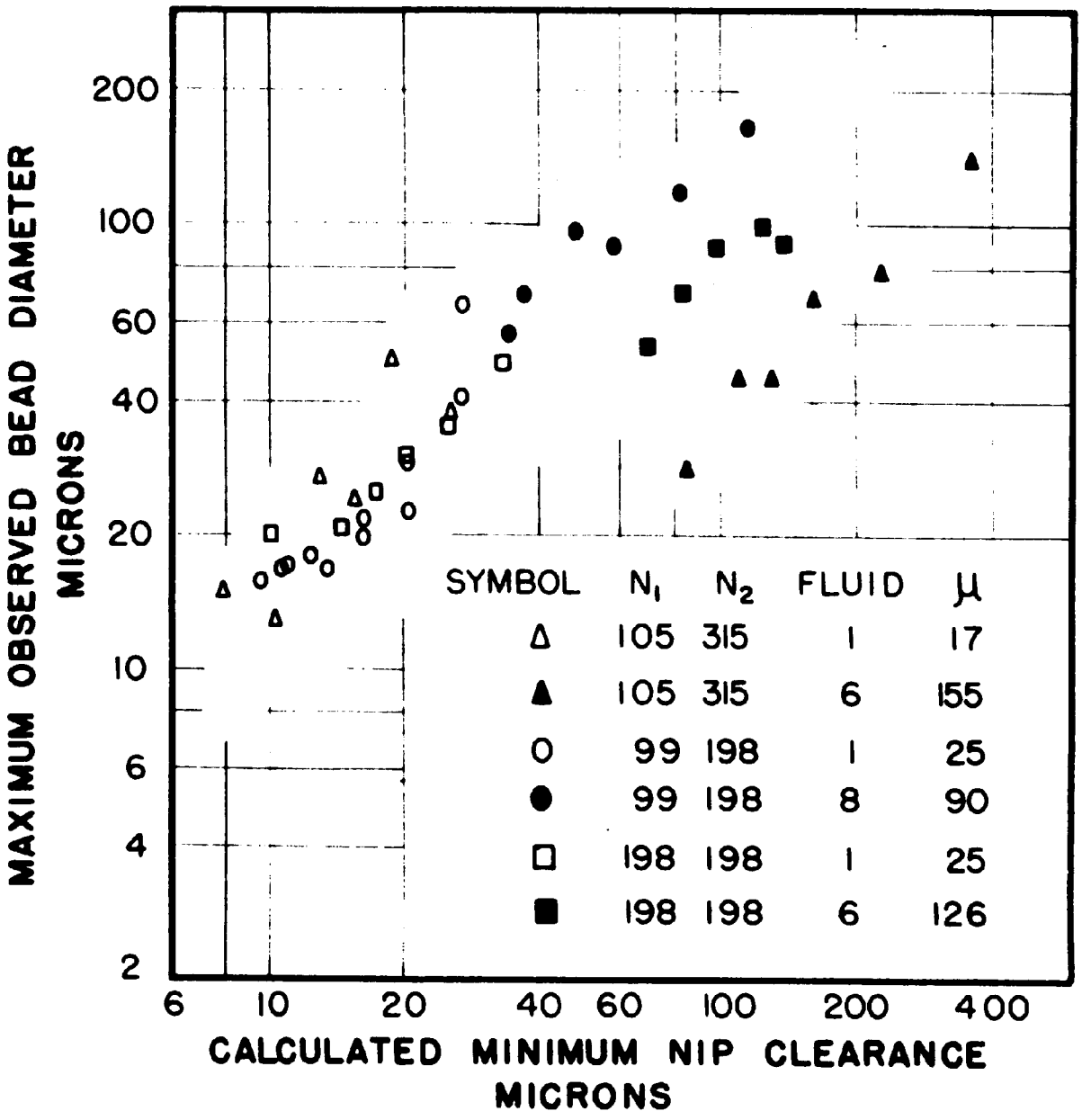

FIGURE 22. MEASURED AND CALCULATED FLOW RATE IN GLASS BEAD SYSTEMS

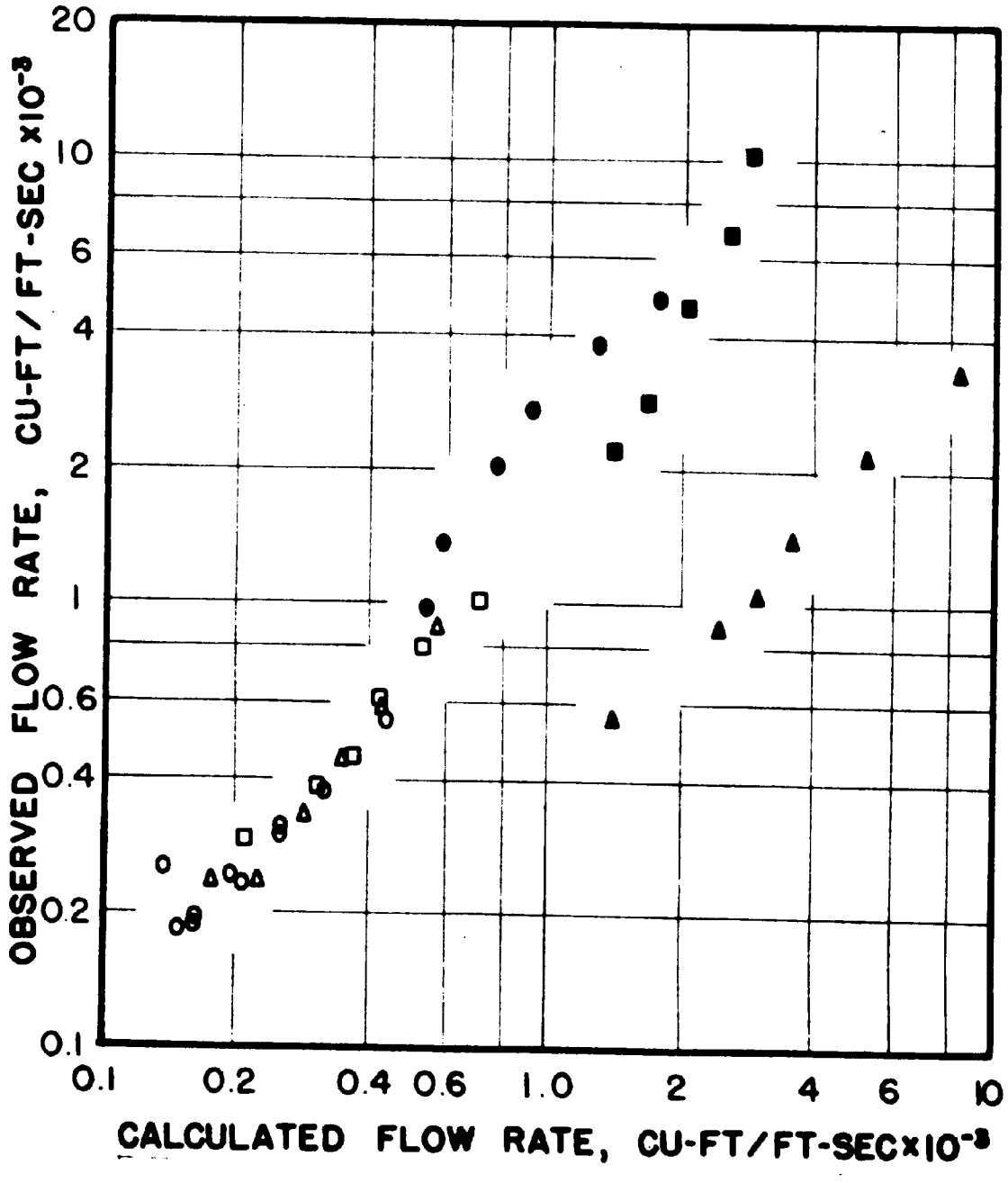

FIGURE 23. GLASS BEAD DIAMETER AND NIP FLOW RATE

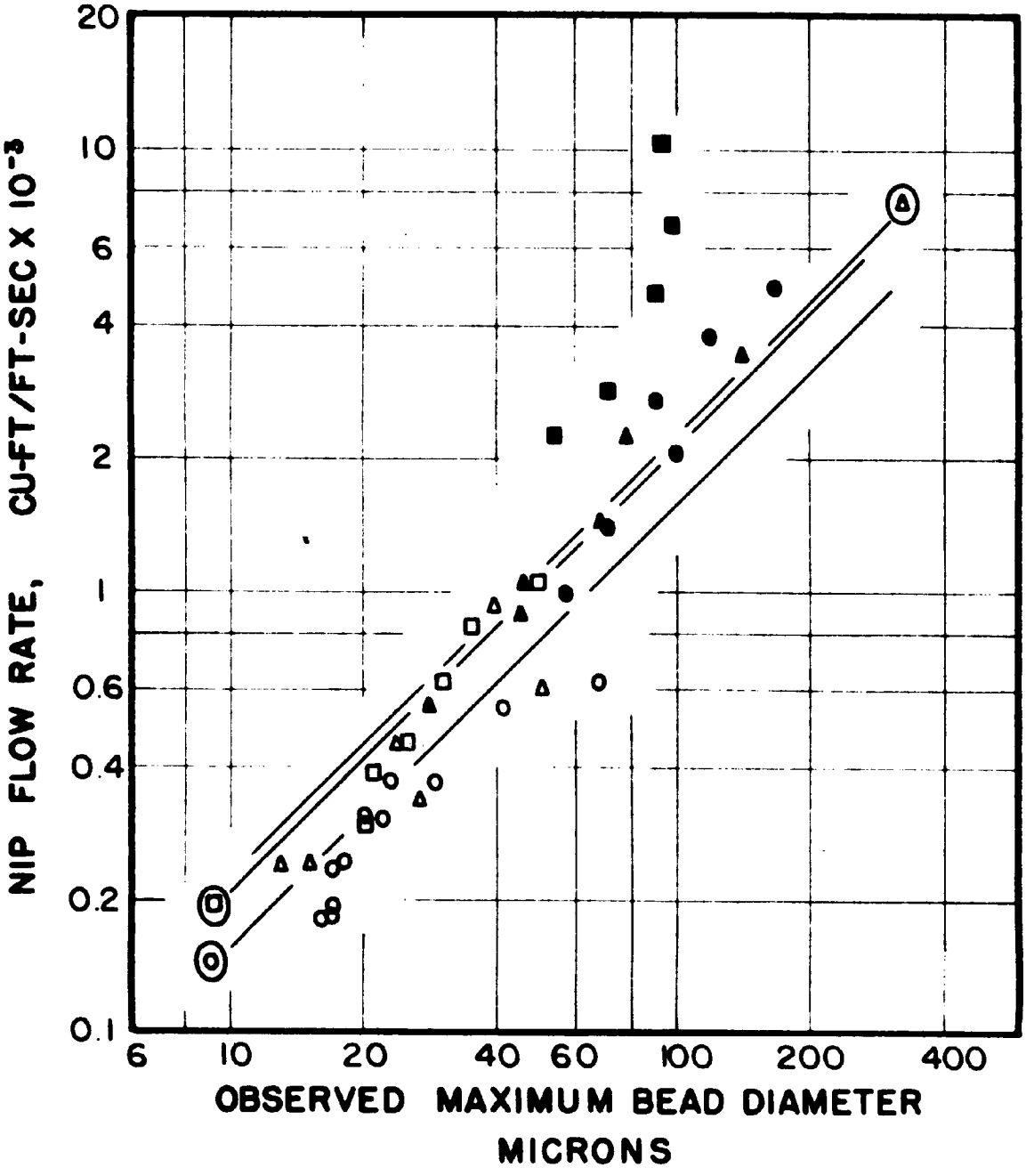

VI. DISCUSSION OF RESULTS

An inspection of Figs. 8 through 19 reveals that the experimental flow rate measurements are in good general agreement with the predictions of the viscous flow nip theory. In some cases almost perfect agreement was observed. In other cases there appeared to be divergence of experiment from theory of a greater magnitude than appeared reasonable on the basis of experimental error. In general, the experiments with low viscosity fluids and 4-inch diameter rolls show better agreement with theoretical predictions than do the high viscosity, 6-inch roll experiments. In most instances, the slope of the curves of log flow rate vs. log reciprocal roll force follow the theoretical predictions even when values differed in absolute magnitude. The mean of the logs of all experimental flow rates corresponded to a flow rate of 4.49×10^{-4} cu-ft/ft-sec. This value was 6.2 percent below the theoretical mean value of 4.78×10^{-4} cu-ft/ft-sec. The only theoretical treatment in the literature that offers a method of estimating the flow rate in such systems is that of Gatcombe (20). By this theory, the flow rate is equal to 4/3 times the product of the average roll velocity and the minimum nip clearance. Gatcombe's theory gives estimated flow rates approximately 8 percent higher than those obtained from the present theory, or an estimated average flow rate of 5.16×10^{-4} cu-ft/ft-sec. It is seen that the theory offered in this dissertation presents a closer estimate of the average flow rate than does the Gatcombe theory, although as is shown later, both may be in substantial error under conditions in which the fluids deviate from the constant viscosity condition.

Presentation of the data as log flow rate vs. log reciprocal force was found bo be more convenient than either direct flow rate vs. force plots or flow rate vs. reciprocal force plots. The former are nearly hyperbolic in shape and do not lend themselves to ready interpolation. While flow rate vs. reciprocal force plots are nearly linear, they crowd the data at high force values and require excessively small scales for presentation of the entire range of data.

Statistical Analysis of Flow Rate Data

The data of Table XXI and Fig. 20 were analyzed statistically to provide a measure of the reliability of the data and the correlation obtained.

Standard Deviation of Experimental Flow Rates. Duplicate measurements were made on most of the experimental runs with the 4-inch diameter rolls. These values provide an extimate of the reproducability of the experimental technique. An inspection of the data indicated that the variance associated with the measurement of flow rate was not independent of the level measured, but increased with increasing flow rate. For this reason a standard deviation calculated directly on the flow rate values would not give a true picture of the reliability of the data. This standard deviation would indicate a higher variance at low flow rates and a lower variance at high flow rates than the data warranted. Since a plot of the data indicated that the percent variation of data was more nearly constant than the absolute magnitude of variation, the standard deviation of the logarithm of the duplicated values was calculated as shown in Table IV, to serve as a measure of the reproducability of the experimental technique.

Table IV

Standard Deviation of Logarithms of

Measured Flow Rate Between 4-Inch Rolls

Source	Sum of Squares	Degrees of Freedom
108 Pairs	0.14838	216
2 Triplications	0.00116	4
1 Quadruplication	0.00750	3
1 Quintiplication	0.01018	4
Total	0.16722	227

Variance = 7.366×10^{-4}

Standard Deviation = 0.0271

The standard deviation obtained here indicates that the 95 % confidence limits of the log of an observed flow rate are ± 0.0531, corresponding to actual flow rate confidence limits of + 13 and - 11.5 %. A portion of the variance in duplicate samples was due to slight temperature differences between duplicates. When only the 74 pairs of measurements made at equal temperatures are considered, the standard deviation of the logarithms is 0.0228, and the 95 % confidence limits of the flow rates are + 10.8 and -9.8 %.

Statistical Measure of Agreement Between Experimental and Theoretical Flow Rates. A statistical study of the comparison between experimental values and calculated values of logarithms of flow rates was conducted to provide answers to the following questions.

1. What are the limits of confidence of a theoretical calculation of log Q?

2. What is the best line relating experimental to calculated flow rates, and what are its confidence limits?

3. Is there any significant difference between the best line through the data and the theoretical line?

4. Do certain experimental conditions give significantly different results than the bulk of the data?

5. Is the slope of the best line through the 4-inch diameter roll data significantly different from that through the 6-inch roll data?

Details of the statistical analysis and results obtained are presented in Appendix V. The principal results are summarized here.

Precision of Theory. On the basis of all the data, the 95 % confidence limits for prediction of a single experimental flow rate from the theory are + 110 % and - 52.4 %. With data for SAIB on 6-inch rolls and No. 8 varnish excluded, the 95 % limits were + 56 % and - 36 %. For the 4-inch roll data alone, the confidence limits were + 45 % and - 31 %.

Effect of Differences in Fluids and Roll Diameters. Separate analysis of the data for No. 1 varnish, No. 8 varnish, intermediate viscosity fluids, and SAIB indicated that only the slope of the

SAIB data deviated to a significant degree from unity. For the other fluids, the slopes of log theoretical vs. log measured flow rate curves did not differ to a significant degree from each other, nor did the pooled slope of the best individual lines deviate to a significant degree from unity. For each of these systems there was a significant difference between the mean of calculated and mean of experimental flow rates.

There was no significant difference between the slopes of the best lines through the 4-inch roll and 6-inch roll data.

Interpretation of Flow Rate Results

The statistical analysis of the flow rate data permits several conclusions to be drawn about the results, but does not explain their origin. Further reasoning into the physical phenomena involved is required for explanation of the deviations and trends observed.

The high level of correlation coefficient, r_T, obtained (Table XV), from the purely theoretical line offers evidence for the general validity of the nip flow theory. On the other hand, the rather wide confidence limits required to include 95 % of the experimental flow rates indicates the operation of variables which contribute considerable uncertainty to an individual calculated value. Furthermore, the fact that the best single line relating the experimental to calculated values deviates to a significant though small degree from the theoretical slope of unity, indicates the operation of a modifying factor which is a function of the level of flow rate tested. Since the slopes of the best lines through the No. 1 varnish, the No. 8 varnish, and the intermediate

viscosity material data, considered as separate sets, do not show a sig- deviation from unity, the cause of the deviation of the slope of the entire body of data does not appear to reside in the roll speed, roll speed ratio, or pressure variable. The similarity of slopes of the 4 - inch roll data and the comparable 6-inch roll data indicates that roll size is not the contributing factor either. The source of this variation becomes apparent from a plot of the means of the data sets for No. 1 varnish, No. 8 varnish, intermediate viscosity fluids, and SAIB on 6-inch rolls shown in Fig. 24. The lines through the individual data sets fall parallel with, but displaced from, the theoretical line. The SAIB appeared to be a special case which will be considered later. The experimental conditions employed resulted in vertical displacement of the mean experimental flow rates for the different sets. The effect of the lateral displacement of the lines coupled with the vertical displacement of the experimental means produced a slope (0.595) different from either unity or zero for the line through the means of the data sets. Had it been possible to choose experimental conditions such that the mean experimental flow rates for each set of fluids were equal, the lateral displacement of the individual data sets would have affected only the scatter of the data but not the slope of the best line through all of the data. The deviation of the slope of the line from unity is there- fore, in a sense, an artifact of the range of experimental conditions chosen. In practice, the range of flow rates obtainable is not entirely under control of the experimenter, since practical considerations in the operation of the equipment permit the highest flow rates to be obtained only with the higher viscosity fluids.

Figure 24. Regression Lines for Individual Data Sets

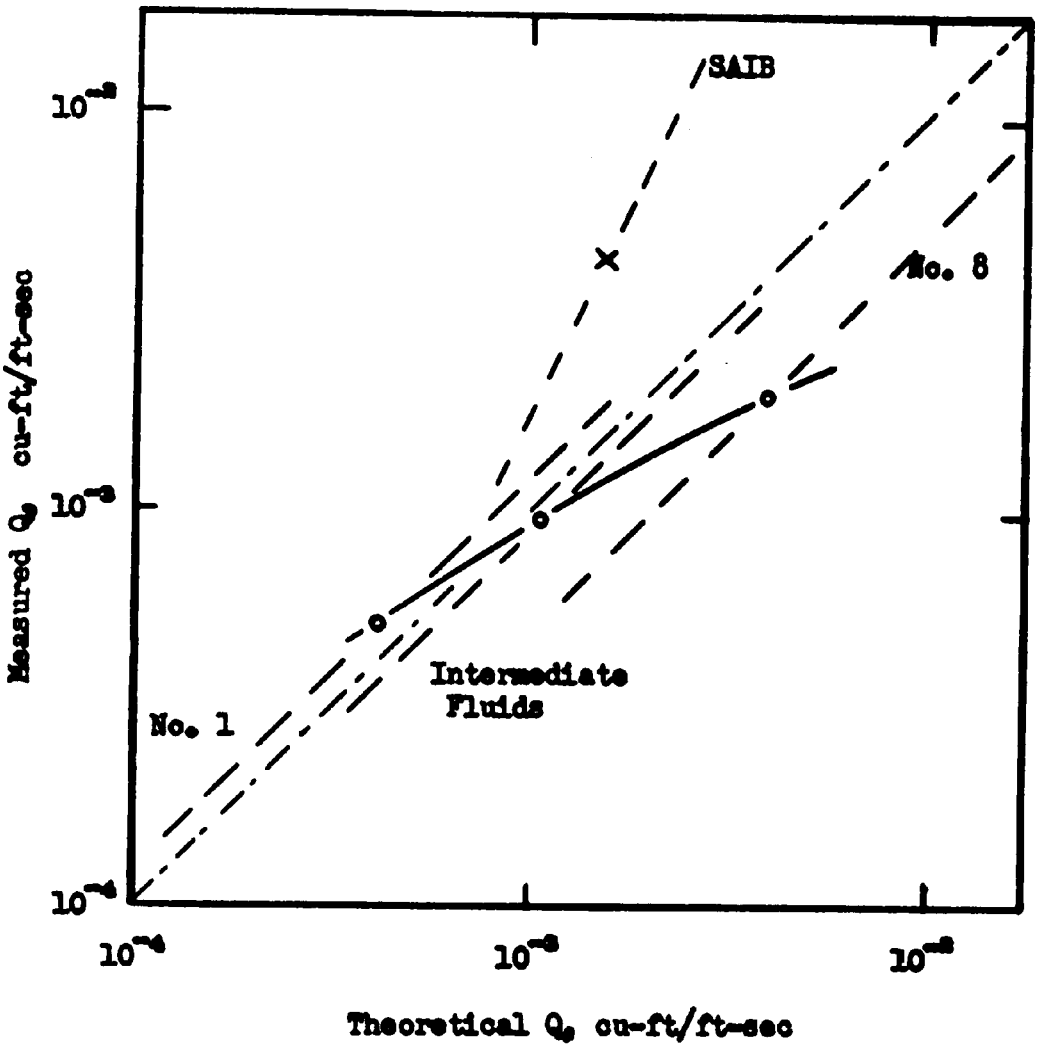

It is concluded that the mean flow rates of the viscous, polymeric fluids tested can be related to the flow rates calculated from the nip flow theory by use of constant multiplying factors. The set of SAIB experiments on 6-inch rolls constitutes the only case in which the deviation from theory varied with changing flow rate. The average correction constants for the polymeric vehicles (all fluids tested except SAIB) on the 6-inch rolls are given in Table V.

Table V

Correction Factors Relating Experimental to Theoretical Flow Rate of Polymeric Vehicles on 6-Inch Rolls

System	$\frac{\text{Experimental } Q}{\text{Theoretical } Q}$	Average Viscosity Poise
No. 1 Varnish	1.234	22.8
Intermediate Fluids	0.894	77.4
No. 8 Varnish	0.499	165.4

The correction factors given in Table V are plotted against the average viscosity of the data sets in Fig. 25, where it is seen that the factors decrease in a regular fashion with increasing fluid viscosity. This consistent deviation is attributed to a factor, or factors, which caused the effective viscosities of the fluids in the nip to differ from the values used in calculating the theoretical flow rates. The higher the viscosity range, the greater was the difference between effective nip

Figure 25. Variation in Ratio of Experimental to Theoretical Flow Rate Means for 6-Inch Roll Data

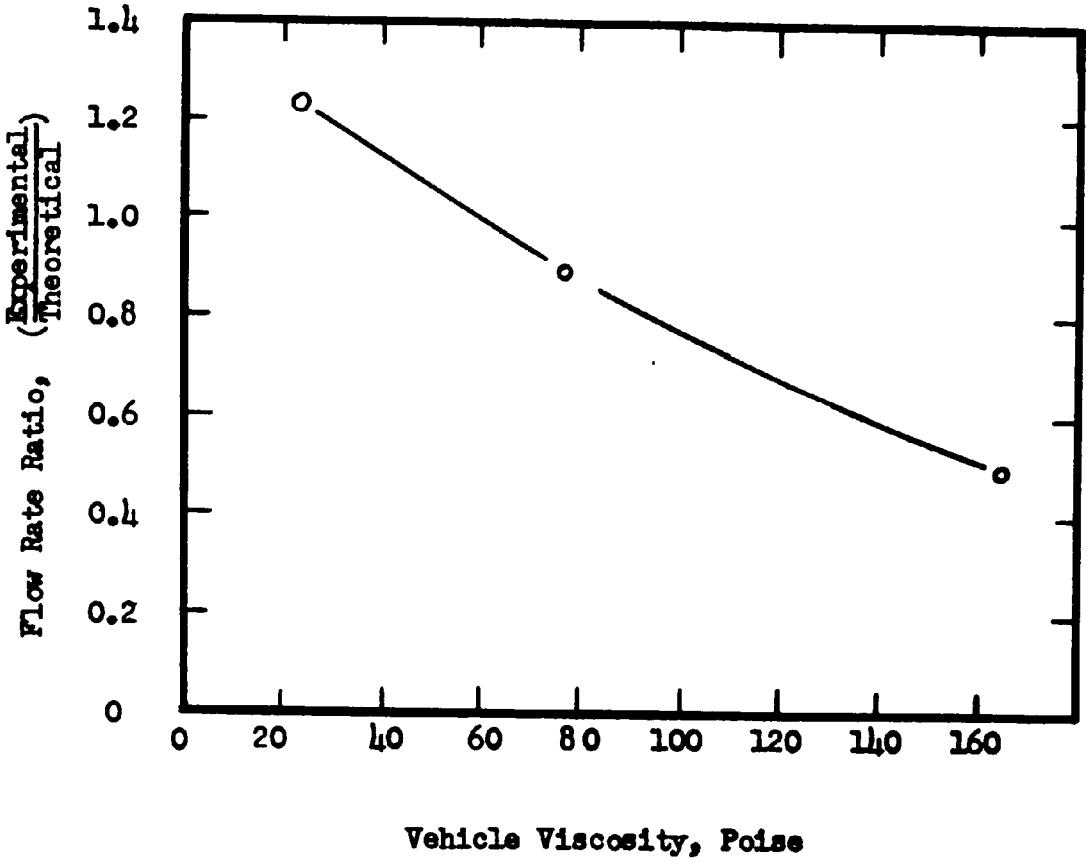

viscosity and viscosity calculated from the measured roll surface temperature.

There are at least four factors which may have contributed to a deviation of the effective nip viscosity from expected viscosity. These are:

1. Experimental method of measuring fluid temperature on roll surface may not give accurate reflection of nip temperature.

2. The viscosity of the fluid may decrease during nip passage due to internal heat generation.

3. The viscosity of the fluid may increase during nip passage due to pressure rise in the nip.

4. The viscosity of the fluid may change under shear in the nip due to non-Newtonian rheological properties.

Without a complete solution to the nip flow equations which considers the case of variable viscosity due to the factors listed above, it is not presently possible to determine which factor controls deviation from the constant viscosity case in a given instance. In the following discussion, order of magnitude approximations are made to illustrate the potential effect of each of these sources of viscosity variation.

Temperature Measurement and Fluid Viscosity in the Nip. The estimation of fluid viscosity in the nip from the film temperature measured by a thermocouple held to the surface of the moving roll was probably the greatest single source of experimental error in the entire program. It was realized from the outset that this measurement could only reflect an approximate value of the effective nip temperature. The problem of measuring the temperature within the nip zone itself is compounded by

the narrow clearances involved, the high stresses encountered, and by the movement of the rolls. These factors prevent the insertion of a temperature sensing element directly into the maximum shear zone. Near the completion of the experimental program, a thermocouple was installed in the bank region just above the nip in such a manner that it encountered the stream of fluid being rejected from the nip. In general the temperatures measured by this thermocouple were comparable to the surface measured temperatures. The bank temperatures were subject to greater fluctuations, probably because of the effect of slight shifts in thermocouple location on the particular stream line encountered. A comparison of average run temperatures measured by the bank and surface thermocouples is given in Table VI. In the case of the No. 1 varnish experiments the bank and surface temperatures are in close agreement. Greater differences were observed in the individual runs with No. 8 varnish, but the average difference for the six conditions investigated was only 2.8 °F. Close agreement between surface and bank temperatures was observed for the SAIB on the 6-inch rolls, but in two runs on 4-inch rolls, an average difference of surface over bank temperature of 15 °F was observed. The close agreement between theoretical and experimental flow rates obtained for SAIB on the 4-inch roll (Figs. 8 and 9) indicates that the surface temperature, which was used for viscosity determination, gave a more nearly correct viscosity than did the bank temperature.

Table VI

Comparison of Fluid Temperatures Measured on Roll Surface and in Bank

Average Run Temperature*, °F		Fluid	Roll RPM		Roll Diameter, In.
Surface	Bank		N_1	N_2	
78.7	79.7	No. 1 Varnish	99	198	6
86	86.2	"	103	310	6
87	86.2	"	105	315	6
89	88.3	"	105	315	6
80	78.5	"	198	198	6
98.8	93.7	No. 8 Varnish	99	198	6
104.7	111.8	"	103	310	6
107	111.8	"	105	315	6
89.3	104.7	"	105	315	6
107.5	117.2	"	105	315	6
114.4	99	"	198	198	6
88.8	90.2	No. 4 Varnish	103	310	6
125.5	123.2	SAIB	72	215	6
128.7	128.8	"	107	215	6
118.3	105.8	"	35	104	4
123	105.3	"	75	155	4

* Each point is average of runs at six values of roll force.

The actual temperature distribution in the nip is unknown, although several statements can be made regarding its limits and its general character. A complete solution of the problem would involve a solution of the differential equations for flow and temperature, with variable viscosity, which was considered to be beyond the scope of the present investigation. Solutions have been obtained for special cases of equilibrium flow in a rotational viscometer by Kuhns and Weltman(41), flow of a viscous polymer through a cylindrical tube by Gee and Lyon[42], and flow of Newtonian viscous fluids between equal speed calendering rolls by Finston[23]. The latter is the most pertinent to the system under consideration here. The general form of the temperature distribution can be understood by consideration of the competition between heat generation due to shear in the fluid and cooling by heat transfer to the walls. Because fresh cool fluid constantly enters the shear zone, the average temperature rises from the nip inlet to the outlet. The result is a three dimensional temperature distribution with minimum values occurring at the cooled roll surfaces. Because maximum shear rates occur at the surfaces, ridges of higher temperature are located near the surfaces. If the rolls are operating at differential speeds the temperature ridge near the slower roll will be greater than that near the fast roll. The level of the valley halfway between the centers increases in the direction of flow. The problem is complicated by the fact that viscosity, temperature, pressure, shear rate and flow rate are all interrelated. The limiting temperature rise from nip inlet to outlet can be estimated from an energy balance on the fluid with the assumption of adiabatic roll surfaces. This is given by,

$$\Delta t = \frac{q}{Q \rho C_p} \quad , \tag{53}$$

where q, the rate of nip energy input is calculated from equation 41, Q is the theoretical nip flow rate, and ρ and C_p are fluid density and heat capacity respectively.

To illustrate the magnitude of this theoretical maximum of the average temperature rise, the calculation was performed for the following case, corresponding to experimental run 64 with No 8 varnish.

μ = 161.3 poise = 0.337 lb-sec/ft^2 .

N_1 = 102 rpm, surface velocity = 2.67 ft/sec .

N_2 = 305 rpm, surface velocity = 7.98 ft/sec .

ρ = 60.4 lb/cu-ft .

h_o = 100 microns = 3.28 x 10^{-4} ft .

R = 3 inches .

Theoretical results obtained for these conditions are as follows:

Point of film split, x^* = 4.336x10^{-3} ft = 0.052-inch ,

Total Roll force F/L = 3745 lb/ft ,

Flow Rate Q = 2.148 x 10^{-3} cu-ft/ft-sec ,

Energy Input q = 3.212 Btu/sec-ft .

If a value of 0.4 Btu/lb-°F is assumed for the heat capacity of the fluid, the average temperature rise under adiabatic conditions would be,

$$\Delta t = \frac{3.212}{2.149 \times 10^{-3} \times 60.4 \times 0.4} = 62°F \quad .$$

This value represents an absolute limit on the bulk average nip temperature rise for these conditions and would not be attained in practice because of heat transfer to the walls.

Another estimate of the limiting value of temperature rise in the nip which takes cooling into account can be obtained by calculating the equilibrium maximum temperature rise in a fluid sheared between two parallel, isothermal plates of infinite extent. For this calculation, the clearance between the plates is assumed to be the minimum nip clearance, and the shear rate between plates is equal to the average effective shear rate at the point of minimum nip clearance. This average effective shear rate is defined as

$$\frac{du}{dy}\ \text{effective} = \left[\frac{1}{h_o}\int_{-h_o/2}^{h_o/2}\left(du/dy\right)^2\,dy\right]^{\frac{1}{2}} \tag{54}$$

and at the point of minimum clearance,

$$\frac{du}{dy}\ \text{effective} = \left[\frac{3U_T^2}{h^2}\left(\frac{h_o^*}{h_o}-1\right)^2+\left(\frac{U_2-U_1}{h_o}\right)^2\right]^{\frac{1}{2}} \tag{55}$$

The equation which gives the maximum temperature in a viscous fluid in simple laminar shear between parallel isothermal plates is

$$t_{max} = t_o + \frac{\mu}{k}\left(\frac{du}{dy}\right)^2\left(\frac{h_o}{8}\right)^2 \tag{56}$$

where:

t_{max}, °F, occurs halfway between surfaces,

t_o is surface temperature

μ is viscosity, lb-sec/ft^2

k is fluid thermal conductivity,

(ft-lb)/ ft^2 - sec - (°F/ft)

For the conditions of the previous example, the effective average shear rate at the nip center is 2.06×10^4 sec^{-1}. For comparison,

the nominal shear rate, roll surface speed difference divided by minimum nip clearance, is 1.62×10^4 sec^{-1}, and the maximum local shear rate is 3.85×10^4 sec^{-1}. Values of the thermal conductivity of the fluids used in this study are not accurately known but for purpose of illustration are assumed to be approximately 0.08 (Btu)/(hr - ft^2 - °F/ft) or 1.73×10^{-2} (ft-lb)/(ft^2 - sec - °F/ft) in common with many other oils[43]. The estimated maximum equilibrium temperature rise for these conditions is,

$$t_{max} - t_o = \frac{0.337}{1.73 \times 10^{-2}} \times (2.06 \times 10^4)^2 \left(\frac{3.28 \times 10^{-4}}{8}\right)^2$$

$t_{max} - t_o$ = 110°F. The bulk average temperature for this parabolic temperature distribution is given by

$$(t_{bulk\ av} - t_o) = 2/3\ (t_{max} - t_o) = 73°F.$$

This represents a limiting maximum temperature for an infinitely long nip with shear rate corresponding to the maximum average value obtained in the example roll nip. For this reason the actual temperature rise in the roll nip will be much lower. From the previous calculation it is seen that the energy balance imposes a lower limit on possible temperature rise than does the equilibrium approach.

Since the surface thermocouple held to the film on the moving roll also forms a nip, the fluid passing under it is heated by shear in a manner similar to that encountered in the roll nip. Because the pressure between thermocouple and roll is low (estimated at approximately 50 lb/ft) there will be little shear due to pressure flow, but even the simple shear due to roll motion past the stationary thermocouple strip is appreciable. Since the thermocouple is uncooled and is essentially insulated by air behind it, it approximates an adiabatic boundary. The maximum equilibrium temperature rise in a fluid

sheared between one isothermal and one adiabatic surface is given by,

$$t_{max} - t_o = \frac{\mu}{k}\left(\frac{du}{dy}\right)^2 \frac{(h_f)^2}{2} \quad , \tag{57}$$

where h_f is film thickness.

This equation predicts a temperature maximum, located at the adiabatic surface, equal to four times the maximum obtained in the case of two isothermal surfaces. The simple laminar shear rate for this case is equal to $\frac{U}{h_f}$, where U is the roll surface velocity. Substitution of this value for $\frac{du}{dy}$ into equation 57 shows that the equilibrium temperature rise is actually independent of the film thickness but depends only on the fluid properties and the surface velocity.

$$t_{max} - t_o = \frac{\mu}{k} \frac{U^2}{2} \tag{57-a}$$

This condition is also true for two isothermal surfaces.

For the conditions used in the previous examples the equilibrium temperature rise at the adiabatic surface would be:

$$t_{max} - t_o = \frac{0.337}{1.73 \times 10^{-2}} \times \frac{(2.67)^2}{2} = 69.5 \text{ °F} \quad ,$$

and

$$t_{max} - t_o = \frac{0.337}{1.73 \times 10^{-2}} \times \frac{(7.98)^2}{2} = 620 \text{ °F}$$

for the slow roll and the fast roll respectively. Again, such temperature rises would never be expected in practice because of the short contact zone between roll and thermocouple. They do illustrate the possibility of the thermocouple temperature being nearly equal to or even greater than the effective nip temperature.

The temperature sensitivity of all the fluids used in this study was large. If the viscosity-temperature relationship of a fluid can

be expressed by, $\mu = (10^{-b})(10^{M/T})$, as it was to a reasonable degree for the fluids used, the rate of viscosity change with temperature is given by;

$$\frac{d\mu}{dT} = -2.303\,\mu\,\frac{M}{T^2} \quad , \tag{58}$$

and the temperature decrease, $T_2 - T_1$, necessary for a doubling of viscosity is,

$$T_2 - T_1 = \left(\frac{\log 2}{M}\right) T_1 T_2 \, . \tag{59}$$

Absolute temperatures are used in these equations.

In the temperature range near 100 °F, most of the fluids in the present study were halved or doubled in viscosity by approximately 20 °F change in temperature. The SAIB requires only about 7.5 °F temperature change to double or halve the viscosity.

The calculations shown here indicate that temperature changes due to shear in the nip and at the thermocouple surface could easily account for the observed deviations of experimental flow rates from the theoretical predictions. Higher than predicted flow rates could arise when shear at the thermocouple gave measured temperatures higher than nip temperature, and lower than predicted flow rates could be due to higher temperature in the nip than at the thermocouple.

Viscosity Change with Pressure. Gatcombe (20) presented a detailed analysis of the effect of pressure on the viscosity of fluids passing between cylinders rotating at the same speed. Viscosity increase with pressure was an important factor in the examples cited in his paper, due to the high pressures encountered. Viscosity variation with pressure is less important in the range of conditions encountered in the present work, although in some cases it may have been significant, as the following examples indicate.

The viscosity - pressure relationships of a number of oils has been summarized by Hersey and Hopkins (44), but data on polymeric vehicles such as those employed here are lacking. For the following examples the pressure-viscosity behavior was estimated from the relationship between viscosity temperature sensitivity and pressure sensitivity proposed by Kiesskalt (45). The Kiesskalt relationship shows a linear relationship between the mean pressure - viscosity coefficient, b_m, and the logarithm of the slope of the viscosity vs. temperature curve. The pressure - viscosity coefficient is used in the equation;

$$\frac{d\mu}{dP} = \frac{b_m}{100}\mu \qquad (60)$$

The viscosity - temperature slope of the No. 8 varnish at a viscosity of 161.3 poise is,

$$\frac{d\mu}{dt} = -2.303 \times 161.3 \times \frac{4335.1}{(564.5)^2} = 5.05 \frac{\text{poise}}{°F} = 5050 \text{ millipoise/°F.}$$

The log of this slope is 3.7033, and the corresponding value of b_m is 0.19 percent per atmosphere, from the Kiesskalt curve for fatty oils (46). The maximum pressure attained in the example taken from run 64 at 100 microns minimum clearance is found by solving equation (33-a) at a value, x, equal to -x*, -4.336×10^{-3} ft. This calculation gives a maximum pressure of 111 atmospheres. The integrated form of equation (60) is,

$$\ln \frac{\mu}{\mu_o} = \frac{b_m}{100} \times P. \qquad (61)$$

Substitution of the example conditions gives,

$$\ln(\mu/161.3) = (0.0019)(111) = 0.211,$$

and $\mu_{111} = (1.234)(161.3) = 199$ poise . The maximum local viscosity rise due to pressure is therefore 23.4 percent in this example.

Table VII

Summary of Theoretical Results for Experimental Conditions of Runs 30 and 64.

Value	Units	Run 30	Run 64
Viscosity,	Poise	23	161.3
"	lb-sec/ft^2	0.048	0.337
Slow Roll Speed	RPM	300	102
"	ft/sec	7.85	2.67
Fast Roll Speed	RPM	300	305
"	ft/sec	7.85	7.98
Density	lb/ft^3	59.6	60.4
Minimum Nip clearance, h_o	microns	20	100
"	ft	6.56×10^{-5}	3.28×10^{-4}
Roll Radius	ft	0.25	0.25
x^*	ft	1.925×10^{-3}	4.336×10^{-3}
h^*/h_o	Dimensionless	1.225	1.229
F/L (total)	lb/ ft	3579	3745
Q	ft^3/sec-ft	6.32×10^{-4}	2.148×10^{-3}
q	Btu/sec-ft	1.09	3.212
Adiabatic Temperature Rise*	°F	72.5	62
Nominal Nip Center Shear Rate	sec^{-1}	0	1.62×10^4
Effective Average Nip Center Shear Rate	sec^{-1}	9.35×10^4	2.06×10^4
Maximum Nip Center Shear Rate	sec^{-1}	1.62×10^5	3.85×10^4
$\partial\mu / \partial t$	millipoise/°F	855	5050
b_m	Viscosity, %/Atm	0.165	0.19
Maximum Nip Pressure	Atm	254	111
Viscosity Ratio $\mu_{P_{max}} / \mu_o$	Dimensionless	1.52	1.234

* Heat capacity assumed 0.4 Btu/lb - °F

The maximum pressure rise and estimated viscosity-pressure rise for Run 30 conditions with No. 1 varnish at 10 microns nip clearance were 254 atmospheres and 52 percent viscosity increase. A summary of important calculated nip flow parameters for the Run 64 and Run 30 conditions are presented in Table VII. The viscosity increases due to pressure shown in these examples were calcualted at the points of maximum pressure. The average viscosity rise would be much less. The viscosity rise from pressure is not estimated to be enough to account for the greater than predicted values of flow rate observed for the No. 1 varnish in many of the experiments, though it undoubtedly was a contributing factor. It is believed that the greatest source of divergence in those cases was the surface temperature measurement.

Non Newtonian Rheological Properties. It has been shown that effects of temperature, temperature measurement, and pressure are of great enough magnitude to account for the observed diviations of the experimental flow rates from those calculated from the constant viscosity theory. This does not rule out the possibility of some non-Newtonian behavior at high rates of shear. Although temperature effects in rotational viscometers have been shown to account for non linearity in measured stress, rate-of-shear curves for some fluids (35,41), other examples have been reported (41) in which the temperature effect does not account for all of the curvature observed. It has also been shown (52) by Pao on theoretical grounds that viscoelastic properties can cause apparent viscosity to decrease with increasing shear rate, and it is to be expected that some of the higher molecular weight polymers such as the No. 8 varnish used in this study will show viscoelastic properties.

The deviations from linearity of the stress, shear-rate curves obtained in this study were usually slight, and could be explained on the basis of temperature effects in the viscometer; although a rather low value of thermal conductivity (0.04 Btu/hr-ft^2-°F/ft) must be assumed to account for the behavior of the No. 8 varnish. The shear rates used in viscosity measurement were below 200 sec^{-1} however, and linearity in this range does not preclude non-Newtonian behavior in the shear rate range of 10^4 to 10^5 sec^{-1} encountered in the mill nip. The effects of any non-Newtonian behavior that may have been pressent are believed to have been minor compared with the effects of temperature and pressure.

Anomalous Behavior of SAIB. Only in the experiments with SAIB on 6-inch rolls did the slope of the experimental to theoretical flow rate curve deviate to a significant extent from unity. Examination of the data (runs 72 and 73 in Table XXI, and Figs. 14, 15, and 20) shows that the deviation of experiment from theory increased with decreasing roll force, and was accompanied by an appreciable increase of measured film temperature and corresponding decrease in estimated fluid viscosity. The data are consistent with the hypothesis that the measured film temperature increased with increasing fluid film thickness, while the effective nip temperature remained constant. A possible explanation of this behavior lies in the effect of the high viscosity-temperature slope (86,400 millipoise/°F at 104 °F) on the velocity profile of the sheared SAIB passing under the thermocouple strip. The rapid decrease with temperature rise near the thermocouple surface would be expected to lead to a tremendous increase in shear rate at that surface. The result would be a condition approaching plug flow where the major portion of the film is hardly sheared at all. This condition would lead to a

high level of energy input at the thermocouple surface, giving a greater than normal temperature reading at that surface. Since the effect of the velocity profile distortion decreases with decreasing film thickness or decreasing surface velocity, the better agreement between theory and experiment observed at high levels of roll force and in the 4-inch roll studies is reasonable.

Nip Clearance and Flow with Glass Bead Systems

Experiments with fluids containing a low concentration of glass beads were designed to provide an independent test of the nip flow theory by giving a measure of the minimum nip clearance which could be compared with the calculated value of ho. In these experiments, several factors decrease the certainty that the largest bead diameter observed is actually equal to the minimum nip clearance.

Factors which could lead to observed bead diameters less than the actual minimum nip clearance are:

1. The possibility that no beads in the system are as large as the nip clearance,
2. The possibility that the largest beads will not be observed in the microscopic examination of the sample,
3. The possibility that the flow in the bank region will cause a rejection of beads larger than some critical size but still less than the minimum nip clearance

Theory of Bead Rejection and Capture. Consideration of the implications of equations 43 through 51, dealing with the location of the stagnation point in the nip and the quantity of flow associated with the fast roll, indicates that the third possibility listed above would not be likely to occur. At the point of flow reversal, x_s , beyond which all fluid travels forward through the nip, the nip clearance is αh^*; α is a function of roll speed ratio, r , defined in equation 45. The stream line associated with the fast roll, which divides the forward moving from reverse flowing fluid, is located at a distance from the fast roll given

by $\frac{1}{2} h_s - y_s$. This value is equal to $\alpha h^*/2 - \beta h^*$ or $(\frac{\alpha}{2} - \beta)h^*$. The value β is a function of r, defined in equation 46 . Because of changes in the velocity profile at the roll surface, this dividing stream line is closer to the roll at points well back in the fluid bank than it is at the stagnation point. The minimum thickness of the layer associated with the roll will be found back in the bank region where the velocity of the fluid layer is equal to that of the roll. In this case the rate of flow associated with the fast roll is given by, $Q_f = U_2 \delta_2$. The distance, δ_2, is the distance from the roll surface to the streamline that leads through the stagnation point. The flow rate associated with the fast roll was related to the velocity profile at the stagnation point in equations 48 and 49 , where it was shown that Q_f is equal to f Q. The coefficient f is a function of roll speed ratio given in equation 51 and listed in Table I. The minimum value of δ_2 can be related to roll speed ratio and nip clearance at the nip exit, h*, by the following considerations.

$$\delta_2 = \frac{Q_f}{U_2} = \frac{fQ}{U_2} = \frac{f}{U_2} \frac{U_t}{2} h^* \qquad (62)$$

Since $U_2 = r U_1$, and $U_t = (U_1 + U_2) = U_1(1 + r)$, it follows that

$$\delta_2 = \left[(f/2)(1 + r)/r\right] h^* \quad . \qquad (63)$$

A similar derivation for the slow roll surface shows that,

$$\delta_1 = \left[(1-f)/2\right] \left[(1+r)/r\right] h^* \qquad (64)$$

Manley and Mason 51 reported experiments in which spheres in sheared suspensions were observed to move along the stream lines passing through their centers. If this behavior applies in the nip inlet, only particles with centers lying between the wall and the stream line that passes through the stagnation point will enter the nip. Under

this criterion, the diameter of the largest beads accepted will be $2\delta_2$. The relationship of the diameter of the largest bead, D_b max, to minimum nip clearance is therefore given by,

$$D_b \text{ max} = \frac{f\,(1+r)}{r}\left(\frac{h^*}{h_o}\right) \quad h_o \quad . \tag{65}$$

In the machine computation of the theoretical flow equations the ratio h^*/h_o was observed to depend primarily on h_o and roll radius. Values ranging from 1.2257 to 1.2975 were obtained for nip clearances from 10 to 400 microns respectively. The relationship of h^*/h_o to nip clearance for four and six inch rolls is shown in Fig. 26. Using a value of h^*/h_o of 1.23, and calculating f from equation 51, values of D_b max/ h_o were determined. These factors, along with values of α, β, f, and δ/h^*, are listed for different roll speed ratios in Table VIII.

Table VIII

Values of Theoretical Nip Stagnation Point

Constants for Various Roll Speed Ratios

Roll Speed Ratio	α Eq. 45	β Eq. 46	f Eq. 51	δ_2/h^*	δ_1/h^*	D_b max/h_o
1	3	0	0.5	0.5	0.5	1.23
2	2.84	-0.244	0.744	0.556	0.384	1.37
3	2.64	-0.354	0.851	0.566	0.298	1.391
4	2.50	-0.416	0.907	0.567	0.232	1.395
10	1.96	-0.546	0.999	0.550	0.002	1.352
∞	1.50	-0.75	1.000	0.500	0.000	1.23

These calculations indicate that particles equal to the minimum nip

Figure 26. Calculated Relationship between Nip Clearance and h^*/h_o

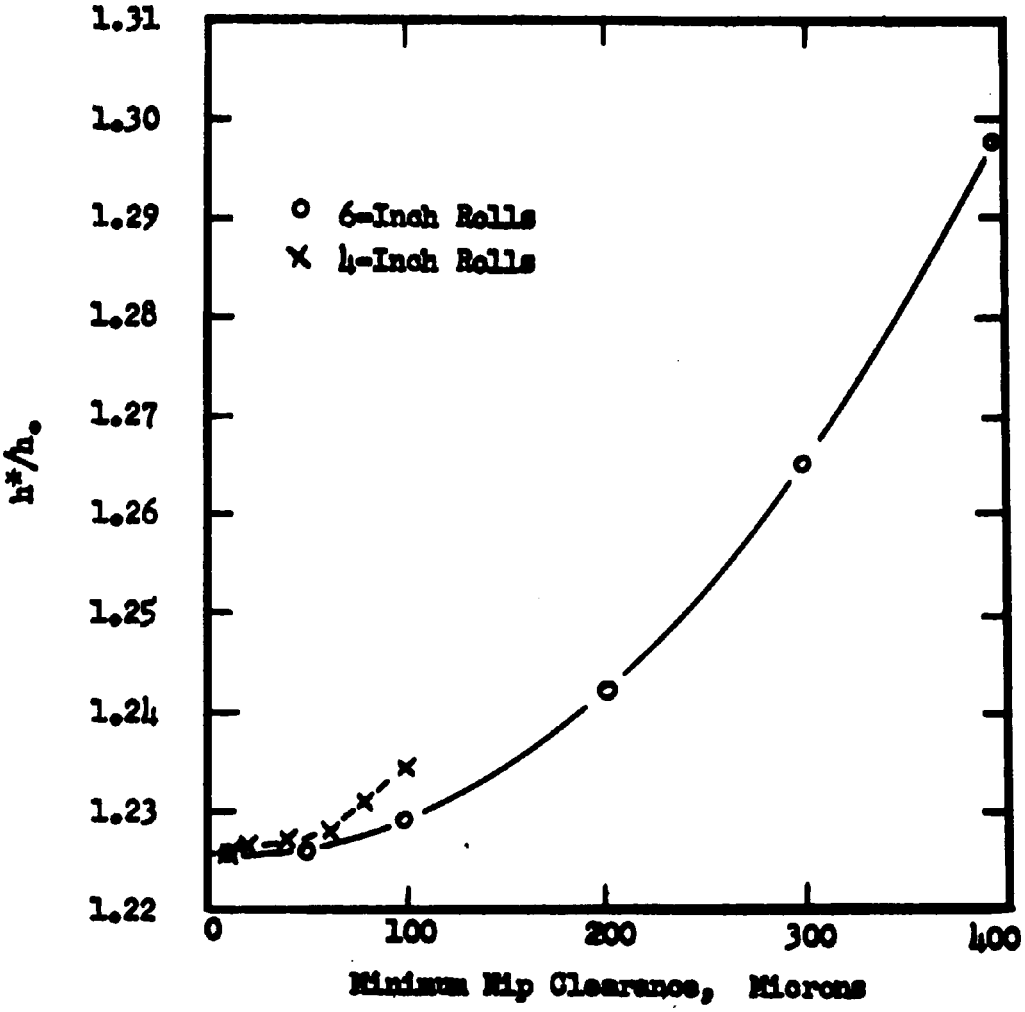

clearance would not be rejected from the nip if they were initially close to the wall. They further indicate that particles adjacent to the fast roll will be crushed only if their diameter is between h_o and h_o times the value of $(D_b \text{ max}/h_o)$ given in Table VIII. Larger particles will be rejected and smaller ones will pass through uncrushed. These calculations ignore the stream line distortion introduced by bead to wall interaction, as well as the fact that beads, being large finite bodies overlap a number of stream lines and may come under the influence of both roll surfaces. The effects of inertial, centrifugal, and gravitational forces in moving beads across stream lines were also neglected. Bead to wall interaction and centrifugal force will tend to move beads away from the wall and lead to the rejection of smaller beads than this simplified theory indicates. On the other hand, gravitation, inertia, and the influence of the second wall lead to capture of larger beads by the nip. In the limitations of the present theory, the magnitude of these competing factors cannot be determined. It is interesting that this theory predicts, for a given nip clearance, a maximum value of the ratio of size of bead captured to nip clearance at a roll speed ratio of about 4. At this ratio however, the slow speed roll is relatively ineffective, and beads on the slow speed side of the dividing stream line would continue to be rejected as long as their diameter were greater than $0.57\ h_o$. At unit roll speed ratio, both halves of the bank would be equally effective in capturing and fracturing beads.

Agreement with Theory. Figure 21 shows that the experimental measurement of size of unbroken beads gives values which are in the same order of size as theoretical values of minimum nip clearance. In the No 1 varnish

and M-2185 copolymer tests, the bead sizes fall on a single curve about 50% greater in value than the predicted nip clearance. With the higher viscosity No 8 varnish, the bead sizes fall below the predicted clearances. For the No 8 varnish test at a roll speed ratio of 3 the bead sizes were only about 40% of the calculated clearance values. In each set of tests the observed bead diameters were nearly proportional to the calculated clearances but deviated by a constant factor.

The observed flow rates are compared with theory in Fig 22 where it is seen that the No 1 varnish values were higher than theoretical by about 40% and the 3-1 ratio No 8 varnish values were only about 40% of the calculated values. The alkyd vehicle and the No 8 varnish at 1-1 ratio deviated to a greater extent, with the observed flow rates being higher than the calculated values. This latter result is the only observed instance in which No. 8 varnish gave higher than theoretical flow rates.

Bead Concentration as a Possible Source of Deviation. The concentration of glass beads in the suspensions was five percent by weight or 2.5 percent by volume. It was originally assumed that at this concentration the beads would not interact with each other, and consequently the effect of beads on viscosity was estimated by the Einstein[47] equation;

$$\frac{\mu_s}{\mu_o} = 1 + 2.5\,\phi \quad , \tag{66}$$

where: μ_s is suspension viscosity.

μ_o is vehicle viscosity.

ϕ is volume fraction of solids in suspension.

From this equation the viscosity of the suspension was estimated to be five percent higher than the pure vehicle at the corresponding

temperature. There is reason to suspect that this estimate of the viscosity gave values which were too low. Evason[48] reported relative viscosity values of 1.09 to 1.11 for 2.5 volume percent suspensions of polymethyl methacrylate and polystyrene spheres in aqueous lead nitrate-glycerol solutions stabilized with a dispersing agent, and it is likely that at this concentration Einstein's assumption of no particle-particle interaction is no longer valid. It is probable that the proximity of the spheres to the roll surfaces in the nip contributes a still higher increase to the effective viscosity. Both of these factors were probably less important, by themselves, than the effect of any increase in bead concentration which may have occurred in the nip region. Such a concentration increase was likely, due to the combined effects of inertia, gravity, and proximity of the beads to the walls. Experimental evidence for the tendency of bead concentration to increase at the roll surface is given in Appendix VII. It appears that measured bead concentrations in the samples scraped from the rolls exceeded the initial five percent concentration in all cases where nip clearance was great enough to pass the larger beads. The unusually low flow rates and bead sizes observed with the No. 8 varnish at 3-1 roll speed ratio do not agree with the other results, but may be due to temperature difference between the nip and thermocouple. Both bead size data and flow rate data are consistent with a viscosity level 72% below that used in the theoretical calculations. The observation that bead size reached a maximum while a flow rate continued to increase in the tests with No. 8 varnish at 1-1 ratio is attributed to a deficiency of larger size beads in the fluid sample employed.

Appearance of Bead Samples. The appearance of the beads after passage through the mill is illustrated in Fig. 27 by photomicrographs at 74x magnification. The samples shown were taken following the lowest force runs, with No. 1 varnish and H 2185 copolymer systems. The somewhat greater fraction of particle breakage in the No. 1 varnish system appeared to be part of a general trend in which the fraction of beads fractured decreased with increasing fluid viscosity. It is believed that this trend was due to the particle size distribution of the beads, which gave a relatively small number of particles in the narrow size range subject to fracture at high nip clearances.

Film Split and Relative Transfer Between Rolls

A film of fluid passing between rotating cylinders is subjected to tension as it moves away from the zone of low clearance, and eventually must split. The location of the line of split relative to the roll surfaces, and the relative quantity of fluid which moves away on each of those surfaces depends not only on hydrodynamic considerations, but on physical properties of the fluid as well. In actual practice the problem is complicated by interaction of the hydrodynamic factors encountered in the nip with the physical properties to produce local variations in these properties.

Hydrodynamic Prediction. At the present state of the theory, the only case which can be treated from the standpoint of purely hydrodynamic considerations is that of rolls totally immersed in a constant viscosity fluid with infinite cohesive strength.

Figure 27. Glass Beads After Passage Between 6-Inch Diameter Rolls at 99, 198 RPM, 74 X

No. 1 Varnish, 23 Poise

H 2185 Copolymer, 90 Poise

for this case there would be no film split, but the relative quantity of flow associated with each of the rolls could be determined. This idealized case gives a pressure profile through the nip which is a symmetrical, odd function of x. That is, $P(x) = -P(-x)$. The pressure gradient is, however, an even function of x, and dP/dx at x is equal to dP/dx at $-x$. The ratio of fast roll flow rate to total flow rate, given by equation 51 and listed in Table I, therefore applies to both inlet and outlet sides of the nip in this special case.

The system studied in this investigation differs in so many respects from the idealized case that the agreement found between the experimental transfer ratios and the predicted f values is remarkable. This relationship is shown in Fig. 28, where experimental transfer fractions, listed in table IX, are compared with theoretical f values calculated from 51.

Effect of Roll Force. The influence of roll force on transfer fraction is shown in Fig. 29, where average transfer fractions for lithographic varnishes on six-inch roll are plotted versus applied roll force. In general, the transfer fractions decrease with increasing force and tend to approach the theoretical f value at high force levels. The same trend can also be observed in the results obtained with four-inch rolls; but in that case the data points are clustered about the theoretical f values at force levels higher than 1000 lb/ft. The transfer behavior of the SAIB was unique in that transfer ratio increased with roll force, contrary to the behavior of the other systems.

Effect of Fluid. The transfer fraction depends on physical properties of the liquid as shown by the increase in transfer with increasing fluid viscosity-temperature sensitivity plotted in Fig. 30. The high

Table IX

Average Fraction of Total Flow Transferred to Fast Roll

4-inch Roll						6-inch Roll*					
1-1 Ratio		2-1 Ratio		3-1 Ratio		1-1 Ratio		2-1 Ratio		3-1 Ratio	
Low Speed	High Speed	Low Speed	High Speed	Low Speed	High Speed	Low Speed	High Speed	Low Speed	High Speed	Low Speed	High Speed
0.454	0.4477	0.7508	0.7487	0.8630	0.8513	0.5324	0.5228	0.8063	0.7835	0.8721	0.8590
0.4508 ± 0.0012		0.7498 ± 0.0007		0.8572 ± 0.0009		0.5286 ± 0.0047		0.7925 ± 0.0024		0.8626 ± 0.014	

* Lithographic varnish Data.

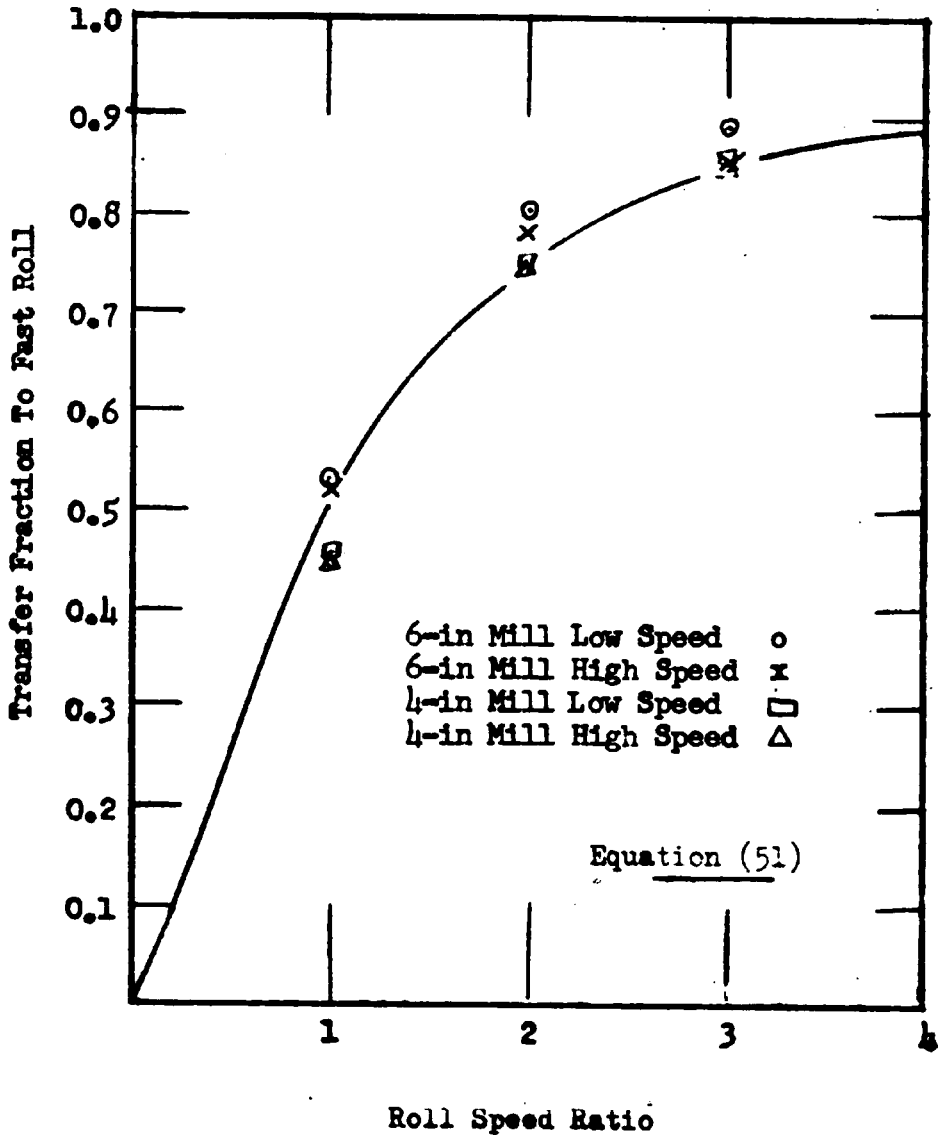

Figure 28. Variation of Transfer Fraction with Roll Speed Ratio

Figure 29. Influence of Roll Force on Fraction of Total Flow Transferred to Fast Roll

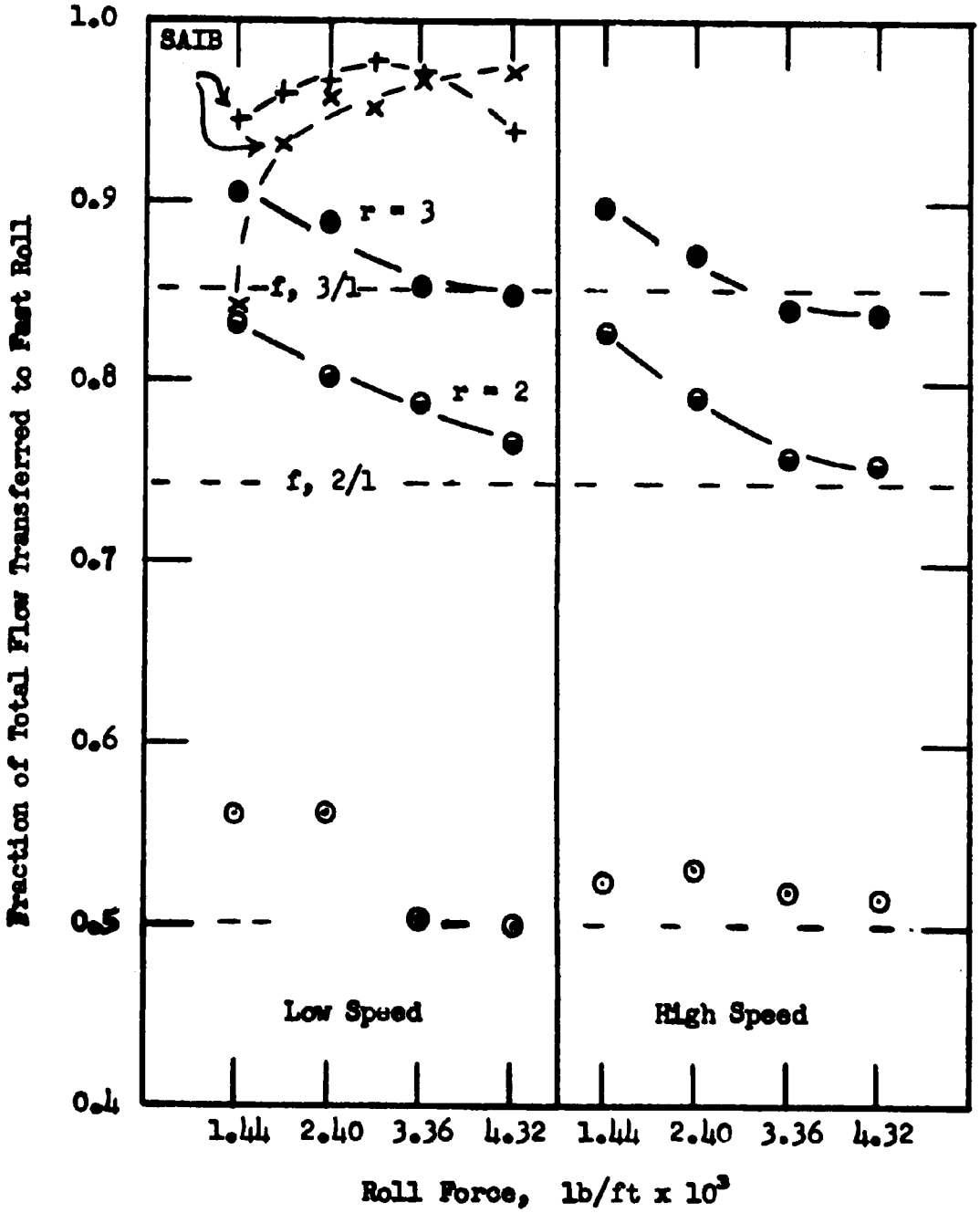

Figure 30. Variation of Ratio of Experimental to Theoretical Transfer Fraction with Viscosity-Temperature Coefficient of Fluid

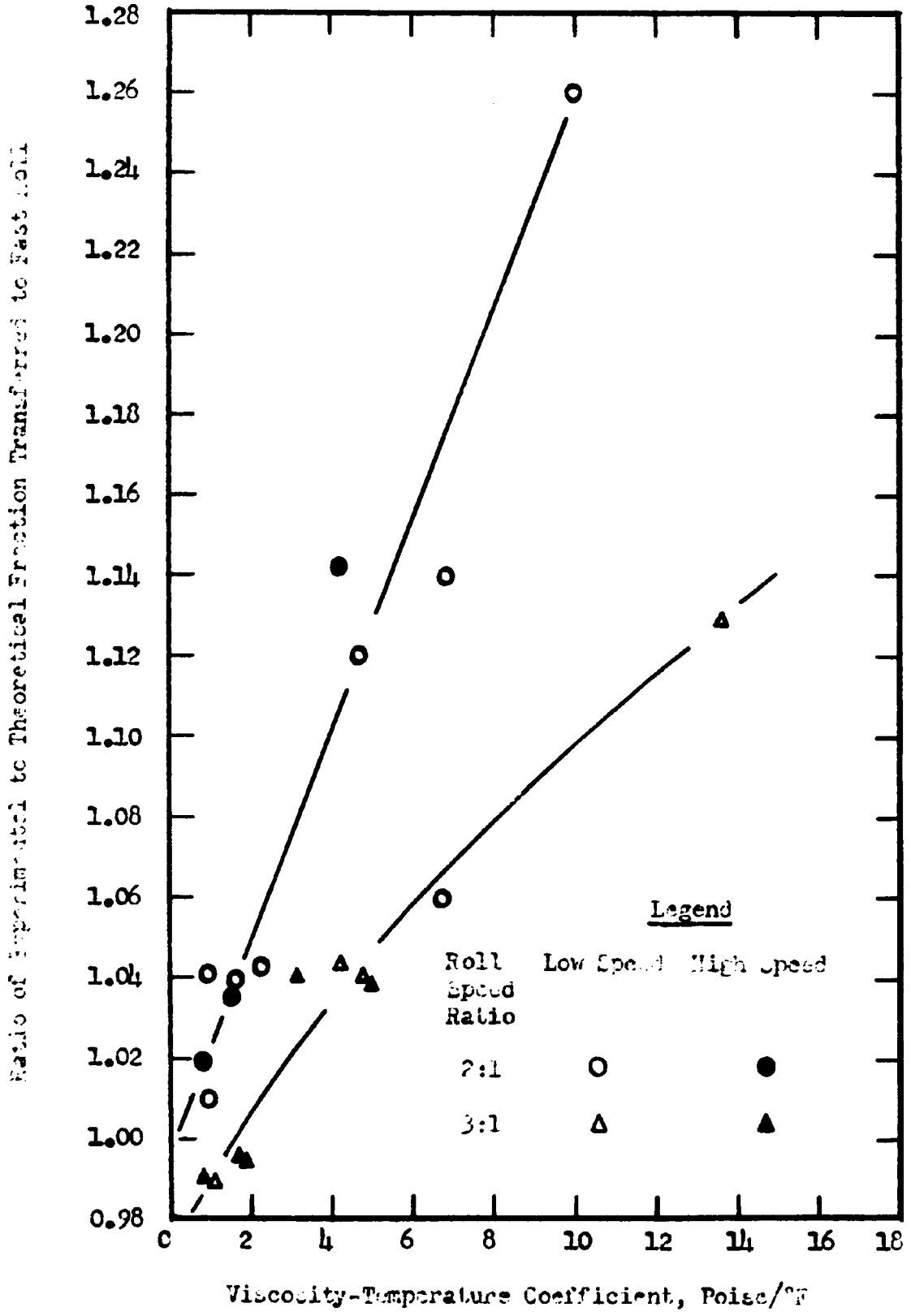

viscosity No. 5 and No. 8 varnishes gave higher transfer than the lower viscosity vehicles. The highest transfer values were observed with SAIB on the 6-inch rolls, where the average SAIB transfer fractions were 0.938 and 0.959 for roll speed ratios of 2 and 3 respectively. On 4-inch rolls, SAIB gave higher transfer ratios than all ather fluids except HF 825 Acroloid, which was equivalent in behavior.

Hypothesis on Film Split Mechanism. The experimental data are consistent with the hypothesis that the theoretical transfer fraction given in equation 51 represents a limiting value which is achieved under ideal conditions. Deviations from the limiting value were consistently in the direction of higher transfer, which ment that the position of film split was closer to the slow roll than predicted. This behavior is reasonable when the effect of shear induced temperature gradients in the nip is considered. As discussed on page 80, the competition of high shear rate at the roll surface with heat transfer to the roll leads to formation of a zone of maximum temperature a short distance into the film from each roll surface. The temperature distribution is symmetrical between the rolls when roll speeds are equal. When the rolls turn at different speeds, the shear rate near the slow roll is greater than that near the fast roll, and an unsymmetrical temperature profile is developed. The maximum temperature will occur near the surface of the slower roll. Because of the temperature sensitivity of the fluid, the maximum temperature zone leads to a local reduction of viscosity, which is further amplified by the tendency of shear rate to increase where viscosity is decreased. The net

result of the temperature effect is the creation of a zone of reduced viscosity in which film rupture can occur most readily when the fluid undergoes tension. Any factor which tends to increase the local rise of temperature and decrease of viscosity will shift the position of film split toward the slow roll surface and increase the fraction of transfer to the faster roll. Factors having this influence are:

1. High fluid viscosity.
2. High viscosity-temperature coefficient.
3. High film thickness.
4. Low thermal conductivity of fluid.
5. Low heat capacity of fluid.
6. High shear rate.
7. Low flow rate.

Increased viscosity and increased shear rate raise the rate of energy input to the system through the relationship,

$$q = \mu \left(\frac{du}{dy}\right)^2 . \qquad (67)$$

The viscosity-temperature coefficient controls the response of the fluid to temperature changes; $d\mu/dt = -2.303 \mu M/T^2$.

The film thickness determines the distance through which heat must diffuse before being removed at the surface. The fluid thermal conductivity controls the rate of heat diffusion through the fluid. The heat capacity controls the rate of temperature rise with energy intake by the fluid. The flow rate influences the local temperature rise since heat is removed from the nip by the passage of fluid through it.

Past roll transfer fractions approaching the theoretical limit are favored by:

1. Low viscosity.
2. Low viscosity-temperature coefficient.
3. Low film thickness.
4. High thermal conductivity.
5. High heat capacity.
6. Low shear rate.
7. High flow rate.

The observed relationship of the transfer fraction to the independent variables can be explained on the basis of these seven factors. The higher transfer fraction found with the higher number varnishes is due both to the increased rate of heat generation with increased viscosity, and to the greater viscosity-temperature sensitivity. The SAIB, with the highest value of $d\mu/dt$ studied, naturally gives the greatest transfer fraction. Increasing roll force produces two competing effects: a decrease in film thickness, and an increase in rate of shear. The decrease in film thickness was the more important effect of pressure under most of the conditions studied; however, with SAIB the increase in shear rate was more important, and the transfer fraction increased. The apparent maximum in the force-transfer curve of SAIB in Fig. 29 may very well be due to a balance of the competing effects of shear rate and film thickness. The average transfer fractions listed in Table IX show a consistent inverse relationship between transfer fraction and roll speed. This effect is not unreasonable if the cooling effect of the increased flow rate offsets the higher shear rate induced by higher roll speed.

Non-Newtonian Viscosity and Film Split. Non-Newtonian fluid flow properties of the type which lead to a decrease of apparent viscosity with increasing rate of shear are expected to affect fluid transfer in the same manner as temperature-sensitive viscosity properties. The mechanism of action is similar to that described for temperature sensitivity, in that high shear rate regions near the slow roll surface create local regions of low viscosity in which film rupture is favored. This local viscosity reduction effect is believed to account for the observed sensitivity of printing ink transfer properties to ink shortness as reported by Sparta[8], Fetsko and Walker[30], Scarr[31], Lin[33], and Zettlemoyer[49]. Modifications of the roll nip theory necessary for application to printing experiments have been discussed by the present author elsewhere[50].

Power Consumption

The theoretical nip power consumption is given by equation 41. Although no experimental study of power consumption was made in this investigation, it is possible to compare numerical results of equation 41 with values calculated from the empirical equation given by Maus[6] for the case of two rolls with a fluid bank. This equation is,

$$\frac{P_o\, g}{\rho L (U_T^3)\, 2R} = 2.58 \left[\frac{h_o\, U_T\, \rho}{g\, \mu}\right]^{-2/3} \left[\frac{U_T^2}{h_o\, g}\right]^{-1/3} \left[\frac{U_T}{U_2}\right] - 1.15 \qquad (68)$$

A comparison of power consumption values calculated by the Maus equation and equation 41, for six sets of typical operating conditions, is shown in Table X.

Table X

Theoretical and Empirical Values of Nip Power Consumption

Variable	Units	Run 3	Run 3	Run 30	Run 62	Run 64
Roll Diameter	ft	0.1667	0.1667	0.25	0.25	0.25
Fast Roll Speed	RPM	155	155	300	310	310
Slow Roll Speed	RPM	77.5	77.5	300	103.3	103.3
Viscosity	Poise	47.8	47.8	23	17.8	161
Nip Clearance	Microns	40	100	20	10	100
Power Consumption Equation 41	$\frac{\text{ft-lb}}{\text{sec-ft}}$	111	19.6	850	1360	2499
Power Consumption Maus	$\frac{\text{ft-lb}}{\text{sec-ft}}$	92	68	735	675	1310

In two of the examples, the results are in close agreement. In two instances the theoretical equation gave results nearly twice those given by the empirical equation, and in the fifth example, the theory gave less than one third the empirical value. The deviation of the nip power equation derived from theory from that obtained by experimental measurements is believed to be due to two factors which the theory does not take in to account. These are:

1. Power consumed in the bank behind the nip.
2. Decrease of nip viscosity with temperature at high levels of power consumption.

Since the total power consumed in the system was measured by Maus, his equation includes the effect of bank power as well as nip power. His results also include the effect of viscosity change with shear conditions in the nip. The viscous flow theory does not allow for these factors, and therefore deviates from the empirical values on the high side at high levels of power consumption, and on the low side at lower power consumption when bank power is an important part of the total. Because of these considerations, the empirical expression is expected to give a better estimate of total power demand than the nip flow theory in its present state of development. In view of the importance of fluid properties observed in this study, it is expected that fluids with different temperature-viscosity coefficients than the polybutenes used by Maus will show deviations from the empirical equation. The difference between observed power consumption and power consumption calculated from the nip theory at low power levels should provide a measure of the actual quantity of energy dissipated in the mill bank. Conditions would have to be chosen where the constant viscosity assumptions of the nip flow theory are valid, for this suggested experiment.

VII. CONCLUSIONS

A theoretical and experimental investigatior of the flow of viscous fluids between the surfaces of mutually external rotating cylinders was conducted. Theoretical methods of prediction of rate of flow, clearance between cylinders, and relative transfer of fluid to faster roll were developed. An experimental study was conducted to test the validity and range of applicability of the theory. The following conclusions were drawn on the basis of this investigation.

1. Experimental flow rates are predicted by the theory with 95 % confidence limits of +35 and - 25 percent when fluid viscosity is less than 90 poise or total roll surface speed is less than 10 feet per second.

2. Ninety-five percent of all data values fell within limits of -52 to + 110 percent of the theoretical flow rates.

3. The flow rate behavior of fluids with viscosities as high as 150 poise can be correlated by use of an empirical correction factor in conjunction with the hydrodynamic theory.

4. The flow behavior of Sucrose Acetate Isobutyrate, a liquid with an unusually high temperature viscosity sensitivity, gave good agreement with theoretical predictions with roll surface speeds of 4 feet per second on four inch diameter rolls. The behavior of this material deviated from theory at total surface speeds equal to and in excess of 7 feet per second.

5. The lower limiting value of the fraction of total flow transferred to the faster of two rolls is governed by hydrodynamic factors, and is primarily a function of roll speed ratio. The limiting value is approached under experimental conditions which give nearly constant viscosity in the nip.

6. The fraction of total flow transferred to the faster roll is equal to or greater than that given by the constant viscosity transfer theory, and is increased by factors which tend to reduce fluid viscosity at the slow roll surface.

X. LIST OF REFERENCES

1. New York Paint and Varnish Production Club, Subcommittee 53: Off. Digest, 286, November, 1948.
2. _____: Off. Digest, 311, December, 1950.
3. _____: Off. Digest, 358, p. 1093, November, 1954.
4. _____: American Paint Journal Convention Daily, Nov. 1, 1957; Off. Digest, 394, p. 1113, November, 1957.
5. Fisher, E. K.: Colloidal Dispersions, pp. 288-9, John Wiley and Sons, Inc., New York, 1950.
6. Maus, L., Walker, W. C., and A. C. Zettlemoyer: I and E. Chem., 47, No 4, p. 696, April, 1955.
7. Taylor, J. H.: "An Investigation of Variables affecting Power Consumption in Three Roll Mills", M.S. Thesis, Lehigh University, Bethlehem, Pa., 1950.
8. Sparta, T.: "Roll Mill Studies III, A Production Rate Equation", M.S. Thesis, Lehigh University, Bethlehem, Pa., 1954.
9. Gamble, E. and T. Sparta: NPIRI Project Report No. 32, National Printing Ink Research Institute, Lehigh University, Bethlehem, Pa., May, 1954.
10. Prandtl, L. and O.G. Tietjens: Fundamentals of Hydro and Aeromechanics, p. 259, Dover Publications, Inc., New York, 1934, Dover ed. 1957. Navier, M.: Mem. Acad. Sci., 6, p. 389, 1827.
11. Prandtl, L. and O.G. Tietjens: Fundamentals of Hydro and Aeromechanics, p. 259, Dover Publications, Inc., New York, 1934, Dover ed. 1957. Poisson, S.P.: J. École Polytech, 13, p. 1, 1831.

12. Prandtl, L. and O.G. Tietjens: Fundamentals of Hydro and Aeromechanics, p. 259, Dover Publications, Inc., New York, 1934, Dover ed. 1957. B. de St Venant: Compt. rend. 17, p. 1240, 1843.

13. Prandtl, L. and O.G. Tietjens: Fundamentals of Hydro and Aeromechanics, p. 259, Dover Publications, Inc., New York, 1934, Dover ed. 1957. Stokes, G.G.: Trans. Cambridge Phil. Soc., 8, 1845.

14. Reynolds, O: Phil. Trans. Roy. Soc., 177, pt. 1, pp. 157-234, 1886.

15. Rayleigh, J.M.S. (Lord): Phil. Mag., 35, pp. 1-12, 1918.

16. Dryden, H.L., F. Murnaghan, and H. Bateman: Hydrodynamics. Bibliography, p. 241, p. 294. Dover Publications Inc., 1956.

17. Frazer, R.A.: Phil. Trans. Roy. Soc., A225, pp. 93-130, 1926.

18. Ardichvili, G.: Kautschuk, 14, pp. 23-25, 41-45, 1938.

19. Eley, D.D.: J. Polymer Sci., 1, No 6, pp. 529-534, 1946.

20. Gatcombe, E.K.: Trans. ASME, 67, pp. 177-188, 1945.

21. Bergen, J.T. and G.W. Scott: J. Appl. Mech., Trans. ASME, 73, p. 101, 1951

22. Gaskell, R.E.: J. Appl. Mech., Trans. ASME, 72, p. 334, 1950.

23. Finston, M.: J. Appl. Mech., Trans. ASME, 73, p. 12, 1951.

24. Paslay, P.R.: J. Appl. Mech., Trans. ASME, 79, p. 602, 1957.

25. Hummel, C.: JOCCA, 39, No. 10, p777, October, 1956.

26. Banks, W.H., and C.C. Mill: J. Coll. Sci., 8, p. 137, 1953.

27. _____: Proc. Roy. Soc., A223, p. 414, 1954.

28. Miller, J.C.: "A Kinematic Study of the Splitting of Thin Liquid Films", Ph. D. Dissertation, Lehigh University, Bethlehem, Pa., 1956.

29. Miller, J.C. and R.R. Myers: Trans. Soc. Rheology, 2, p. 237, 1958.

30. Fetsko, Jacqueline M., and W.C. Walker: Am. Ink Maker, 33, No. 11, p. 38, and No. 12, p. 38, 1955.

31. Scarr, R.F.: "The Effects of Dynamic Ink and Press Variables on Ink Transfer", M.S. Thesis, Chem. Dept., Lehigh University, Bethlehem, Pa., 1956.

32. Hammel, J.J.: "Influence of Dispersion Components on Transfer and Optical Properties of Black Prints", M.S. Thesis, Chem. Dept., Lehigh University, Bethlehem, Pa., 1959.

33. Lin, L.C.: "The Effect of Printing Conditions On The Ink Transfer and Print Quality of Non Porous Stock", M.S. Thesis, Chem. Dept., Lehigh University, Bethlehem, Pa., 1958.

34. Schlichting, H.: Boundary Layer Theory, Chapter VI, p. 83. Translated by J. Kestin, McGraw-Hill Book Co., New York, 1955.

35. Lower, G.W.: "Consistency Studies of Printing Ink I. Modified Rotational Viscometer and the Calcium Carbonate-Polybutene System", Ph. D. Dissertation, Lehigh University, Bethlehem, Pa., 1950.

36. Banks, W.H., and C.C. Mill: J. Colloid Sci., 8, No. 1, p. 139, Feb. 1953. Vincent and Simmonds: Proc. Phys. Soc. (Lon.) p. 380, 1943.

37. Banks, W.H., and C.C. Mill: J. Colloid Sci., 8, No. 1, p. 139, Feb. 1953. Trevenna: Proc. Phys. Soc. (Lon) 65, p. 46, 1952.

38. Volk, W.: Applied Statistics for Engineers, Chapter 8, pp. 224-94, McGraw-Hill Book Co., New York, 1958.

39. Ibid: p. 146.

40. Brownley, K.A.: Industrial Experimentation, p. 149, Chemical Publishing Co., Brooklyn, N.Y., 1947.

41. Kuhns, P.W. and Ruth N. Weltmann: J. Colloid Sci., 7, p. 218, 1952.

42. Gee, R.E. and J.B. Lyon: I. and E. Chem., 49, No. 6, p. 956, June 1957.

43. McAdams, W.H.: Heat Transmission, p. 456, 3d ed. McGraw-Hill Book Company, Inc., New York, 1954.

44. Hersey, M.D., and R.R. Hopkins: Viscosity of Lubricants under Pressure, American Society of Mechanical Engineers, New York, 1954.

45. Hersey, M.D., and R.F. Hopkins: Viscosity of Lubricants under Pressure, American Society of Mechanical Engineers, New York, 1954. Kiesshalt, S.: Z. Vereines deutsches Ingenieure, 73, pp. 1502-03, 1929.

46. Ibid: Fig. 20, p. 60.

47. Einstein, Albert: Ann. d. Physik, 19, p. 289, 1896; 34, 591, 1911.

48. Eveson, G.F.: JOCCA, 40, No. 6, pp. 456-477, June, 1957.

49. Zettlemoyer, A.C., R.F. Scarr, and W.D. Schaeffer: Proc. 9th Annual Meeting Tech. Assoc. Graphic Arts, Inc. A, pp. 75-85, May 14, 1957. Int. Bull. Print. and Allied Trades, No. 80, pp. 88-96, 1958.

50. Taylor, J.H. and A.C. Zettlemoyer: TAPPI, 41, No. 12, pp. 749-757, Dec., 1958.

51. Manley, J., and S.F. Mason: J. Colloid Sci., 7, p. 354, 1952.

52. Pao, Yoh-Han: J. Appl. Physics, 28, No. 5, pp. 591-8, May, 1957.

APPENDICES

APPENDIX I

THREE-ROLL MILL MATERIAL BALANCE

The rate-of-flow of fluid through a three-roll mill is determined by the flow rate through the feed nip, the relative transfer fractions from nip to faster roll, and by the effeciency of the take-off knife. The interrelationship of these factors is shown in the following material balance. A diagram of the system under consideration is shown in Fig. 1 of the text.

Nomenclature

Q — Flow rate through feed nip, volume/time-unit roll length.

f — Feed nip transfer factor, the fraction of ink passing feed nip which is transferred to center roll.

a — Apron nip transfer factor, the fraction of ink passing apron nip which is transferred to apron roll.

t — Take-off-knife factor, the fraction of ink carried by apron roll which is removed by take-off-knife.

R — Mill throughput rate, the volume of ink removed from mill per unit time per unit roll length.

Derivation

1. By definition the rate of ink flow through the feed nip is Q.
2. The rate of ink flow forward on the center roll is equal to (f) (Q).
3. Define the rate of flow to apron nip as W.
4. Then the rate of flow forward on the apron roll is (a)(W).

5. The take off of ink is R, and is equal to (t) (a) (W).

6. The flow under the take-off-knife- returns to the apron nip on the bottom of the apron roll. This flow rate is equal to

$$(1 - t)\ (a)\ (W)\ .$$

7. The total flow to the apron nip is made up of that returned on the apron roll bottom and that brought forward on the center roll.

$$W = (1 - t)\ (a)\ (W) + f\ Q\ .$$

8. $$W\left[1 - (1 - t)(a)\right] = f\ Q\ .$$

9. $$W = \frac{f\ Q}{1 - a + a\ t}\ .$$

10. The expression for W from step 9 is substituted for W in step 5 to give,

$$R = \frac{(t)\ (a)\ (f)}{1 - a + a\ t}\ Q\ .$$

APPENDIX II

VISCOUS FLOW THEORY FOR REGION DISTANT FROM THE NIP

In 1926, R. A. Frazer published a paper (17) titled, "On the Motion of Circular Cylinders in a Viscous Fluid", which contained an exhaustive treatment of the general hydrodynamic theory of viscous flow associated with the rotation of two cylinders of infinite length, immersed in a fluid of infinite extent. General functions for the stream lines were obtained, and several special cases were treated. Although Frazer's general theory should apply to the roll mill problem, the shear complexity of the equations obtained renders it unwieldy and inconvenient. The special case considered by Frazer, in which the cylinders are assumed to be in contact along a line of tangency, does yield a reasonably simple expression for the stream lines in the region removed from the zone of narrow clearance. This expression was used in deriving the pressure distribution in the mill bank region, and provided a rational boundary condition for solution of the nip flow problem. The general approach employed by Frazer, and the results obtained, as applied to the mill problem, are presented in this appendix.

Equation for Stream Function

The basic Navier-Stokes equations, reduced to the form shown in equations 6 and 7 of the text, serve as the starting point for solution of the two dimensional viscous flow problem. The condition of continuity expressed by equation 8 also must apply. In the solution of these

equations, a stream function, ψ, is defined by the relationships;

$$u = -\frac{\partial \psi}{\partial y} \quad , \tag{A II 1}$$

$$v = \frac{\partial \psi}{\partial x} \quad . \tag{A II 2}$$

The stream function defines streamlines, ψ = constant, in the flow pattern across which no flow occurs. Inserting the stream function into equations 6 and 7 gives;

$$\frac{\partial P}{\partial x} = \mu \left(-\frac{\partial^3 \psi}{\partial x^2 \partial y} - \frac{\partial^3 \psi}{\partial y^3}\right) \quad , \tag{A II 3}$$

$$\frac{\partial P}{\partial y} = \mu \left(\frac{\partial^3 \psi}{\partial x^3} + \frac{\partial^3 \psi}{\partial x \partial y^2}\right) \quad . \tag{A II 4}$$

Differentiating (A II 3) with respect to y and (A II 4) with respect to x gives;

$$\frac{\partial^2 P}{\partial x \partial y} = \mu\left(-\frac{\partial^4 \psi}{\partial x^2 \partial y^2} - \frac{\partial^4 \psi}{\partial y^4}\right) \quad , \tag{A II 5}$$

$$\frac{\partial^2 P}{\partial y \partial x} = \mu\left(\frac{\partial^4 \psi}{\partial x^4} + \frac{\partial^4 \psi}{\partial x^2 \partial y^2}\right) \quad . \tag{A II 6}$$

Subtracting (A II 5) from (A II 6) gives,

$$\frac{\partial^4 \psi}{\partial x^4} + 2\frac{\partial^4 \psi}{\partial x^2 \partial y^2} + \frac{\partial^4 \psi}{\partial y^4} = 0 \quad . \tag{A II 7}$$

Bipolar Coordinate System

Equation (A II 7) can be expressed in terms of complex variables defined by :

$$\lambda = x + i\,y \qquad \text{(A II 8)}$$

$$\mu = x - i\,y\,, \qquad \text{(A II 9)}$$

where, $$i = \sqrt{-1}\,. \qquad \text{(A II 10)}$$

In these variables, equation (A II 7) becomes,

$$\frac{\partial^4 \psi}{\partial \lambda^2 \partial \mu^2} = 0 \qquad \text{(A II 11)}$$

In order to solve equation (A II 11), Frazer made a further transformation to a bipolar coordinate system, using the following transformation of variables:

$$\lambda = x + i\,y = -i\gamma \coth\left(\frac{\rho + i\sigma}{2} + \delta\right) \equiv i\gamma \coth\left(\Omega + \delta\right) \qquad \text{(A II 12)}$$

$$\mu = x - i\,y = +i\gamma \coth\left(\frac{\rho - i\sigma}{2} + \delta\right) \equiv i\gamma \coth\left(\omega + \delta\right) \qquad \text{(A II 13)}$$

Note that in the equations being derived here, the symbol μ represents the coordinate defined in equation (A II 9), and not viscosity as used elsewhere. The nomenclature has been used here to conform with that originally employed by Frazer.

In the bipolar coordinate system defined by equations (A II 12) and (A II 13), circles are defined by $\rho =$ constant. The constants γ and δ can be selected to define two mutually external circles corresponding to $\rho = -K$ and $\rho = +K$ respectively. If $\underline{a}$ and $\underline{b}$ denote the radii and $\underline{D}$ the distance separating the centers, then:

$$\gamma = a \sinh (K - 2\delta) = b \sinh (K + 2\delta) \qquad \text{(A II 14)}$$

and, $$\gamma D = a\, b \sinh 2K \qquad \text{(A II 15)}$$

If, as in the case of interest here, the radii of the circles which represent cylinders are equal, then;

$$a = R = b, \text{ and it follows that } \delta = 0 \; . \qquad \text{(A II 16)}$$

Then, $$\gamma = R \sinh K \; , \qquad \text{(A II 17)}$$

$$\gamma = \frac{R^2}{D} \sinh 2K \; , \qquad \text{(A II 18)}$$

and $$\frac{\sinh 2K}{\sinh K} = \frac{D}{R} = \frac{2R + h_o}{R} = 2 + \frac{h_o}{R} \; ; \qquad \text{(A II 19)}$$

where, h_o is the minimum distance separating the roll surfaces.

Since $\sinh 2K = 2 \sinh K \cosh K$, equation (A II 19) can be reduced to,

$$\cosh K = 1 + \frac{h_o}{2R} \; , \qquad \text{(A II 20)}$$

or, $$K = \cosh^{-1} \left(1 + \frac{h_o}{2R} \right) \; . \qquad \text{(A II 21)}$$

Thus,

$$\cosh^2 K = 1 + \sinh^2 K = 1 + \frac{h_o}{R} + \frac{h_o^2}{4R^2} \; , \qquad \text{(A II 22)}$$

and $$\sinh K = \sqrt{h_o / R \left(1 + h_o / 4R \right)} \; . \qquad \text{(A II 23)}$$

Substitution of (A II 23) into (A II 17) shows that,

$$\gamma = \sqrt{R\, h_o \left(1 + h_o / 4R \right)} \; . \qquad \text{(A II 24)}$$

Points in the bipolar coordinate system are defined by the coordinates ρ and σ . The relationship between these coordinates and the rectangular system is shown in Fig. A-1 .

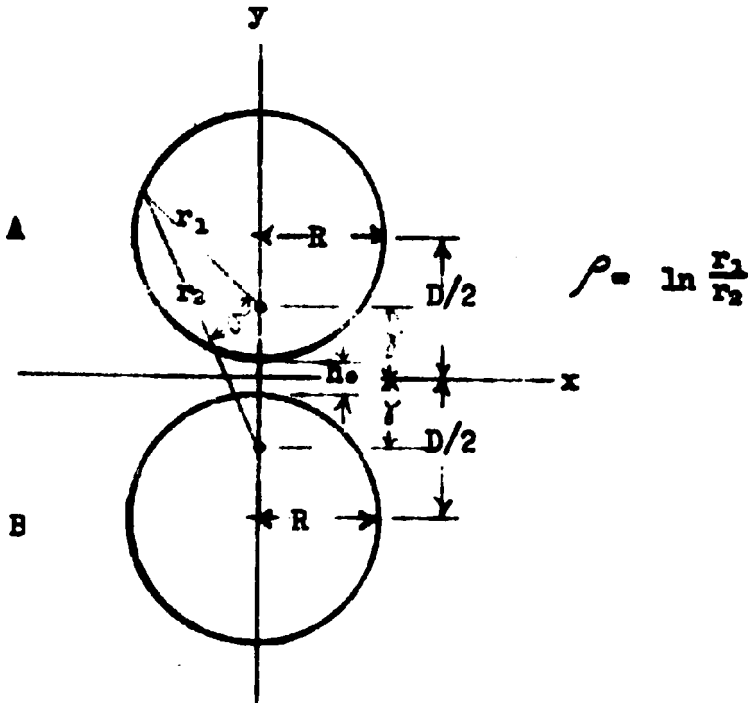

Figure A-1. Bipolar Coordinate System

Foci of the system are located at distances $\pm \gamma$ from the origin. The coordinate ρ is defined as the log to base e of the ratio of the distances r_1 and r_2 from a point to the two foci. The coordinate σ is the angle between r_1 and r_2. The boundary of the upper cylinder, A, corresponds to $\rho = -K$, while the lower cylinder, B, is given by $\rho = +K$. Other relationships between the rectangular and bipolar coordinate systems are listed here for convenience.

$$x = -\frac{\gamma \sin\sigma}{\cosh\rho - \cos\sigma} \quad . \qquad \text{(A II 25)}$$

$$y = -\frac{\gamma \sinh\rho}{\cosh\rho - \cos\sigma} \quad . \qquad \text{(A II 26)}$$

$$\rho = \frac{1}{2} \ln \frac{x^2 + (y-\gamma)^2}{x^2 + (y+\gamma)^2} \quad . \qquad \text{(A II 27)}$$

$$\sigma = \tan^{-1}\left(\frac{2x\gamma}{\gamma^2 - x^2 - y^2}\right) \quad . \qquad \text{(A II 28)}$$

General Stream Function

Frazer solved equation (A II 7) by a method of successive reflections of conjugate functions and obtained a general solution for the stream function when cylinders are rotating in a viscous fluid of infinite extent. When both cylinders have the same diameter the stream function may be written as follows.

$$\begin{aligned} c\psi = &- \mathfrak{A}\Big\{\sum_{s=1}^{\infty} a_s\left[2 \sinh S(\rho - K)\cos S\sigma\right] \\ &+ A_1\left[2\cosh(\rho - K)\cos\sigma - 2\cosh K\right] \\ &+ 2a_0\left[\rho - K\right]\Big\} \\ &+ \mathfrak{B}\Big\{\sum_{s=1}^{\infty} b_s\left[2\sinh S(\rho + K)\cos S\sigma\right] \\ &+ B_1\left[2\cosh(\rho + K)\cos\sigma - 2\cosh K\right] \\ &+ 2b_0\left[\rho + K\right]\Big\} \\ &+ 4\gamma^2 \operatorname{ctnh} K\Big\{\ln \frac{1/2\left[\cosh 2\rho + \cosh 4K\right] - \cos\sigma\left[2\cosh 2K\cosh\rho\right] + \cos^2\sigma}{2(\cosh\rho - \cos\sigma)} \\ &+ \sum_{s=1}^{\infty} \frac{e^{-3SK}}{S}\left(\frac{2\cosh S\rho\cos S\sigma}{\cosh SK}\right)\Big\} + \left(\frac{\alpha_0\gamma^2}{\sinh^2 K}\right)(\rho) \quad . \qquad \text{(A II 29)} \end{aligned}$$

Terms used in equation (A II 29) have the following significance.

$$\mathfrak{A} = \frac{2\gamma^2 \sinh(\rho + K)}{\sinh^2 K (\cosh\rho - \cos\sigma)} \quad . \qquad \text{(A II 30)}$$

$$\mathfrak{B} = -\frac{2\gamma^2 \sinh(\rho - K)}{\sinh^2 K (\cosh\rho - \cos\sigma)} \quad . \qquad \text{(A II 31)}$$

$$a_s = b_s = \frac{\sinh^2 2K}{(\sinh^2 2SK - S^2 \sinh^2 2K)} \left[\frac{2S \cosh K \sinh K}{\sinh 2SK} - \frac{(S-1)\sinh(S+1)K}{\sinh 2(S+1)K} \right.$$

$$\left. - \frac{(S+1)\sinh(S-1)K}{\sinh 2(S-1)K} \right] \quad . \qquad \text{(A II 32)}$$

The conditions which serve to determine the constants of equation (A II 29) are as follows:

$$(a_1 + b_1) = -\frac{\gamma \tanh 2K}{D} \quad , \qquad \text{(A II 33)}$$

$$D = a \frac{\sinh 2K}{\sinh K} \quad , \qquad \text{(A II 34)}$$

$$C_o = \frac{1}{2K}\left\{ \frac{\gamma \tan 2K}{D} - \sum_{s=2}^{\infty} \left[a_s \frac{\sinh SK}{\sinh K} + b_s \frac{\sinh SK}{\sinh K} \right] \right\} \quad , \qquad \text{(A II 35)}$$

$$a_o = \frac{C_o}{b} = b_o = \frac{C_o}{a} \quad , \qquad \text{(A II 36)}$$

$$(A_1 + B_1) = -\left[\frac{1}{\gamma D (O_a a^2 + O_b b^2)} \right] \left\{ \gamma^2 (O_a a^2 - O_b b^2) \right.$$

$$\left. + C_o \left[2K a^2 b^2 (O_a - O_b) + \gamma D (O_a a^2 - O_b b^2) \right] \right\} \quad , \qquad \text{(A II 37)}$$

$$\alpha_o = -4 (A_1 + B_1) \cosh 2K \quad , \qquad \text{(A II 38)}$$

$$C = \left[\frac{8}{(\Omega_a a^2 + \Omega_b b^2)}\right]\left\{ \gamma^2 + C_o\left[K (a^2 + b^2) + \gamma D\right]\right\} . \qquad \text{(A II 39)}$$

The constants Ω_a and Ω_b are the angular velocities of the cylinders A and B respectively, taken as positive in the counter-clockwise sense.

Solution for Rolls in Contact

Reduction of the stream function given by equation (A II 29) to a form suitable for engineering calculations of pressure distribution and flow rate between rotating cylinders presents several practical difficulties. When the distance between roll surfaces becomes small compared with the roll diameters, the values of K and sinh K become extremely small, and the series terms involving these factors converge quite slowly. The result obtained by Frazer for the case of cylinders assumed to be in actual contact is more readily useful. This solution, of course, is not valid in the nip region between rolls, where the minimum nip clearance is an important fraction of the total distance between roll surfaces. In the bank region, however, the influence of the nip clearance becomes negligible; and deductions from the no-clearance theory should provide a reasonable esitmate of the stream lines and pressure distribution.

The stream function for the rolls-in-contact case is;

$$\psi = A \frac{y^2}{x^2 + y^2} + C (x^2 + y^2) + F y + G \frac{y^3}{(x^2 + y^2)^2} . \qquad \text{(A II 40)}$$

The constants in (A II 40) are defined by the following relationships.

$$A = -\frac{R^2}{2}(\sigma_a + \sigma_b) \quad , \qquad \text{(A II 41)}$$

$$C = \frac{\sigma_a + \sigma_b}{8} \quad , \qquad \text{(A II 42)}$$

$$F = \frac{R}{4}(\sigma_a - \sigma_b) \quad , \qquad \text{(A II 43)}$$

$$G = -R^3(\sigma_a - \sigma_b) \, . \qquad \text{(A II 44)}$$

In order to relate the general expression to the case of interest here, the rolls A and B are defined as the fast roll and slow roll respectively. Dimensionless variables may be defined as follows:

$$\eta = y/R, \qquad y = R\eta \quad , \qquad \text{(A II 45)}$$

$$\zeta = x/R, \qquad x = R\zeta \quad , \qquad \text{(A II 46)}$$

In these dimensionless variables, equation (A II 40) becomes,

$$\psi/R^2 = \frac{A}{R^2}\left(\frac{\eta^2}{\eta^2+\zeta^2}\right) + C(\eta^2+\zeta^2) + \frac{F}{R}\eta + \frac{G}{R^3}\frac{\eta^3}{(\eta^2+\zeta^2)^2} \quad ,$$

where; (A II 47)

$$A/R^2 = -\left(\frac{\sigma_a + \sigma_b}{2}\right) \quad , \qquad \text{(A II 48)}$$

$$C = \left(\frac{\sigma_a + \sigma_b}{8}\right) \quad , \qquad \text{(A II 49)}$$

$$F/R = \frac{O_a - O_b}{4} \quad , \qquad \text{(A II 50)}$$

$$G/R^2 = (O_b - O_a) \quad . \qquad \text{(A II 51)}$$

When flow through the nip between rolls is taken in the positive x direction, roll A turns in a counterclockwise direction and roll B in a clockwise direction. For this case the angular velocity of the rolls is related to the speed of rotation in revolutions per minute by:

$$O_a = \pi N_2/30 \, , \qquad \text{(A II 52)}$$

$$O_b = -\pi N_1/30 \, , \qquad \text{(A II 53)}$$

where N_1 and N_2 are the RPM of the slow and fast rolls respectively.

The equation of a dimensionless stream function is obtained by substitution of the constants and RPM expressions, given above, into (A II 47) and rearranging. This procedure gives,

$$\phi = \left[-\frac{60}{\pi R^2 (N_2 - N_1)}\right] = \frac{\pi^2}{\eta^2 + \zeta^2} - \frac{\eta^2 + \zeta^2}{4} - K'\left[\eta - \frac{4\eta^3}{(\eta^2 + \zeta^2)^2}\right] . \qquad \text{(A II 54)}$$

K is a function of roll speed ratio, r, defined by,

$$K = \frac{1}{2}\,\frac{r+1}{r-1} \quad . \qquad \text{(A II 55)}$$

Dividing Stream Line. The stream line which divides the flow associated with the fast roll from that associated with the slow roll is found by setting equation (A II 54) equal to zero and solving for η as a function of ζ. The equation has six solutions given by:

$$\eta = -1 \pm \sqrt{1-\zeta^2}\,, \qquad \text{(A II 56)}$$

$$\eta = +1 \pm \sqrt{1-\zeta^2}\,, \qquad \text{(A II 57)}$$

$$\eta = -2K \pm \sqrt{4K^2-\zeta^2}\,. \qquad \text{(A II 58)}$$

The zeros of principle interest are:

$$\eta = -1+\sqrt{1-\zeta^2}\,, \qquad \text{(A II 56-a)}$$

$$\eta = +1-\sqrt{1-\zeta^2}\,, \qquad \text{(A II 57-a)}$$

$$\eta = -2K+\sqrt{4K^2-\zeta^2}\,. \qquad \text{(A II 58-a)}$$

These three equations correspond to the top of the lower roll, B, the bottom of the upper roll, A, and to the dividing stream line respectively. The locations of the dividing stream lines relative to the roll surfaces, for roll speed ratios of 2 and 3, are shown in Fig. A-2.

Figure A-2. Location of Dividing Stream Lines on Inlet Side of Roll Nip

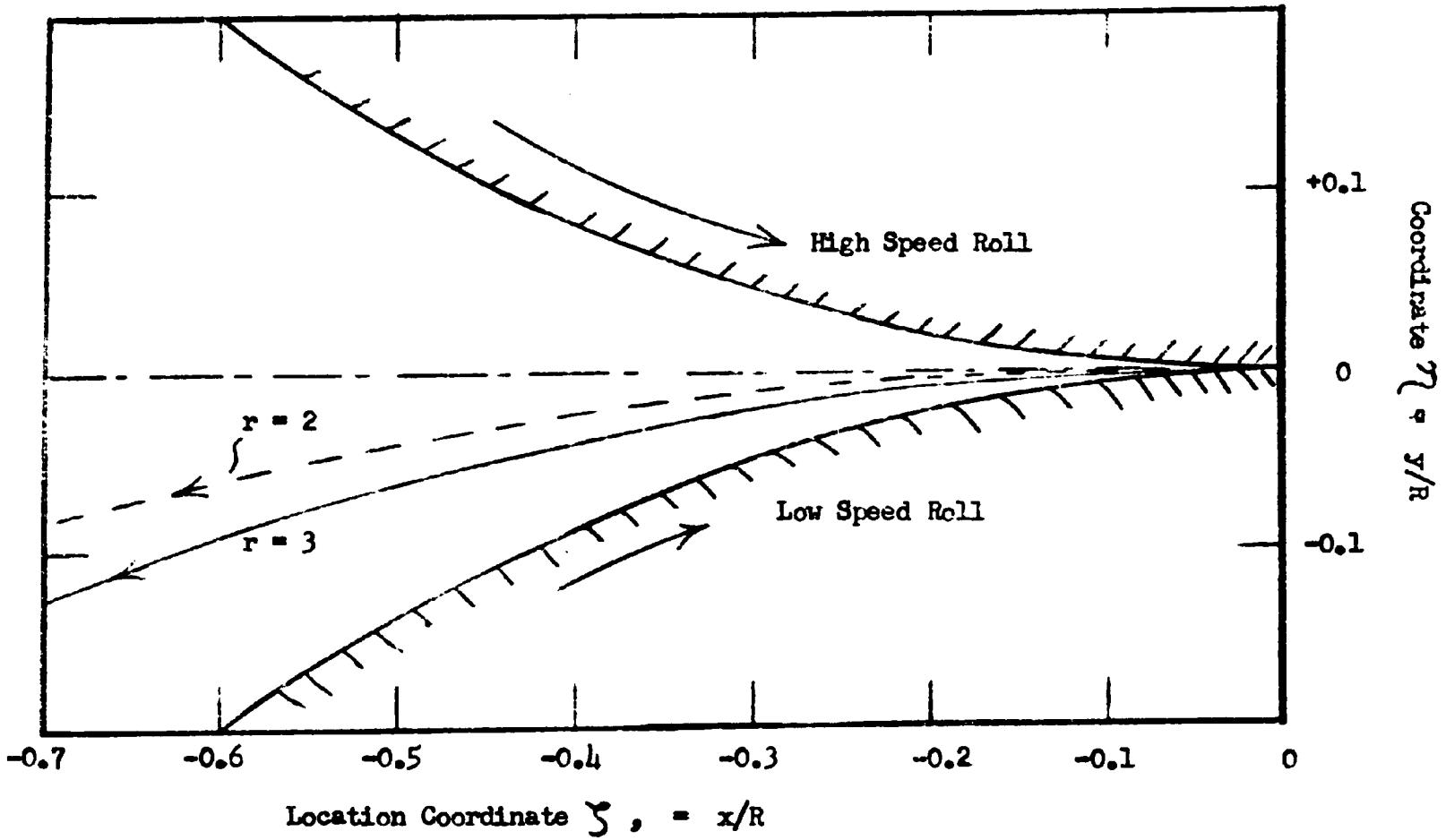

Derivatives of Stream Function. Appropriate differentiation of the stream function leads to expressions for the flow velocity components and the pressure gradients, as shown in equations (A II 1) through (A II 4). The results of these differentiations are shown here.

Velocity Components. The fluid velocity components, u and v, are found by differentiating equation (A II 40) with respect to y and x respectively.

$$u = -2A\left[\frac{y\,x^2}{(x^2+y^2)^2}\right] - 2\,C\,y - F - G\left[\frac{3x^2y^2 - y^4}{(x^2+y^2)^3}\right] . \qquad \text{(A II 59)}$$

$$v = -2A\left[\frac{x\,y^2}{(x^2+y^2)^2}\right] + 2\,C\,x - 4\,G\left[\frac{x\,y^3}{(x^2+y^2)^2}\right] . \qquad \text{(A II 60)}$$

Shear Rate. Shear rate equations are obtained by differentiation of equations (A II 59) and (A II 60).

$$\frac{\partial u}{\partial x} = -4A\left[\frac{x\,y\,(y^2-x^2)}{(x^2+y^2)^3}\right] - 12\,G\,x\,y^2\left[\frac{y^2-x^2}{(x^2+y^2)^4}\right] . \qquad \text{(A II 61)}$$

$$\frac{\partial u}{\partial y} = -2\,A\,x^2\left[\frac{x^2-3y^2}{(x^2+y^2)^3}\right] - 2C - 2G\,y\left[\frac{3x^4 - 8x^2y^2 + y^4}{(x^2+y^2)^4}\right] . \qquad \text{(A II 62)}$$

$$\frac{\partial v}{\partial x} = -2\,A\,y^2\left[\frac{y^2-3x^2}{(x^2+y^2)^3}\right] + 2C - 4G\,y^2\left[\frac{y^2-5x^2}{(x^2+y^2)^4}\right] . \qquad \text{(A II 63)}$$

$$\frac{\partial v}{\partial y} = -4\,A\,xy\left[\frac{x^2-y^2}{(x^2+y^2)^3}\right] - 12\,G\,xy^2\left[\frac{x^2-y^2}{(x^2+y^2)^4}\right] . \qquad \text{(A II 64)}$$

Pressure Gradients. Pressure gradients in the x and y directions are found from equations (A II 3) and (A II 4), or from equations 6 and 7 of the text, which are their equivalents.

$$\frac{\partial P}{\partial x} = \mu \left\{ -4 A y \left[\frac{y^4 - 2x^2y^2 - 3x^4}{(x^2 + y^2)^4} \right] - 6Q \left[\frac{y^6 - 5x^2y^4 - 5x^4y^2 + x^6}{(x^2 + y^2)^5} \right] \right\} . \tag{A II 65}$$

$$\frac{\partial P}{\partial y} = \mu \left\{ -4 A x \left[\frac{x^4 - 2x^2y^2 - 3y^4}{(x^2 + y^2)^4} \right] - 24 Q xy \left[\frac{x^4 - y^4}{(x^2 + y^2)^5} \right] \right\} . \tag{A II 66}$$

Pressure Distribution. Integration of equations (A II 65) and (A II 66) would lead to a solution of the pressure distribution in the fluid in regions other than the zone of roll tangency. An approximation of this pressure distribution is provided by the fact that along the path, y = 0, the pressure gradient in the x direction is independent of y. That is, equation (A II 65), up the center line between rolls, reduces to:

$$\frac{\partial P}{\partial x} = -6\mu Q x^{-4} \Big|_{y=0} . \tag{A II 67}$$

Integration of equation (A II 67) along the y = 0 path from the limits $-\infty$ to x gives,

$$P = 2 \mu Q x^{-3} + \text{const.} \tag{A II 68}$$

The constant is the value of the pressure at $y = 0$, $x = -\infty$.

Application to Roll Mill. The bank of fluid behind the feed nip of a roll mill is finite in extent, contrary to the assumption of an infinite fluid body employed in the derivation of Frazer's equations. Consideration of the pressure distribution indicated by equation (A II 68) shows that the greatest portion of the pressure rise is found between x equal to -R and x equal to zero. For this reason it is believed that the pressure distribution along the center line of the bank of fluid can be approximated by integrating equation (A II 67) from the location of the free fluid surface to a given point x, along the path, y = 0. When the free surface is located at x = -R, and when the value of G from equation (A II 44) is substituted into (A II 67), the integration gives,

$$P = -\frac{\pi}{15}\mu (N_1 + N_2)\left[\frac{R^3}{x^3} + 1\right] . \qquad \text{(A II 69)}$$

Adding the hydrostatic pressure of the fluid head in the bank, and converting to dimensionless variables, the final bank pressure equation is obtained.

$$P = R\rho\left[\zeta + 1\right] - \frac{\pi}{15}(N_1 + N_2)\mu\left[\left(\frac{1}{\zeta}\right)^3 + 1\right], \qquad \text{(A II 70)}$$

where $\zeta = x/R$.

The sign of ζ is negative in the inlet or bank region of the mill.

APPENDIX III

NIP STAGNATION POINT

The stagnation point is that point in the nip inlet beyond which all fluid moves in the forward direction, and behind which part of the fluid is rejected into the bank. It is located at the point where both shear rate, du/dy and velocity, u , are equal to zero.

Equations 14 and 16 express shear rate and velocity as follows:

$$du/dy = \frac{1}{\mu} \frac{dP}{dx} y + C_1 = 0 \quad , \qquad \text{(A III 1)}$$

$$u = \frac{1}{\mu} \frac{dP}{dx} \frac{y^2}{2} + C_1 y + C_2 = 0 \quad . \qquad \text{(A III 2)}$$

Solution of (A III 2) by the quadratic equation gives,

$$y_s = \frac{- C_1 \pm \sqrt{C_1^2 - 2 \frac{C_2}{\mu} \frac{P}{x}}}{\frac{1}{\mu} \frac{dP}{dx}} \quad . \qquad \text{(A III 3)}$$

From (A III 1),

$$y_s = - \frac{C_1 \mu}{dP/dx} \quad . \qquad \text{(A III 4)}$$

Equations (A III 3) and (A III 4) are equated and the resulting expression is simplified to give,

$$C_1^2 - 2 \frac{C_2}{\mu} \frac{dP}{dx} = 0 \quad . \qquad \text{(A III 5)}$$

Substitution for C_1, C_2 and dP/dx from equations 20 , 18 , and 32, and reducing with the use of equation 34 gives;

$$0 = \left(\frac{U_2 - U_1}{h_s}\right)^2 - \left[\frac{12 U_t}{h_s^2}\right]\left[1 - \frac{h^*}{h_s}\right]\left[\frac{U_t}{2} - \frac{3}{4} U_t \left(1 - \frac{h^*}{h_s}\right)\right] \quad . \qquad \text{(A III 6)}$$

Further simplification yields,

$$0 = \left[(U_2-U_1)^2 + 3\,U_t^2\right] h_s^2 \quad -(12U_t^2\, h^*)\, h_s + 9\,U_t^2\, h^{*2} . \qquad \text{(A III 7)}$$

Equation (A III 7) is solved for h by the quadratic equation, which after reduction gives,

$$h_s = \frac{3\,U_t^2 \pm 3\,U_t \sqrt{U_t^2 - (U_1^2 + U_1U_2 + U_2^2)}}{2\,(U_1^2 + U_1U_2 + U_2^2)}\, h^* . \qquad \text{(A III 8)}$$

Equation (A III 8) can be reduced to a function of the roll speed ratio r, and h^*, by using the relationships,

$$U_2 = r\,U_1 , \qquad \text{(A III 9)}$$

and

$$U_t = U_1\,(1+r),$$

giving;

$$h_s = \frac{3}{2}(1+r)\,\frac{(1+r \pm \sqrt{r})}{1+r+r^2}\, h^* . \qquad \text{(A III 10)}$$

Equation (A III 10) may be written,

$$h_s = \alpha h^* , \qquad \text{(A III 10-a)}$$

where

$$\alpha = \frac{3}{2}(1+r)\,\frac{(1+r+\sqrt{r})}{(1+r+r^2)} .$$

The x coordinate of the inlet stagnation point is found by substitution of (A III 10-a) into equation 29 ;

$$\alpha h^* = h_o + \frac{x_s^2}{R} .$$

$$x_s = \sqrt{R\,(\alpha h^* - h_o)} . \qquad \text{A III 11)}$$

The y coordinate is found by substitution of equation (A III 10-a) into equation (A III 4), which gives,

$$y_s = \left(\frac{1}{6}\right)\frac{1-r}{1+r}\,\left(\frac{\alpha^2}{\alpha-1}\right)\, h^*, \qquad \text{(A III 12)}$$

or,

$$y_s = \beta\, h^* , \qquad \text{(A III 12-a)}$$

where

$$\beta = \frac{1}{6}\,\frac{(1-r)}{(1+r)}\,\frac{(\alpha^2)}{(\alpha-1)} .$$

APPENDIX IV

COMPUTER SOLUTION FOR FORCE AND FLOW RATE EQUATIONS

In order to make solution of the equations for nip force and flow rate practical from the standpoint of effort and time consumption, the equations were programmed for solution by the Royal-McBee, LGP-30, stored program, digital computer. This program was written to be used with the LGP-30 floating point program which automatically places decimal points.

Discussion of Program

The program consists of two principal divisions: calculation of point of minimum nip pressure, the assumed point of film split, from equations 9 and 33-a; and calculation of throughput rate and total force on rolls from equations 34 and 39. The program starts with an assumed value of minimum nip clearance; and, using data values of fluid viscosity and density, roll radius, slow roll rpm, and fast roll rpm, calculates the flow rate and nip force that would result. The program then subtracts a given decrement from nip clearance, and repeats the calculation. This repetition is continued until a nip clearance of zero is reached, when the program causes the machine to stop and await new data. Both starting values and decremental values of minimum nip clearance, in microns, are supplied as data. The transfer control button on the machine provides a choice of decremental values of nip clearance. When the button is "up" the decrement is always 10 microns. When the transfer button is depressed, the decrement is taken as the data value inserted at location 0462. The program requires four memory tracks of program and data, and an additional memory track for storage of intermediate results. After receiving data, the machine begins computation

and, in 10 seconds, prints out the calculated value of roll force due to the bank. This value is independent of nip clearance. The machine then begins computing the point of minimum nip clearance, or film split, x^* in equation 33a. This calculation requires approximately 90 seconds. The value of x^* in feet is printed followed almost immediately by Q, the throughput rate, in cu-ft/ft-sec. The force between rolls due to the nip is then calculated and printed, taking about 20 seconds. After nip force, the machine calculates and prints total roll force, reciprocal roll force, and nip clearance, in microns, in quick succession. These calculations constitute one point on a curve of roll force vs. throughput rate, roll force vs. nip clearance, or nip clearance vs. throughput rate. The machine then goes immediately to the next lower value of nip clearance and repeats the calculations. The data for a five point curve of force vs. production rate are calculated in approximately ten minutes compared with approximately 15 hours by desk calculator methods. A sample page of computer results for 6-inch diameter rolls, 102-305 rpm, with 161.3 poise fluid, is presented as Table XI. The results of intermediate calculations for these conditions at 100 microns clearance are shown in Table XII. The values shown in Table XII were obtained by use of an auxiliary computer program which causes the computer to print out the contents of the floating point accumulator after executing previously "tagged" operations.

Details of Program

The computer program is based on solution of equations 9, 33-a, and 39, given in the text. Equations 29 and 34 are auxiliary relationships employed in the program. Sub-routines for logarithm to base e

TABLE XI

Sample Table of Computer Results for Conditions of Run 64

Run 64 228-148 No. 8 Varnish
102-305 RPM 161.3 Poise
6-Inch Roll

Data Input

+045437!	1613000!	-0000000!	Viscosity
+075438!	9961000!	-0000000!	Sp Gr
+045439!	1020000!		N_1
	3050000!	-0000000!	N_2
+065441!	3000000!	-0000000!	R
+045444!	2000000!	-0000000!	h_o starting
+055462!	5000000!	-0000000!	h_o decrement

Results

.1416209 04 Bank Force, lb/ft

x* ft	Q cu-ft/ft-sec	Nip F/L lb/ft	Total F/L lb/ft	Total L/F ft/lb	h_o Microns
.6304466 02-	.4342818 02-	.7273607 03	.2143569 04	.4665116 03-	.2000000 03
.5370678 02-	.3236538 02-	.1252892 04	.2669101 04	.3746580 03-	.1500000 03
.4335518 02-	.2148470 02-	.2328822 04	.3745030 04	.2670205 03-	.1000000 03
.3047139 02-	.1071820 02-	.5629593 04	.7045802 04	.1419285 03-	.5000000 02

Table XII. Intermediate Computer Results

Instruction Executed	Accumulator Contents		
0005	.2500000	00	R, ft
0010	.1554613	02	
0013	.1399152	02	
0016	.4070000	03	
0019	.3367943	00	
0024	.3426882	02	
0027	.2869426	05	P_1 lb/ft^2
0030	.1414635	04	
0036	.1416209	04	F/L bank
0044	.2500000	01-	
0045	.2500000-	01-	
0049	.6249999	03-	
0051	.2500000	02-	
0053	.1000000	03	
0056	.3280833	03-	h_0 , ft
0058	.2828083	02-	h_1 , ft
0061	.8839909-	01	
0063	.3125760-	04	
0102	.8202082	04-	
0104	.9056624	02-	
0108	.2760465	02	
0112	.1223237-	01	
0118	.8521389-	02	
0122	.1979251-	06	
0131	.8696277-	02	
0134	.4295918	02-	first trial x*
0139	.1845492	04-	
0141	.7381967	04-	
0143	.2250028	00	
0146	.4019029	03-	
0149	.1068895	02	
0151	.7954670-	02	
0155	.4429096	01	
0159	.6113183	01	
0200	.4126450	01	
0211	.4507730	00	$\phi(x^*)$ 1st trial
0223	.4507730	00	
0225	.4295918	02-	
0228	.4300214	02-	x^* 2d trial
0139	.1849184	04-	
0141	.7396736	04-	
0143	.2254530	00	
0146	.4020506	03-	
0149	.1069570	02	
0151	.7957593-	02	
0155	.4432967	00	
0159	.6118526	01	
0200	.4138320	01	
0211	.4021368	00	$\phi(x^*)$ 2d trial
0245	.4863620	01-	
0253	.4335728	02-	x^* 3d trial
0255	.4021368	00	
0257	.4300213	02-	
0259	.4335727	02-	
0139	.1879854	04-	
0141	.7519415	04-	
0143	.2291922	00	
0146	.4032774	03-	
0149	.1075123	02	
0151	.7981874-	02	
0155	.4464918	00	
0159	.6162625	01	
0200	.4237277	01	
0211	.2379656-	02-	$\phi(x^*)$ 3d trial
0245	.4045164	00	
0253	.4335518	02-	x^* 4th trial
0255	.2379656-	02-	
0257	.4335727	02-	
0259	.4335518	02-	
0139	.1879672	04-	
0141	.7518689	04-	
0143	.2291701	00	
0146	.4032702	03-	
0149	.1075090	02	
0151	.7981731-	02	
0155	.4464730	00	
0159	.6162366	01	
0200	.4236690	01	
0211	.0000000	00	$\phi(x^*)$ 4th trial
0302	.2148470	02-	Q
0309	.8324128	00	
0316	.6616544	01	
0318	.2563543	04	
0321	.2266149-	05	
0323	.7076572	05	
0326	.8656326-	05	
0331	.8854302	05	
0340	.6241420-	03	
0343	.3535964	03	
0352	.1758454	04	
0355	.1008175	03-	
0363	.8820009	02-	
0402	.3058093	01-	
0409	.1402946-	04	
0420	.3745030	04	F/L total
0428	.5000000	02	new h_0
0056	.1640416	03-	Starting new point
0058	.2664041	02-	h_1 , ft
0061	.9384238-	01	
0063	.3522557-	04	
0102	.4101041	04-	
0104	.6404000	02-	

and arc tangent are required in addition to the basic floating point sub-routine with square root and data input-output routines.

Bank Force. The computer program first converts data from the convenient input units to consistent engineering units, i.e. radius from inches to ft., nip clearance from microns to ft., viscosity from poise to lb-sec/ft^2, density from specific gravity to lb/cu-ft, and roll rpm to surface velocity in ft/sec. The force due to the bank region is then calculated and printed in the portion of the program from locations 0019 to 0036, using the first two terms of equation 39.

Point of Minimum Pressure. For convenience in computer solution, equation 33-a was rearranged in the following manner:

$$\frac{2}{3}\frac{ho}{U_t}\left(\frac{P_1-P^*}{\mu}\right) - 2\left(\frac{x_1}{h_1} + \sqrt{\frac{R'}{h_o}}\tan^{-1}\frac{x_1}{\sqrt{Rh_o}}\right)$$

$$+h^*\left[\frac{x_1}{h_1^2} + \frac{3}{2h_o}\left(\frac{x_1}{h_1} + \sqrt{\frac{R'}{h_o}}\tan^{-1}\frac{x_1}{\sqrt{Rh_o}}\right)\right]$$

$$+\frac{1}{2}\sqrt{\frac{R'}{h_o}}\tan^{-1}\frac{x^*}{\sqrt{Rh'_o}} - \frac{3}{2}\sqrt{\frac{R}{h_o}}\left(\tan^{-1}\frac{x^*}{\sqrt{Rh_o}}\right)\left(\frac{x^{*2}}{Rh_o}\right) - \frac{3}{2}\frac{x^*}{h_o}$$

$$+\frac{x^*}{h^*} = 0 \qquad \text{(A IV 1)}$$

The first two terms and the major portion of the third term of (A IV 1) are independent of x^*, and may be calculated once for each set of data. Since the equation is solved by an iteration process, the terms involving x^* and h^* must be recalculated for each trial value of x^*. The pressure, P_1, at the nip inlet ($x_1 = -0.1R$) is calculated from equation 9 in which ζ is set equal to -0.1, in program locations 0019-0027. The minimum pressure, P^*, is taken as zero, but could be any value if

a more accurate knowledge of the cavitation threshold pressure of the fluid were known. In locations 0038 through 0134, the program computes constant values used in equation (A IV 1) and obtains a first estimate of the value of x^* from the relationship,

$$\text{1st trial } x^* = 0.47434 \sqrt{Rh_o} \qquad \text{(A IV 2)}$$

Steps 0135 and 0136 set to zero a counter for number of trial x^* calculations completed. Steps 0137 through 0211 calculate the remaining terms of (A IV 1), giving a term, $\phi(x)$, for the sum of left hand terms of (A IV 1). The trial counter is incremented by 1 in steps 0212 through 0214; and in steps 0215 through 0242, the value of $\phi(x)$ is tested for equality to zero. If $\phi(x)$ is not less than $1x10^{-5}$ or greater than $-1x10^{-5}$, a second estimate of x^* is obtained, and the routine returns to step 0137 for calculation of a new value of $\phi(x)$. The logical sequence of steps 0215 through 0242 are summarized in the flow diagram of Table XIII.

In this program $\phi(x^*)$ is tested for magnitude between $\pm 10^{-5}$ and if greater or less, the trial x^* is increased or decreased respectively, by a factor of 1.001. After the second trial, values of x^* are improved by a linear interpolation routine in locations 0243 through 0260. This routine makes use of the two preceeding values of x^* and $\phi(x^*)$ to calculate a new value of x^* by the relationship,

$$x^*_{n-1} = x^*_n + \phi n \left[x^*_{n-1} - x^*_n\right] / \left[\phi_{n-1} - \phi_n\right], \qquad \text{(A IV 3)}$$

where subscript n refers to trial just completed, n-1 to preceeding trial, and n-1 to next trial.

In the example of Table XII, a satisfactory value of x^* was obtained in four tries, with $\phi(x^*)$ testing out to 0.0000000 on the fourth trial.

Table XIII

Logical Sequence for Testing $\phi(x^*)$ and Estimating Second x^* Trial Value

Location	Instruction	Result
0230	a0453	add 10^{-5}
0231	t0233	minus test
0232	u0261 (+)	$\phi(x^*)$ good
0233	e0526 (−)	count trial
0234	z0001 (not first)	test for first trial
0235	u0243	interpolate
0236	b0504 (first)	bring $\phi(x^*)$
0237	h0505	store $\phi(x^*)$
0238	b0558	bring (x^*)
0239	h0506	store (x^*)
0240	d0455	$(x^*)+1.001$
0241	h0558	store new (x^*)
0242	u0137	return for new trial

Location	Instruction	Result
0215	b0504	bring $\phi(x^*)$
0216	t0230 (−) (+)	minus test
0217	s0453	subtract 10^{-5}
0218	t0261 (−)	$\phi(x^*)$ good
0219	e0526 (+)	count trial
0220	z0001 (not first)	test for first trial
0221	u0243	interpolate
0222	b0504 (first)	bring $\phi(x^*)$
0223	h0505	store $\phi(x^*)$
0224	b0558	bring (x^*)
0225	h0506	store (x^*)
0226	u0000	place (x^*)
0227	m0455	$(x^*)(1.001)$
0228	h0558	store new (x^*)
0229	u0137	return for new trial

Normally, from three to six trials were required, depending on operating data used. After a satisfactory value of x^* is obtained, it is printed.

Nip Flow Rate. The value of Q is calculated from equation 34 once x^* has been evaluated. This calculation takes three steps given by locations 0263, 0300, and 0301. Since a computer track runs from locations nn00 through nn63, location 0300 follows 0263.

Nip Force. The nip force is calculated by a straight forward calculation of the last four terms of equation 39. Use is made of many previously calculated partial results. This section of the program includes locations 0304 through 0416. The nip force is printed at instruction 0417, the bank force is added, and total force is printed by instruction 0419. The reciprocal of total force is calculated and then printed at 0423. The value of minimum nip clearance, in microns, in use is then brought to the accumulator and printed. Depending on whether the transfer control is up or down, the contents of data locations 0459 or 0462 are subtracted from the nip clearance. Location 0459 contains the value 10, which must not be changed since it is used in other steps as well. Location 0462 contains any desired value of clearance decrement.

Completion of Program. After subtracting the decrement and storing the new minimum nip clearance, the value of 1.0 is subtracted, and a minus test is made of the result. If the result is minus, the program exits from floating print and returns to the initial location to call for new data. If the result of subtraction of 1 from h_o is not negative, the program returns to location 0054 to begin computation of flow rate and force for the new clearance. The program may always be entered

at location 0000 since all initialization procedures are accomplished in early stages of the program.

The program, data locations, and intermediate data storage locations follow as part of this Appendix. Note that the program input code is written for insertion of the program starting at location 5000, with floating point interpretative routine starting at location 1100. A summary of the Floating Point Interpretative System, Floating Point Orders, and Data Input and Output Format, are also appended.

Program for the Computation of Force and Rate of Flow Between Rotating Cylinders

This program is used with Floating Point sub-routine 24.0, Input-output routine 11.3 - 12.3, Arctangent routine 16.2, and Logarithm routine 18.1. The program uses the transfer control to select decrements of minimum nip clearance; transfer up, decrement is 10 microns, transfer down, the decrement is selected from data location 0462.

Program Input Code	Location	Instruction	Contents of address
/0005000			
;0005000	0000	xR1100	
	01	xu1100	
	02	xi0000	
	03	b0441	R, in.
	04	d0460	12
	05	h0534	R, ft
	06	xu0000	
	07	m0438	sp gr
	08	xu0000	
	09	m0452	62.4
	10	h0541	$R\rho$
	11	xu0000	
	12	m0445	0.9
	13	h0535	$0.9R\rho$
	14	b0439	N_1
	15	a0440	N_2
	16	h0536	N_t
	17	p0437	poise
	18	m0461	viscosity conversion
	19	h0537	μ
	20	xu0000	
	21	m0536	N_t
	22	xu0000	
	23	m0534	R
	24	h0539	$R \mu N_t$
	25	m0446	$999\pi/15$
	26	a0535	$0.9R\rho$
	27	h0540	P_1
	28	p0539	$R \mu N_t$
	29	m0448	$197.1\pi/15$
	30	h0542	$197.1\pi/15\ R \mu N_t$
	0031	p0541	$R\rho$

Location	Instruction	Contents
0032	m0534	R
33	xu0000	
34	m0447	
35	a0542	
36	h0543	F/L bank
37	xp0000	
38	p0534	
39	m0536	
40	xu0000	
41	m0449	
42	h0544	U_t
43	b0534	
44	d0459	
45	xt0000	make minus
46	h0545	x_1
47	xu0000	
48	m0545	
49	h0546	x_1^2
50	d0534	
51	h0547	x_1^2/R
52	b0444	h_o
53	h0443	working h_o
54	p0443	
55	m0450	
56	h0548	h_o, ft
57	a0547	
58	h0549	h_1
59	b0545	
60	d0549	
61	h0550	x_1/h_1
62	d0549	
0063	h0551	x_1/h_1^2
0100	p0534	
01	m0548	
02	h0520	Rh_o
03	xr0000	take sq rt
04	h0552	$\sqrt{Rh_o}$
05	xu0000	
06	d0548	
07	xr0000	take sq rt
08	h0553	$\sqrt{R/h_o}$
09	b0545	
10	d0552	
11	xa0000	take $\tan^{-1}$
12	h0554	$\tan^{-1} x_1/\sqrt{Rh_o}$
13	xu0000	
14	m0553	
15	a0550	
16	xu0000	
17	m0457	
18	h0555	
19	m0456	
20	d0548	
21	a0551	
22	h0556	
23	b0442	
24	s0540	
25	d0537	
26	d0456	
27	d0544	
28	xu0000	
29	m0548	
30	a0555	
0131	h0557	

Location	Instruction	Contents
0132	p0552	
33	m0451	
34	h0558	trial x*
35	e0137	initialize counter
36	y0526	
37	xu0000	x* to mult
38	m0558	
39	h0559	
40	d0534	
41	h0560	
42	d0548	
43	h0561	
44	b0560	
45	a0548	
46	h0562	h*
47	xu0000	h* to mult
48	d0562	
49	h0563	x*/h*
50	m0556	h* times (0556)
51	h0527	
52	b0558	
53	d0552	
54	xa0000	take $\tan^{-1}$
55	h0501	
56	xu0000	
57	m0553	
58	d0457	
59	h0502	
60	xu0000	
61	m0561	
62	xu0000	
0163	m0458	

Location	Instruction	Contents
0200	h0503	
01	b0456	
02	d0548	
03	xu0000	
04	m0558	
05	xy0000	change sign
06	a0527	
07	s0503	
08	a0563	
09	a0502	
10	s0557	
11	h0504	ϕ (x*)
12	e0526	
13	xi0001	increment count
14	y0526	
15	b0504	
16	t0230	
17	s0453	
18	t0261	
19	e0526	
20	xz0001	test count
21	u0243	
22	b0504	
23	h0505	
24	b0558	
25	h0506	
26	xu0000	
27	m0455	
28	h0558	new x*
29	u0137	
30	a0453	
0231	t0233	

Location	Instruction	Contents	Location	Instruction	Contents
0232	u0261		0300	m0544	
33	e0526		01	d0457	
34	xs0001	test count	02	h0509	Q
35	u0243		03	xp0000	print Q
36	b0504		04	xu0000	
37	h0505		05	m0456	
38	b0558		06	d0548	
39	h0506		07	xy0000	
40	d0455		08	a0544	
41	h0558	new x*	09	h0510	
42	u0137		10	b0537	
43	b0505		11	d0548	
44	s0504		12	xu0000	
45	h0507		13	m0458	
46	b0506		14	xu0000	
47	s0558		15	m0509	
48	d0507		16	h0511	
49	xu0000		17	m0510	
50	m0504		18	h0512	
51	xy0000	change sign	19	xu0000	
52	a0558		20	m0550	
53	h0508		21	h0513	
54	b0504		22	m0553	
55	h0505		23	h0514	
56	b0558		24	xu0000	
57	h0506		25	m0554	
58	b0508		26	h0515	
59	h0558	new x*	27	p0511	
60	u0137		28	m0551	
61	b0558		29	s0513	
62	xp0000	print x*	30	s0515	
0263	p0562		0331	h0516	

Location	Instruction	Contents	Location	Instruction	Contents
0332	b0562		0400	p0545	
33	d0549		01	m0554	
34	xn0000	take ln	02	h0523	
35	xu0000		03	p0558	
36	m0512		04	m0501	
37	xu0000		05	s0523	
38	m0534		06	a0522	
39	d0457		07	xu0000	
40	h0517		08	m0514	
41	b0454		09	h0524	
42	d0549		10	b0558	
43	h0518		11	s0545	
44	b0454		12	xu0000	
45	d0562		13	m0516	
46	s0518		14	a0519	
47	xu0000		15	a0524	
48	m0511		16	a0517	
49	xu0000		17	xp0000	print F/L nip
50	m0534		18	a0543	
51	d0457		19	xp0000	print total F/L
52	h0519		20	h0525	
53	b0520		21	b0454	
54	a0559		22	d0525	
55	h0521		23	xp0000	print total L/F
56	b0520		24	b0443	
57	a0546		25	xp0000	print working h.
58	d0521		26	800t0434	transfer control
59	xn0000	take ln	27	s0459	
60	xu0000		28	h0443	new h.
61	m0552		29	s0454	1.0
62	d0457		30	t0432	
0363	h0522		0431	u0054	go to new point

Location	Instruction	Contents
0432	xe0000	exit floating point
33	u0000	return for new data
34	s0462	alternate decrement h_o
35	u0428	
36	xs0000	

DATA

0437	Viscosity	Poise
38	specific gravity	
39	N_1, slow roll rpm	
40	N_2, fast roll rpm	
41	R, roll radius, inches	
42	P*, cavitation pressure	
43	working h_o, changes	
44	Starting h_o, microns	
45	0.900000	
46	209.2300	$999\pi/15$
47	0.4050000	
48	41.28053	$197.1\ \pi/15$
49	0.1047198	$\pi/30$
50	3.280833×10^{-6}	ft/microm
51	0.47434	factor for trial x*
52	62.40000	lb/cu-ft for sp gr = 1
53	1.0×10^{-5}	
54	1.000000	
55	1.001000	
56	1.500000	
57	2.000000	
58	3.000000	
59	10.00000	
60	12.00000	
61	2.088000×10^{-3}	$lb\text{-}sec/ft^2$ per poise
62	decrement h_o	

Location of Results of Intermediate Calculations

Location	Contents of Location
0500	----
01	$\tan^{-1}(x^*/\sqrt{Rh_\circ})$
02	$1/2\sqrt{R/h_\circ}\ \tan^{-1}(x^*/\sqrt{Rh_\circ})$
03	$3/2\ x^{*2}/Rh_\circ\sqrt{R/h_\circ}\tan^{-1}(x^*/\sqrt{Rh_\circ})$
04	$\phi(x^*)_n$
05	$\phi(x^*)_{n-1}$
06	x^*_{n-1}
07	$\phi_{n-1} - \phi_n$
08	x^*_{n+1}
09	Q
10	$U_t - 1.5Q/h_\circ$
11	$3\mu Q/h_\circ$
12	$(3\mu/h_\circ)(U_t - 1.5Q/h_\circ)$
13	$(x_1/h_1)(3\mu/h_\circ)(U_t - 1.5Q/h_\circ)$
14	$(\sqrt{R/h_\circ})(3\mu/h_\circ)(U_t - 1.5Q/h_\circ)$
15	$[\tan^{-1}(x_1/\sqrt{Rh_\circ})](\sqrt{R/h_\circ})(3\mu/h_\circ)(U_t-1.5Q/h_\circ)$
16	$(x_1/h_1^2)(3\mu Q/h_\circ)-(0513)-(0515)$
17	$(R/2)(0512)(\ln h^*/h_1)$
18	$1/h_1$
19	$(3\mu Q/h_\circ)(R/2)(1/h^* - 1/h_1)$
20	$Rh_\circ$
21	$Rh_\circ + x^{*2}$
22	$\frac{1}{2}\sqrt{Rh_\circ}\ \ln[(Rh_\circ+x_1^2)/(Rh_\circ+x^{*2})]$
23	$x_1\tan^{-1}(x_1/\sqrt{Rh_\circ})$
24	$(0514)[(x^*\tan^{-1}\ x^*/\sqrt{Rh_\circ})-(0523)+(0522)]$
25	F/L total
26	s0000 (counter for trials of x*)
27	$h^*\ \{(x_1/h_1^2)+(1.5/h_\circ)[(x_1/h_1)+(\sqrt{R/h_\circ}\tan^{-1}(x_1/\ Rh_\circ)]\}$
28	----
29	----
30	----
0531	----

Location	Contents of Location
0532	----
33	----
34	R ft
35	0.9 Rρ
36	N_t
37	μ lb-sec/ft^2
38	μN_t
39	$R \mu N_t$
40	$0.9R\rho+(999\pi/15)\mu N_t = P_1$
41	R ρ
42	$(197.1\pi/15)(R \mu N_t)$
43	F/L bank
44	U_t
45	x_1
46	$(x_1)^2$
47	$(x_1)^2/R$
48	$h_\circ$ ft
49	h_1
50	x_1/h_1
51	$x_1/(h_1)^2$
52	$\sqrt{Rh_\circ}$
53	$\sqrt{R/h_\circ}$
54	$\tan^{-1}(x_1/\sqrt{Rh_\circ})$
55	$2\left[(x_1/h_1)+(\sqrt{R/h_\circ})\tan^{-1}(x_1/\sqrt{Rh_\circ})\right]$
56	$(x_1/h_1{}^2)+(1.5/h_\circ)\left[(x_1/h_1)+(\sqrt{R/h_\circ})\tan^{-1}(x_1/\sqrt{Rh_\circ})\right]$
57	$h_\circ(P^* - P_1)/(1.5\mu U_t)$ + (0555)
58	x* trial
59	x^{*2}
60	x^{*2}/R
61	$x^{*2}/Rh_\circ$
62	h*
0563	x*/h*

FLOATING POINT INTERPRETIVE SYSTEM

INPUT:

Floating point numbers on tape or in memory, or numbers in the pseudo registers resulting from previous operations.

CALLING SEQUENCE:

Loc.	Inst.	Add	
α	R	Lo	
$\alpha + 1$	U	Lo	
$\alpha + 2$	.	.	
$\alpha + 3$	.	.	Floating point operations
.	.	.	
.	.	.	
.	.	.	
$\alpha + n$	E	0000	"Exit" instruction
$\alpha + n + 1$	etc.		Resume fixed point operation.

INTERNAL NUMBER FORMAT:

A standard floating point number as carried in memory consists of sign and 24 bits for characteristic (x) and sign and 5 bits for the exponent (y). However, all intermediate calculations (i.e., numbers appearing only in accumulator and multiplier registers) are carried with 30 bits of characteristic and 30 bits of exponent. Each factor of any calculation must be in standard floating point form. ($N = x.2^y$; $.5 \leq |x| < 1$. or $x = 0$; $-31 \leq y \leq 31$). Numbers appearing in accumulator M registers are in the range $.25 \leq |x| < .5$ or $x = 0$.

The standard floating point binary form:

X	.XX.....XX	X	XXXXX
Sign of Characteristic 0 for plus 1 for minus	Characteristic 24 bits.	Sign of exponent 0 for plus 1 for minus	Exponent 5 bits. Power of2

DATA TAPE PREPARATION:

1. All characters of the I.D. word should be punched. e.g. -012040' must contain eight characters including the stop code. The stop code (') must be the last character punched.
2. Punch only those I.D. words appearing on the load sheet. Do not punch the stop code if an I.D. word is not present.
3. The sign and any leading zeros of a positive number need not be punched. To enter all zeros merely punch a stop code. The sign and all seven digits of a negative number must be punched.
4. Be sure to check each load sheet to see whether an additional stop code should follow the last number punched.

EXIT:

The interpretive routine exits to the first location following the E 0000 instruction.

SUBROUTINE MEMORY RELATIONSHIPS:

The arithmetic, logical, address modification, and auxiliary instructions have been coded as a unified group on a single set of coding sheets ("Floating Point Interpretive Routine"). A single corresponding tape has been punched for this set. In many instances the programmer will wish to use just this part of the floating point system; if so, only this tape need be stored in the memory. This will leave 54 tracks for program instructions and data in contrast to 41 when the entire system is used.

In other cases the Input-Output and/or function evaluation routines may be needed. Only those routines actually used need be stored on the drum. These required routines must be stored on the drum in the following relationship:

Program	Routine	Start Fill	Set Modifier	No. of Tracks
24.0	Interpretive (Includes $\sqrt{\ }$)	Lo	Lo	10
11.3-12.3	Input-Output	Lo + 1000	Lo + 1000	6
14.1	Sine-Cosine	Lo + 1600	Lo	2 1/2
16.2	Arctangent	Lo + 1832	Lo	1 1/2
18.1	Logarithm	Lo + 2000	Lo	1
17.1	Exponential	Lo + 2100	Lo	2

All track 63 except sectors 10, 15, 16, 18, 23, 27, 29, 34, 36, 40, 47 thru 50, 52, 56 thru 58, 60 and 63 is used for temporary storage by various parts of the system. Therefore Lo should be set such that no part of the floating point system used is stored in track 63.

PROGRAM STOPS:

Loc.	Order	Meaning and Remedy
Lo + 0654	Z 0000	Programmed stop. Depress "start" to continue.
Lo + 0556	H XXXX or C XXXX	Exponent is too large. Location of instruction being executed is in the real accumulator. Start to continue.
Lo + 0556	R 0000	Accumulator is negative. Location of instruction being executed is in the real accumulator. Start to continue.
Lo + 1152	I 0000	Input data has too large an exponent. A start will store a zero for that word and continue with next word on tape.
Lo + 0612	D XXXX	Division by zero or a non-floated number. Do not continue.
Lo + 2005	N 0000	Accumulator is ≤ 0. A start continues with an answer of zero.
Lo + 2028 or Lo + 2030	N 0000	Accumulator exponent is not in range. Do not continue.

NOTES:

1. The floating point system may be left and re-entered without destroying the contents of the registers.

2. The exponent of a number in a register which is to be stored in memory must be less than +32, or a range error will result. If it is less than -31, the number is replaced by zero.

3. It is strongly suggested that the initial location occupied by the system be the 00 sector of a track. If it is not, many of the addresses that refer to track 63 are not optimum.

4. It is also suggested that the entire system be placed in memory and punched out in parts by program 13.1. Then the parts needed may be loaded by program 10.1 and each check sum may be verified.

5. All instructions with zero addresses have special interpretations. None of these zero addresses refer to memory location "zero", (0000), but rather designate a special interpretive instruction. This floating point system employs sixteen such special instructions. Furthermore, the two shift instructions (D 000y, N 000y) utilize the next nine addresses (0001 through 0009); hence the divide and reset and multiply instructions cannot use these addresses.

DATA INPUT FORMAT

Data input is accomplished by reading a prepunched decimal tape. The tape consists of groups of the following:

1. One identification word. This consists of a sign and two decimal digits for P, followed by four decimal digits for initial location to begin storing the converted floating point binary numbers.

2. Signed decimal numbers. Each number consists of a sign (if negative) and seven decimal digits.

3. A "minus zero" word. This consists of a minus sign followed by seven zeros. This number is not stored in memory, but is used by the routine to signal the end of the group.

A stop code must follow the last "minus zero" word. This is interpreted as a "zero" identification (I.D.) word since it follows the "minus zero" data word. It causes the system to exit from the subroutine, carriage return, and interpret the instruction following the I 0000 instruction.

P denotes the number of decimal places following the point in the seven digit field. $-3 \leq P \leq 15$. Internally the exponent must be in the range $-31 \leq$ Exp. ≤ 31.

DATA OUTPUT FORMAT

The printed output consists of a decimal point followed by seven decimal digits of the characteristic and its sign. Following the sign there are two spaces followed by the exponent and its sign (if the sign is negative).
e.g. .5060000- 02 is -50.60000. A tab is executed after printing.

FLOATING POINT ORDERS

Thirty-three orders are available. The list of these orders and their meaning follows. In the following exposition the term "accumulator" refers to the two memory cells of the floating point accumulator as defined above.

A. Arithmetic Instructions
Memory location XXXX is the address of one floating point number in standard form as defined in Part 2.

1. B XXXX. Bring
The contents of memory location XXXX replace the contents of the accumulator.

2. A XXXX. Add
The contents of the accumulator plus the contents of memory location XXXX replace the contents of the accumulator.

3. S XXXX. Subtract
The contents of the accumulator minus the contents of memory location XXXX replace the contents of the accumulator.

4. D XXXX. Divide
The contents of the accumulator divided by the contents of memory location XXXX replace the contents of the accumulator.

5. P XXXX. Place
The contents of memory location XXXX replace the contents of the M register.

6. M XXXX. Reset and Multiply
The contents of the M register multiplied by the contents of memory location XXXX replace the contents of the accumulator.

7. N XXXX. Cumulative Multiply
The contents of the M register multiplied by the contents of memory location XXXX and added to the contents of the accumulator replace the contents of the accumulator.

8. D 000y. Right Shift
The contents of the accumulator divided by 2^y replace the contents of the accumulator. The contents of accumulator remain in floating point form.
$0 \leq y \leq 9$

9. M 000y. Left Shift
The contents of the accumulator multiplied by 2^y replace the contents of the accumulator. The contents of accumulator remain in floating point form.
$0 \leq y \leq 9$

10. H XXXX. Hold
Place the contents of the accumulator in memory location XXXX.

11. C XXXX. Clear
Place the contents of the accumulator in memory location XXXX and set the accumulator to zero.

B. Logical or Transfer Instructions

12. U XXXX. Unconditional Transfer
The next instruction to be interpreted is in memory location XXXX. This order cannot be used to exit from the floating point interpretive system.

13. T XXXX. Test
The next instruction to be interpreted is in memory location XXXX if the accumulator is negative. Otherwise the first successive location will be interpreted.

14. 800T XXXX. Transfer Control
The next instruction to be interpreted will be in memory location XXXX if either the accumulator has a negative characteristic or the transfer control switch is down. Otherwise the first successive location will be interpreted.

C. Address Modification Instructions
Location XXXX implies a fixed point address.

15. E XXXX. Enter
The address portion of memory location XXXX replaces the contents of the address accumulator.

16. I XXXX. Increment
The address accumulator is incremented by the address XXXX. This order can be used to decrement the address accumulator by complementing the address portion of the I XXXX order.

17. Y XXXX. Store Address
The address portion of the address accumulator replaces the contents of the address portion of memory location XXXX.

18. Z XXXX. Zero Test
The address of the "Z" instruction is subtracted from the contents of the address accumulator. If the result is not zero, the first successive instruction is interpreted. If the result is zero, the first successive instruction is skipped and the second successive instruction is interpreted.

D. Auxiliary Instructions

19. R XXXX. Return Address
The location of this instruction is increased by 2 and is stored in the address portion of memory location XXXX.

20. U 0000. Reverse Registers
The contents of the M register and accumulator are interchanged.

21. B 0000. Set Sign Plus
The sign of the accumulator is made positive if not already so.

22. T 0000. Set Sign Minus
The sign of the accumulator is made negative if not already so.

23. Y 0000. Change Sign
The sign of the accumulator is reversed.

24. Z 0000. Stop
Computation is halted unless break point switch No.16 is down. Depressing the start button causes the next instruction to be interpreted.

25. E 0000. Exit
Exit from the floating point interpretive system. Control is returned to the location following the location of the E 0000 instruction.

E. Input-Output Instructions

26. I 0000. Input
Control is transferred to a floating point data input subroutine which reads decimally punched numbers on tape, converts them to floating binary, and stores them. The next instruction is interpreted after the proper exit code has been read from tape. See Section V, Part 1 for tape format and input details.

27. P 0000. Print
Print the contents of the accumulator. The contents of the accumulator are not destroyed. See Section VI, Part 1 for Output format.

F. Function Evaluation Instructions

23. R 0000. Square Root
The square root of the contents of the accumulator replaces the contents of the accumulator

29. S 0000. Sine
The sine of the contents of the accumulator replaces the contents of the accumulator. The accumulator must be in radian measure.

30. C 0000. Cosine
The cosine of the contents of the accumulator replaces the contents of the accumulator. The accumulator must be in radian measure.

31. A 0000. Arctangent
The arctangent of the contents of the accumulator replaces the contents of the accumulator. Output is in radian measure.

32. N 0000. Natural Logarithm
The natural logarithm of the contents of the accumulator replaces the contents of the accumulator.

33. H 0000. Exponential
The quantity e^x replaces the contents of the accumulator, where x is initially the contents of the accumulator.

APPENDIX V

STATISTICAL ANALYSIS OF NIP FLOW RATE RESULTS

A statistical study of the agreement between computed values and experimental values of nip flow rate was performed. The magnitude of the absolute deviations was observed to be nearly proportional to the level of flow rate studied, and for that reason, the analysis was performed on the logarithms of the flow rate values. Variance of the logarithms was independent of flow rate magnitude.

The nomenclature and methods used in this analysis follow those described by Volk (38). The logarithm of the measured flow rate is designated as E and that of the theoretical flow rate as T. The symbol $\hat{E}$ represents a value of log flow rate calculated from a regression equation of the form,

$$\hat{E} = a + bT.$$

Because of the appearance of the results shown in Fig. 20, there is reason to suspect that the behavior of the No. 8 varnish and the SAIB in the 6-inch roll experiments was different from that of the other materials tested. For this reason, the No. 8 varnish and SAIB results were given special consideration in the statistical treatment, and separate analyses were made of the data with and without these materials.

The first step in the analysis was to calculate the sums of squares of the experimental and theoretical flow rate logarithms for various arrangements of the data. To simplify the arithmetic the data were coded by adding 5 to each logarithm. Thus the logarithm of 0.4858 $\times 10^{-3}$ cu-ft/ft-sec, which is actually 1.68646-5, was expressed as 1.68646.

Values listed in Table XIV based on these coded values were calculated in the following manner:

n = number of data points,

ΣE = total of coded logs of observed flow rates,

ΣT = total of coded logs of theoretical flow rates,

$$\Sigma E^2 = E_1^2 + E_2^2 + \ldots E_n^2$$

$$\Sigma T^2 = T^2 + T_2^2 + \ldots T_n^2$$

$$\Sigma ET = E_1T_1 + E_2T_2 + \ldots E_nT_n$$

$$\bar{E} = \frac{\Sigma E}{n}$$

$$\bar{T} = \frac{\Sigma T}{n}$$

$$\Sigma' E^2 = \Sigma(E-\bar{E})^2 = \Sigma E^2 - \frac{(\Sigma E)^2}{n}$$

$$\Sigma' T^2 = \Sigma(T-\bar{T})^2 = \Sigma T^2 - \frac{(\Sigma T)^2}{n}$$

$$\Sigma' ET = \Sigma(E-\bar{E})\ (T-\bar{T}) = \Sigma ET - \frac{\Sigma E \Sigma T}{n}$$

b = slope = $\Sigma' ET / \Sigma' T^2$

$a = \bar{E} - b\bar{T}$ = intercept of coded logarithms

$a_c = a-5(1-b)$ = intercept of actual logarithms

$C^2 = b\Sigma' ET$

$$\Sigma' \hat{E}^2 = \Sigma(E-\hat{E})^2 = \Sigma' E^2 - \Sigma' C^2$$

$$r^2 = \Sigma' C^2 / \Sigma' E^2$$

$r = \sqrt{r^2}$ = correlation coefficient

$S^2(\hat{E}) = \Sigma' \hat{E}^2/n-2$ = variance of estimate, residual variance associated with "error".

$S(\hat{E})$ = standard deviation of estimate.

Table XIV

Regression Analysis of Experimental and Theoretical Roll Nip Flow Rate Logarithms

Source	Four Inch Roll	Six Inch Roll							Four inch, Six inch No 1 Varnish, Intermediate,	All Runs
		No 1 Varnish	Intermediate Fluids	No 8 Varnish	SAIB	No 1 Varnish Intermediate fluids	No 1 Varnish Intermediates No 8 Varnish	All Fluids Tested		
n	244	51	56	41	12	107	148	160	351	404
ΣE	342.79052	87.58534	111.04470	94.21691	31.83138	198.63004	292.84695	324.67833	541.42056	667.46876
ΣT	349.20093	82.93015	113.76028	106.58941	26.13791	196.69043	303.27984	329.41775	545.89136	678.61868
ΣE^2	524.40571	155.56182	227.55473	223.20634	85.19647	383.11655	606.32289	691.51936	907.52226	1215.92510
ΣT^2	550.33687	139.65726	237.89348	282.46318	57.06186	377.55074	660.01392	717.07578	927.88761	1267.41265
ΣET	536.54966	147.29240	232.17694	250.60817	69.60575	379.46934	630.07751	699.68326	916.01900	1236.23292
$\bar{E}$	1.40488	1.71736	1.98294	2.29797	2.65262	1.85636	1.97870	2.02924	1.54251	1.65215
$\bar{T}$	1.43115	1.62608	2.03143	2.59974	2.17816	1.83823	2.04919	2.05886	1.55525	1.67975
$\Sigma' E^2$	42.82645	5.11630	7.35963	6.69071	0.76007	14.38858	26.86792	32.66925	72.37633	113.16632
$\Sigma' T^2$	50.57749	4.80609	6.79703	5.35843	0.12934	15.98882	38.53648	38.85044	78.89224	127.50346
$\Sigma' ET$	45.96454	4.87151	6.59701	5.66870	0.27194	14.34198	29.97902	31.21573	73.97682	115.0528
$\Sigma' Q^2$	41.77232	4.93782	6.40288	5.99692	0.57176	12.66476	23.32184	25.08136	69.367657	103.81794
$\Sigma' \hat{E}^2$	1.05413	0.20848	0.95675	0.70179	0.18831	1.52382	3.54608	7.58789	3.00867	9.34838
b	0.90879	1.01361	0.97057	1.05790	2.10252	0.89700	0.77794	0.80348	0.93769	0.90235
a	0.10427	0.06915	0.01129	-0.45229	-1.9270	0.20745	0.3846	0.37499	0.08417	0.13643
a_c	-0.3518	0.1372	-0.1359	-0.1628	3.1990	-0.3076	-0.7257	-0.6076	-0.2274	-0.3518
r^2	0.975	0.959	0.870	0.895	0.75225	0.8941	0.86802	0.7677	0.95843	0.91755
r	0.988	0.980	0.933	0.946	0.867	0.946	0.932	0.876	0.979	0.958
$S^2(\hat{E})$	0.004355	0.004087	0.01772	0.01799	0.01883	0.01451	0.02429	0.04802	0.00862	0.02325
$S(\hat{E})$	0.0660	0.0639	0.133	0.134	0.137	0.120	0.156	0.219	0.0928	0.152

Precision of Flow Rate Theory

The precision of the theoretical prediction of flow rates is tested by calculating the sum of squares, mean square and root mean square deviations of the experimental from theoretical values. This was done separately for all of the points, the 4-inch roll points, and the 6-inch roll points with SAIB and No. 8 varnish runs excluded, and for the 4-inch roll points. Results are shown in Table XV.

Table XV

Deviation of Experimental Flow Rate Logarithms from Theory.

	Total	Less SAIB No 8	4-inch Roll
$\sum(E-T)^2 = \sum E^2 - 2\sum ET + \sum T^2$	10.87191	3.37187	1.64326
$\sum(E-T)^2/n$ = variance from theory	0.02691	0.009606	0.00674
$\sqrt{\sum(E-T)^2/n}$ = Standard deviation from theory	0.164	0.0980	0.0821
$\sum' E^2 - \sum(E-T)^2$	102.24441	69.00446	41.18319
$(\sum' E^2 - \sum(E-T)^2)/\sum' E^2 = r_T^2$	0.9035	0.9534	0.9616
r_T	0.951	0.976	0.981

These root mean square deviations correspond to 95% confidence limits of 1.966 x 0.164 = ± 0.322 for the logarithm of flow rate if all the fluids are considered, or ± 1.967 x 0.0980 = ± 0.19277 for the log of flow rate if the No. 8 varnish and SAIB on 6-inch rolls are excluded. These limits correspond to percentage deviation limits in actual flow rates of +110 - 52.4%, +56 - 36%, and + 45 - 31% for total data, data without 6-inch SAIB, and 4-inch roll data respectively. The r_T values are the correlation coefficients of the data with the theory.

Regression Lines

The best straight line for all the data relating the experimental values to the theoretical values of log flow rate is seen from column 10, Table XIV to be,

$$\hat{E} = 0.9024\ T - 0.3518$$

or,

$$\hat{Q} = 0.445\ Q_T^{\ 0.9024}$$

where $\hat{Q}$ is the predicted flow rate and Q_T is the theoretical flow rate. The 95% confidence limits for single values of flow rate estimated from this equation are +99 and -49.8 percent.

If the No. 8 varnish and 6-inch roll SAIB conditions are excluded, the best line for the remaining data is given by

$$\hat{Q} = 0.592Q_T^{\ 0.9377}$$

with 95% confidence limits of +52.2 and -34.3 percent.

The question of whether or not the regression line, $\hat{E} = a + b\ T$ gives a significant improvement over the theory alone ($E = T$), can be resolved by determining if the sums of squares of deviations removed by the regression equation is significant. The criterion used is Snedecor's F test (39). The sum of square of deviations associated with the theoretical line is $\sum(E-T)^2$ and the number of degrees of freedom, D.F., is n. The sum of squares of deviations from the regression line is $\sum(E-\hat{E})^2$ at (n-2) D.F. The difference is

$$\sum(E-T)^2 - \sum(E-\hat{E})^2 \text{ with 2 D. F.}$$

The test is made by calculating the ratio of the mean square of the difference to the mean square of the regression line deviation and

comparing this ratio to the value of F that would be exceeded by chance if there were no real difference between the theoretical line and the regression line. This test is summarized in Table XVI for all the data and for the data with No. 8 varnish and large roll SAIB excluded.

Since the F values calculated from the data greatly exceed the 0.1% probability level F values for the same number of degrees of freedom, the differences between the theoretical line and the best regression lines through the data are, statistically, highly significant.

Not only are the positions of the best lines different from that of the theoretical line, but the slopes are also significantly different as is shown by a t test. In this test,

$$t = \frac{b - B}{S(b)} \text{ , where :}$$

b is the slope of the regression line,

B is a slope under test, B = 1 ,

S(b) is standard deviation of slope of regression line.

$$S(b) = \frac{S^2 \hat{E}}{\Sigma' T^2} .$$

For all the data points ;

$$S(b) = \frac{0.02325}{127.5035} = 1.350 \times 10^{-2} ,$$

$$b = 0.9024 ,$$

$$t = 7.23 , \quad DF = 402 .$$

For the case of the data without the No. 8 varnish and 6-inch SAIB points, $S(b)$ is 1.045×10^{-2} and t is 5.96. Since the 99.9% confidence levels of t for 402 and 349 D.F. are approximately 3.315 and 3.319 respectively [41], there is less than one chance in a thousand that the

Table XVI

F Test for Significance of Improvement Given by Regression Line

	Total Data		
	Sum of Squares	DF	Mean Square
Theoretical Line	10.87191	404	0.02691
Regression Line	9.34838	402	0.02325
Difference	1.52353	2	0.7618

	Excluding 6-in SAIB and No 8		
	Sum of Squares	DF	Mean Square
Theoretical Line	3.37187	351	0.009606
Regression Line	3.00867	349	0.008620
Difference	0.36320	2	0.1816

F total Data $= \frac{0.7618}{0.02325} = 32.77$ At 2,402,F $^{(40)}_{.001} = 7.02$

F-8, SAIB $= \frac{0.1816}{0.00862} = 21.07$ At 2,349,F .001 = 7.04

differences between both regression line slopes and unity are not real. Although, within the range of experimentation tested, the theoretical line falls well within the 95% confidence limits of single values of $\hat{E}$ estimated from the regression line, the 95% confidence limits of the slope of the regression lines do not include unity, the theoretical value.

High Viscosity Fluid Results. An inspection of the results plotted in Fig. 20 shows immediately that the results obtained with SAIB on the 6-inch diameter roll deviate to a considerable extent from the predicitions of the flow theory. The results obtained with No. 8 varnish also appear to deviate from the theory to a greater extent and in a different manner than do most of the fluids tested. A "t" test was employed to determine if the deviation of the slope of the experimental versus theoretical log flow rate curve for No. 8 varnish from that of the other material was actually significant. For this test, t is calculated from the expression,

$$t = \frac{b_1 - b_2}{S(b)\ \text{pooled}}$$

where b_1 and b_2 are the slopes of the two lines, and $S(b)$ pooled is the pooled estimate of the standard deviation of the slope.

$$S^2(b)_{\text{pooled}} = \left(\frac{(n_1-2)\ \ S^2(\hat{E}_1) + (n_2-2)\ S^2(\hat{E}_2)}{(n_1-2) + (n_2-2)}\right)\left(\frac{1}{\sum T_1^2} + \frac{1}{\sum T_2^2}\right)$$

Taking values from Table XIV for the No. 8 varnish regression line (subscript 1) and the regression line for points other than No. 8 varnish and SAIB (subscript 2), the following results were calculated.

$$S_{(b)\ \text{pooled}} = \left\{\left[\frac{(39)\ (0.01799) + (349)(0.00862)}{39 + 349}\right]\left[\frac{1}{5.35843} + \frac{1}{78.89224}\right]\right\}^{\frac{1}{2}}$$

$S_{(b)}$ pooled = 4.36×10^{-2}

and $t = \dfrac{1.0579 - 0.93769}{4.36 \times 10^{-2}}$

$$t = 2.76 \quad , \quad DF = 388$$

This value of t exceeds 2.598, the value of t .01 at 388DF, and the difference is significant between the slope obtained with No. 8 varnish and that obtained with the other test materials. A similar test applied to the 6-inch roll SAIB data gives 0.263 for the estimated standard deviation of the pooled slope and a t of 4.43 which represents a highly significant difference in slopes.

To test whether the slope of the No. 8 varnish data considered separately is significantly different from the theoretical line, a t test is performed on it.

For No. 8 varnish, $S_{(b)} = \dfrac{0.01799}{5.35843} = 0.0579$,

$$t = \frac{1.0579 - 1.0000}{0.0579} = 1.000,$$

D.F. = 39

From the table of t values, there is about a 30 percent probability that this test value of t would be exceeded by chance, and consequently the difference between the slope of the No. 8 varnish data and the theoretical slope of 1 cannot be declared significant.

The position of the line is significantly different from that predicted by theory as shown by a t test on the mean value of E for No. 8 varnish.

For No. 8 varnish, $S(\bar{E}) = \sqrt{\dfrac{0.01799}{41}} = 0.0209$

The test is between the theoretical value of E and the experimental value.

$$t = \frac{2.59974 - 2.29797}{0.0209} = 14.4$$

D.F. = 39

t 0.001 at 39 D. F. = 3.6

The difference of the mean of the No. 8 varnish data from the theoretical value is therefore highly significant.

The t test for the difference between unity and the slope of the 6-inch roll SAIB data gives:

$$S_{(b)} = 0.382,$$

$$t = 2.886$$

D.F. = 10

The difference is significant at the 98% probability level since $t_{0.02}$, 10 D.F. is 2.764.

The difference between the theoretical and experimental SAIB mean is also significant.

No. 1 Varnish. The runs with No. 1 varnish constitute the lowest viscosity conditions tested. To evaluate the significance of any difference between the behavior of this material and the remaining fluids, the slope of the 6-inch roll - No. 1 varnish runs was compared with that of the 6-inch roll data with intermediate viscosity fluids, that is, all fluids except No. 1 and No. 8 varnish and SAIB. The slopes and means of both sets of data were compared with the theoretical values. The results are summarized below.

Difference in Slopes, No. 1 Varnish and other Materials.

Slope	No. 1 varnish	1.01361
Slope	Other materials	0.97057
Pooled	$S_{(b)}$	0.0632
t		0.681
D.F.		103

The difference is not significant.

Difference in Slope Between No. 1 Varnish and 1.000

Slope No. 1 varnish	1.01361
$S_{(b)}$	0.0292
t	0.4661
DF	49

The difference is not significant.

Difference in Slope Between Intermediate Fluid Data and 1.000

Slope	0.97057
$S_{(b)}$	0.0511
t	0.576
DF	54

The difference is not significant.

Difference in Mean between No. 1 Varnish and Theory.

$\bar{E}$	1.71736
$\bar{T}$	1.62608
$S(\bar{E})$	0.00895
t	10.99
DF	49
$t_{.001,49}$	3.468

The difference in means is highly significant.

Difference in Mean between Intermediate Fluids and Theory

$\bar{E}$	1.98294
$\bar{T}$	2.03143
$S\bar{E}$	0.0178
t	2.724
DF	54
$t_{.01,54}$	2.67

The difference between experimental and theoretical means is significant.

Since no significant differences were found between unity and the best slopes of the individual lines through the No. 1, No. 8, and intermediate fluid data sets, it was suspected that the data for these sets could be represented satisfactorily by lines with equal slopes. An analysis of variance on the slopes of these lines strongly supported this conclusion. Table XVII contains the sums of squares of the factors used in this test.

With the exception of sums of squares of means and difference, these values are taken from Table XIV. Sums of squares of means, $\sum' \bar{E}^2$, $\sum' \bar{T}^2$, and $\sum' \bar{E}\bar{T}$, were calculated as follows.

$$\sum' \bar{E}^2 = \frac{(\sum E_1)^2}{n_1} + \frac{(\sum E_2)^2}{n_2} + \frac{(\sum E_3)^2}{n_3} - \frac{(\sum E)^2}{n}$$

where subscript 1 refers to No. 1 varnish data, subscript 2 to No. 8 varnish data, subscript 3 to intermediate fluid data, and no subscript to total of the three data sets. For example, $\sum' \bar{E}^2$ is given by,

Table XVII

Sums of Squares for Comparison of 6-Inch Roll Correlations on No. 1 Varnish, No. 8 Varnish, and Intermediate Fluids.

Source	$\Sigma' E^2$	$\Sigma' T^2$	$\Sigma' ET$	$\Sigma' C^2$	$\Sigma' e^2$	b
Total	26.86792	38.53648	29.97902	23.32184	3.54608	0.77794
Means	7.66360	21.57511	12.841.96	7.64380	0.0198	0.595
Difference	19.20432	16.96137	17.13706	17.31457	1.88975	1.01036
No 1	5.14630	4.80609	4.87151	4.93782	0.20848	1.0136
No 8	6.69871	5.35843	5.66870	5.99692	0.70179	1.0579
Others	7.35963	6.79703	6.59701	6.40288	0.95675	0.9706
Sum	19.20464	16.96155	17.13722	17.33762	1.86702	

$$\sum'\bar{E}^2 = \frac{(87.58534)^2}{51} + \frac{(94.21691)^2}{41} + \frac{(111.04470)^2}{56} - \frac{(292.84695)^2}{148}$$

The sums of squares for means are the respective values for the best straight line drawn through the means of each set of data weighted according to the number of points which make up the set. The sum of squares of difference row is calculated by subtracting each sum of squares of means from the corresponding total sum of squares, for $\sum'T^2_w$, $\sum'E^2_w$, and $\sum'ET_w$. The sum of squares removed by correlation, $\sum'C^2w$, is calculated from,

$$\sum'C_w^2 = (\sum'ET_w)^2 / \sum'T^2w,$$ and residual sum of squares $\sum'\hat{E}^2_w$ is equal to

$$\sum'E^2_w - \sum'C^2_w .$$

In Table XVII, the values of $\sum'\hat{E}^2$ represent the residual sum of squares of deviations. The minimum value, 1.86702 from the sum of sums row is obtained when the best separate lines are drawn through the separate sets of data and is taken as the "error" sum of squares. The residual sum of squares from the "difference" row, 1.88975, is obtained when separate lines with equal slope are drawn through the two sets of data. The residual from the "total" row, 3.54608 is associated with the best single line through all of the data. The significance of the difference between these correlations is evaluated by the F test as shown in Table XVIII. The between slopes mean square is an estimate of the reduction in residual variance obtained by using individual slopes for each set of data rather than equal pooled slopes. The ratio of this mean square to the "error" mean square is calculated for the F test.

Table XVIII

Analysis of Variance for Comparison of 6-Inch Roll Correlations of No. 1 Varnish, No. 8 Varnish, and Intermediate Fluids

Source	Sum of Squares	D.F.	Mean Square
Means Correlation	0.0198	1	0.0198
Difference	1.63653	1	1.63653
Between Slopes	0.02273	2	0.011365
Error	1.86702	142	0.013148
Total	3.54608	146	

Variance Ratio = 11365/13148 = 0.864

The difference between the correlation obtained by using separate lines with individual slopes, through the No. 1 varnish, No. 8 varnish, and intermediate fluids data and that obtained by using separate lines with equal pooled slopes is not significant, since the between slopes variance estimate is actually less than the error variance estimate.

The value of the pooled slope is 1.0104, and the standard deviation of this slope is 0.0277 at 145 D.F. A t test for the significance of the deviation of this pooled slope from 1.000 shows that there is no significant difference from the theoretical slope.

Four and Six Inch Roll Results. To answer the question of whether or not separate lines drawn through the 4-inch roll data and 6-inch roll data would provide significantly better correlation than a single line through both sets of data, an analysis of variance of the correlations of these two sets of data was performed. The sums of squares, $\Sigma'E^2$, $\Sigma'T^2$, $\Sigma'ET$, $\Sigma'C^2$ and $\Sigma'\hat{E}^2$ are listed for the 4-inch data, the 6-inch data, the total data, the means of the data, and difference

between total and mean in Table XIX. SAIB points and No. 8 varnish points were excluded from the six inch roll set because of the evidence that the SAIB behavior was different from that of the other fluids, and because there were no No. 8 varnish data for the 4-inch roll.

The analysis of variance outlined in Table XX provides the test of whether or not use of individual slopes for the 6-inch and 4-inch roll data gives a significantly better correlation than two lines with equal pooled slopes. The between slopes mean square is less than the "error" mean square, and the difference between the slopes of the best individual lines through the 4-inch and 6-inch roll data is insignificant. On the other hand, a highly significant improvement in correlation is obtained by using separate lines with equal pooled slopes rather than a single line through all the data. This is shown by the ratio of the mean square for difference between single line and pooled slope to the mean square for pooled slope correlation. This ratio, 429/7.4 = 58, greatly exceeds 11, the value for F at the 0.001 significance level with 1 and 348 D. F.

Relationship of Experimental Error to Variance from Correlation Lines. The variance associated with the experimental measurement of log flow rate was estimated from sets of duplicate experiments in Table VI and was found to be approximately 7.4×10^{-4}. This variance was exceeded to a significant amount by the residual variance from all of the correlations. For example, the residual variance from the best correlation line through the 4-inch roll data was 43.6×10^{-4}, and the ratio, 43.6/7.4, gives 5.9 compared with 1.4, the F 0.0001 value associated with 242 and 227 degrees of freedom. Therefore the unaccounted

Table XIX

Sums of Squares for Comparison of 4-Inch Roll and 6-Inch Roll Correlations

Source	$\Sigma' E^2$	$\Sigma' T^2$	$\Sigma' ET$	$\Sigma' C^2$	$\Sigma' \frac{1}{E}^2$	b
Total	72.37633	78.89224	73.97682	69.36766	3.00867	0.9377
Means	15.16130	12.32592	13.67030	15.16130	0.00000	1.1091
Difference	57.21503	66.56632	60.30652	54.63538	2.57965	0.9060
4-in	42.82645	50.57749	45.96454	41.77232	1.05413	0.9088
6-in	14.38858	15.98882	14.34198	12.86476	1.52382	0.897
Sum	57.21503	66.56631	60.30652	54.63708	2.57795	

Table XX

Analysis of Variance for Comparison of 4-Inch Roll and 6-Inch Roll Correlations

Source	Sum of Squares	DF	Mean Square
Means Correlation	0.0000	0	- -
Difference	0.42902	1	0.42902
Between Slopes	0.00170	1	0.00170
Error	2.57795	347	0.0074
Total	3.00867	349	

With Pooled Slope

Means	0.0000	0	- -
Difference	0.42902	1	0.42902
Error	2.57965	348	0.00741
Total	3.00867	349	

for deviation from the linear correlations is greater than can be explained on the basis of the random experimental error.

APPENDIX VI

FORCE AND FLOW RATE RESULTS

Table XXI

Experimental and Theoretical Results for the Force and Flow Rate Between Rotating Cylinders

Notebook and Page No.	Liquid Used	Roll Radius in.	Slow Roll rpm	Fast Roll rpm	Roll Force lb/ft	Film Temp °F	Viscosity Poise	Nip Flow Rate cu ft/ft-sec x 10^{-3} Observed	Nip Flow Rate cu ft/ft-sec x 10^{-3} Theoretical	Transfer Fraction f	Speed Ratio r	Run No.
222-124	1	2	51.7	155	255	80	22.0	0.4858	0.3132	0.904	3	10
"	"	"	"	"	255	80	22.0	0.4919	0.3132	0.912	"	"
"	"	"	"	"	525	82	20.4	0.1417	0.1366	0.849	"	"
"	"	"	"	"	525	82	20.4	0.1388	0.1366	0.850	"	"
"	"	"	"	"	1373	86	17.7	0.0740	0.0445	0.831	"	"
"	"	"	"	"	1373	87	17.1	------	0.0429	-----	"	"
"	"	"	"	"	2280	87	17.1	0.0433	0.0259	0.827	"	"
"	"	"	"	"	2280	87	17.1	0.0495	0.0259	0.853	"	"
222-126	3	2	51.7	155	255	87	37.2	0.5245	0.5693	0.859	3	11
"	"	"	"	"	255	87	37.2	0.5143	0.5693	0.862	"	"
"	"	"	"	"	525	86	38.6	0.2596	0.2652	0.870	"	"
"	"	"	"	"	525	86	38.6	0.2723	0.2652	0.858	"	"
"	"	"	"	"	1373	90	33.4	0.0917	0.0847	0.841	"	"
"	"	"	"	"	1373	90	33.4	0.0963	0.0847	0.840	"	"
"	"	"	"	"	2280	90	33.4	0.0613	0.0507	0.833	"	"
"	"	"	"	"	2280	90	33.4	0.0553	0.0507	0.814	"	"
222-128	12	2	51.7	155	525	85	50.9	0.3813	0.3567	0.861	3	12
"	"	"	"	"	525	85	50.9	0.3774	0.3567	0.858	"	"
"	"	"	"	"	1373	88	46.4	0.1301	0.1184	0.833	"	"
"	"	"	"	"	1373	88	46.4	0.1362	0.1184	0.836	"	"
"	"	"	"	"	2280	88	46.4	0.0915	0.0714	0.830	"	"
"	"	"	"	"	2280	91	42.3	0.0926	0.0651	0.834	"	"

Table XXI - Continued

Notebook and Page No.	Liquid Used	Roll Radius in.	Slow Roll rpm	Fast Roll rpm	Roll Force lb/ft	Film Temp °F	Viscosity Poise	Nip Flow Rate cu ft/ft-sec x 10^{-3} Observed	Nip Flow Rate cu ft/ft-sec x 10^{-3} Theoretical	Transfer Fraction f	Speed Ratio r	Run No.
222-142	10	2	51.7	155	300	87	99.6	1.037	1.470	0.893	3	24
"	"	"	"	"	300	87	99.6	1.046	1.470	0.900	"	"
"	"	"	"	"	900	95	73	0.2665	0.2969	0.894	"	"
"	"	"	"	"	900	95	73	0.3069	0.2969	0.890	"	"
"	"	"	"	"	1500	96	70	0.1727	0.1664	0.924	"	"
"	"	"	"	"	1500	96	70	0.1490	0.1664	0.906	"	"
"	"	"	"	"	2400	93	78.6	0.0907	0.1147	0.893	"	"
"	"	"	"	"	2400	93	78.6	0.0848	0.1147	0.883	"	"
231-34	11	2	35	104	900	116	342	0.6515	0.745	0.883	3	74
"	"	"	"	"	1200	116	342	0.4459	0.510	0.885	"	"
"	"	"	"	"	1500	120	244	0.2451	0.276	0.863	"	"
"	"	"	"	"	1800	120	244	0.2515	0.224	0.884	"	"
"	"	"	"	"	2100	120	244	0.1375	0.190	0.865	"	"
"	"	"	"	"	2700	118	289	0.2458	0.172	0.906	"	"
222-90	1	2	77.5	155	300	76	25.6	0.3476	0.3956	0.7595	2	1
"	"	"	"	"	300	76	25.6	0.3555	0.3956	0.7634	"	"
"	"	"	"	"	300	76	25.6	0.3695	0.3956	0.7497	"	"
"	"	"	"	"	600	78	23.8	0.1512	0.1763	0.6944	"	"
"	"	"	"	"	600	78	23.8	0.1920	0.1763	0.7552	"	"
"	"	"	"	"	600	76	25.6	0.1989	0.1901	0.7617	"	"
"	"	"	"	"	600	77	24.7	0.1959	0.1830	0.7779	"	"
"	"	"	"	"	600	77	24.7	0.1962	0.1830	0.7487	"	"
"	"	"	"	"	900	77	24.7	0.1188	0.1208	0.7626	"	"
"	"	"	"	"	900	78	23.8	0.1162	0.1164	0.7358	"	"
"	"	"	"	"	1200	78	23.8	0.0890	0.0866	0.7461	"	"
"	"	"	"	"	1200	78	23.8	0.0847	0.0866	0.7308	"	"

Table XXI - Continued

Notebook and Page No.	Liquid Used	Roll Radius In.	Slow Roll rpm	Fast Roll rpm	Roll Force lb/ft	Film Temp °F	Viscosity Poise	Nip Flow Rate cu ft/ft-sec x 10^{-3} Observed	Nip Flow Rate cu ft/ft-sec x 10^{-3} Theoretical	Transfer Fraction f	Speed Ratio r	Run No.
222-92	1	2	77.5	155	1500	80	22.0	0.0637	0.0643	0.6782	2	1
"	"	"	"	"	1500	79.5	22.5	0.0787	0.0655	0.7624	"	"
"	"	"	"	"	1500	79	22.9	0.0712	0.0668	0.7416	"	"
"	"	"	"	"	1500	79	22.9	0.0624	0.0668	0.7372	"	"
"	"	"	"	"	1800	78	23.8	0.0624	0.0577	0.7179	"	"
"	"	"	"	"	1800	78	23.8	0.0586	0.0577	0.7167	"	"
"	"	"	"	"	1800	77	24.7	0.0741	0.0599	0.7490	"	"
"	"	"	"	"	1800	80	22.0	0.0728	0.0536	0.7459	"	"
"	"	"	"	"	2100	80	22.0	0.0583	0.0459	0.7307	"	"
"	"	"	"	"	2100	79	22.9	0.0602	0.0476	0.7126	"	"
222-94	2	2	77.5	155	300	76	40	0.5759	0.6463	0.774	2	2
"	"	"	"	"	300	76.5	39.2	0.5349	0.6344	0.752	"	"
"	"	"	"	"	600	77	38.5	0.2757	0.2907	0.776	"	"
"	"	"	"	"	600	78	37.1	0.2694	0.2801	0.767	"	"
"	"	"	"	"	900	79.5	35	0.1712	0.1733	0.761	"	"
"	"	"	"	"	900	80	34.5	0.1784	0.1701	0.761	"	"
"	"	"	"	"	1200	80	34.5	0.1127	0.1267	0.732	"	"
"	"	"	"	"	1200	80	34.5	0.1131	0.1267	0.744	"	"
"	"	"	"	"	1200	80	34.5	0.0840	0.1009	0.738	"	"
"	"	"	"	"	1500	80	34.5	0.0742	0.1009	0.724	"	"
"	"	"	"	"	1800	80	34.5	0.0834	0.0837	0.755	"	"
"	"	"	"	"	1800	80	34.5	0.0761	0.0837	0.775	"	"
"	"	"	"	"	1800	80	34.5	0.0797	0.0837	0.727	"	"
"	"	"	"	"	2100	80	34.5	0.0665	0.0716	0.744	"	"
"	"	"	"	"	2100	80	34.5	0.0655	0.0716	0.758	"	"

Table XXI - Continued

Notebook and Page No.	Liquid Used	Roll Radius In.	Slow Roll rpm	Fast Roll rpm	Roll Force lb/ft	Film Temp °F	Viscosity Poise	Nip Flow Rate cu ft/ft-sec x 10^{-3} Observed	Nip Flow Rate cu ft/ft-sec x 10^{-3} Theoretical	Transfer Fraction f	Speed Ratio r	Run No.
222-96	3	2	77.5	155	300	79	50	0.8227	0.8638	0.776	2	3
"	"	"	"	"	300	79	50	0.8342	0.8638	0.784	"	"
"	"	"	"	"	600	80	48	0.3553	0.3714	0.790	"	"
"	"	"	"	"	600	79	50	0.3808	0.3855	0.790	"	"
"	"	"	"	"	900	80	48	0.2158	0.2404	0.763	"	"
"	"	"	"	"	900	81.5	46.4	0.2186	0.2361	0.778	"	"
"	"	"	"	"	1200	83	43	0.1443	0.1596	0.741	"	"
"	"	"	"	"	1200	82	44.6	0.1543	0.1656	0.759	"	"
"	"	"	"	"	1500	82	44.6	0.1069	0.1318	0.735	"	"
"	"	"	"	"	1500	82	44.6	0.1175	0.1318	0.739	"	"
"	"	"	"	"	1800	83	43	0.0945	0.1056	0.735	"	"
"	"	"	"	"	1800	84	41.5	0.0924	0.1018	0.753	"	"
"	"	"	"	"	2100	84	41.5	0.0728	0.0758	0.732	"	"
"	"	"	"	"	2100	83	43	0.0789	0.0786	0.733	"	"
222-110	12	2	77.5	155	540	84	52.4	0.4946	0.4553	0.773	2	6
"	"	"	"	"	540	82	55.8	0.5012	0.4846	0.776	"	"
"	"	"	"	"	1365	86	49.4	0.1877	0.1604	0.758	"	"
"	"	"	"	"	1365	86	49.4	0.1824	0.1604	0.755	"	"
"	"	"	"	"	2250	88	46.4	0.0928	0.0906	0.812	"	"
"	"	"	"	"	2250	88	46.4	0.1082	0.0906	0.741	"	"
222-102	9	2	77.5	155	240	86-98	86	1.394	2.040	0.681	2	5
"	"	"	"	"	240	89-98	82.7	1.423	1.960	0.691	"	"
"	"	"	"	"	240	101	65.8	1.019	1.560	0.757	"	"
"	"	"	"	"	240	102	63	0.9828	1.500	0.750	"	"
"	"	"	"	"	810	101	65.8	0.4120	0.3757	0.754	"	"
"	"	"	"	"	810	101	65.8	0.3939	0.3757	0.748	"	"

Table XXI - Continued

Notebook and Page No.	Liquid Used	Roll Radius in.	Slow Roll rpm	Fast Roll rpm	Roll Force lb/ft	Film Temp °F	Viscosity Poise	Nip Flow Rate cu ft/ft-sec x 10^{-3} Observed	Nip Flow Rate cu ft/ft-sec x 10^{-3} Theoretical	Transfer Fraction f	Speed Ratio r	Run No.
222-102	9	2	77.5	155	1365	103	60.5	0.1935	0.1987	0.736	2	5
"	"	"	"	"	1365	103	60.5	0.2167	0.1987	0.758	"	"
"	"	"	"	"	2250	107	51	0.1145	0.1002	0.747	"	"
"	"	"	"	"	2250	107	51	0.1065	0.1002	0.721	"	"
222-144	10	2	77.5	155	300	87	99.9	1.423	1.950	0.833	2	25
"	"	"	"	"	300	87	99.9	1.478	1.950	0.831	"	"
"	"	"	"	"	900	90-94	81.9	0.4216	0.4223	0.735	"	"
"	"	"	"	"	900	90-94	81.9	0.3668	0.4223	0.736	"	"
"	"	"	"	"	1500	98	65	0.1481	0.1947	0.800	"	"
"	"	"	"	"	1500	98	65	0.1493	0.1947	0.788	"	"
"	"	"	"	"	2100	98	65	0.0656	0.1203	0.664	"	"
"	"	"	"	"	2100	98	65	0.0662	0.1203	0.694	"	"
231-36	11	2	77.5	155	900	124	175	0.8295	1.075	0.797	2	75
"	"	"	"	"	1200	124	175	0.7614	0.739	0.815	"	"
"	"	"	"	"	1500	120	244	0.6847	0.788	0.832	"	"
"	"	"	"	"	1800	124	175	0.4580	0.455	0.822	"	"
"	"	"	"	"	2100	124	175	0.3877	0.382	0.832	"	"
"	"	"	"	"	2700	122	207	0.4344	0.345	0.835	"	"
222-112	1	2	155	155	255	81	21.3	0.6536	0.7042	0.487	1	7
"	"	"	"	"	255	81	21.3	0.6414	0.7042	0.497	"	"
"	"	"	"	"	525	84	19	0.2787	0.2895	0.482	"	"
"	"	"	"	"	525	84	19	0.2767	0.2895	0.478	"	"
"	"	"	"	"	1373	85	18.4	0.1223	0.1039	0.566	"	"
"	"	"	"	"	1373	85	18.4	0.1169	0.1039	0.445	"	"
"	"	"	"	"	2280	90	15.3	0.0727	0.0522	0.452	"	"
"	"	"	"	"	2280	88	16.5	0.0680	0.0561	0.404	"	"

Table XXI - Continued

Notebook and Page No.	Liquid Used	Roll Radius In.	Slow Roll rpm	Fast Roll rpm	Roll Force lb/ft	Film Temp °F	Viscosity Poise	Nip Flow Rate cu ft/ft-sec x 10^{-3} Observed	Nip Flow Rate cu ft/ft-sec x 10^{-3} Theoretical	Transfer Fraction f	Speed Ratio r	Run No.
222-114	3	2	155	155	255	85	40	1.075	1.475	0.485	1	8
"	"	"	"	"	255	85	40	1.078	1.475	0.485	"	"
"	"	"	"	"	525	88	36	0.4959	0.5680	0.441	"	"
"	"	"	"	"	525	88	36	0.5077	0.5680	0.444	"	"
"	"	"	"	"	1373	95	28.1	0.1372	0.1623	0.491	"	"
"	"	"	"	"	1373	96	27.1	0.1423	0.1567	0.482	"	"
"	"	"	"	"	2280	93	30.1	0.0997	0.1029	0.459	"	"
"	"	"	"	"	2280	95	28.1	0.0874	0.0959	0.412	"	"
222-116	12	2	155	155	525	93	39.8	0.6149	0.6399	0.451	1	9
"	"	"	"	"	525	92	41	0.6230	0.6594	0.458	"	"
"	"	"	"	"	1373	95	37.5	0.2001	0.2157	0.437	"	"
"	"	"	"	"	1373	96	36.4	0.2067	0.2094	0.451	"	"
"	"	"	"	"	2280	98	34.3	0.1265	0.1188	0.415	"	"
"	"	"	"	"	2280	96	36.4	0.1304	0.1261	0.460	"	"
228-8	10	2	155	155	300	90	88.5	1.878	3.040	0.4932	1	26
"	"	"	"	"	300	90	88.5	1.816	3.040	0.4889	"	"
"	"	"	"	"	900	96	70.0	0.5182	0.6631	0.4423	"	"
"	"	"	"	"	900	97	67.4	0.5107	0.6381	0.4509	"	"
"	"	"	"	"	1500	98	65	0.2212	0.3511	0.4000	"	"
"	"	"	"	"	1500	98	65	0.2702	0.3511	0.4370	"	"
"	"	"	"	"	2400	98	65	0.1506	0.2135	0.3674	"	"
"	"	"	"	"	2400	98	65	0.1333	0.2135	0.3607	"	"

Table XXI - Continued

Notebook and Page No.	Liquid Used	Roll Radius In.	Slow Roll rpm	Fast Roll rpm	Roll Force lb/ft	Film Temp °F	Viscosity Poise	Nip Flow Rate cu ft/ft-sec x 10^{-3} Observed	Nip Flow Rate cu ft/ft-sec x 10^{-3} Theoretical	Transfer Fraction f	Speed Ratio r	Run No.
222-130	1	2	81.67	245	255	87	17.1	0.4294	0.6150	0.830	3	21
"	"	"	"	"	255	88	16.6	0.3866	0.5928	0.811	"	"
"	"	"	"	"	525	90	15.3	0.2954	0.2562	0.846	"	"
"	"	"	"	"	525	90	15.3	0.2988	0.2562	0.850	"	"
"	"	"	"	"	1373	93	13.8	0.1036	0.0882	0.816	"	"
"	"	"	"	"	1373	96	12.4	0.1222	0.0791	0.819	"	"
"	"	"	"	"	2280	95	12.8	0.080	0.0493	0.826	"	"
"	"	"	"	"	2280	95	12.8	0.081	0.0493	0.823	"	"
222-132	3	2	81.67	245	255	92	31.2	1.119	1.238	0.871	3	22
"	"	"	"	"	255	92	31.2	1.115	1.238	0.870	"	"
"	"	"	"	"	525	94	29.0	0.4706	0.5030	0.853	"	"
"	"	"	"	"	525	94	29.0	0.4966	0.5030	0.862	"	"
"	"	"	"	"	1373	98	25.3	0.1423	0.1606	0.832	"	"
"	"	"	"	"	1373	99	24.5	0.1424	0.1552	0.829	"	"
"	"	"	"	"	2280	100	23.6	0.0808	0.0894	0.841	"	"
"	"	"	"	"	2280	100	23.6	0.0844	0.0894	0.816	"	"
222-134	12	2	81.67	245	810	94	38.6	0.4565	0.4306	0.843	3	23
"	"	"	"	"	810	94	38.6	0.4696	0.4306	0.851	"	"
"	"	"	"	"	1373	96	36.4	0.2797	0.2324	0.854	"	"
"	"	"	"	"	1373	96	36.4	0.2678	0.2324	0.849	"	"
"	"	"	"	"	2280	98	34.3	0.1434	0.1319	0.831	"	"
"	"	"	"	"	2280	98	34.3	0.1418	0.1319	0.831	"	"
222-148	10	2	81.67	245	300	100	60	1.673	2.25	0.912	3	27
"	"	"	"	"	300	100	60	1.821	2.25	0.906	"	"
"	"	"	"	"	900	107	46.3	0.4287	0.4648	0.866	"	"

Table XXI - Continued

Notebook and Page No.	Liquid Used	Roll Radius In.	Slow Roll rpm	Fast Roll rpm	Roll Force lb/ft	Film Temp °F	Viscosity Poise	Nip Flow Rate cu ft/ft-sec x 10^{-3} Observed	Nip Flow Rate cu ft/ft-sec x 10^{-3} Theoretical	Transfer Fraction f	Speed Ratio r	Run No.
222-148	10	2	81.67	245	900	107	46.3	0.4696	0.4648	0.880	3	27
"	"	"	"	"	1500	112	38.4	0.1700	0.2268	0.881	"	"
"	"	"	"	"	1500	111	39.8	0.1967	0.2352	0.890	"	"
"	"	"	"	"	2400	114	35.8	0.1043	0.1302	0.868	"	"
"	"	"	"	"	2400	112	38.4	0.1155	0.1400	0.884	"	"
222-104	1	2	122.5	245	255	86	17.7	0.7048	0.8232	0.757	2	14
"	"	"	"	"	255	85	18.35	0.7949	0.8541	0.767	"	"
"	"	"	"	"	310	88	16.45	0.2346	0.2244	0.759	"	"
"	"	"	"	"	810	88	16.45	0.2308	0.2244	0.740	"	"
"	"	"	"	"	1373	91	14.8	0.1117	0.1175	0.710	"	"
"	"	"	"	"	1373	91	14.8	0.1041	0.1175	0.718	"	"
"	"	"	"	"	1971	92	14.25	0.0926	0.0788	0.703	"	"
"	"	"	"	"	1971	92	14.25	0.0861	0.0788	0.702	"	"
222-106	3	2	122.5	245	255	91	32.3	1.305	1.679	0.756	2	15
"	"	"	"	"	255	91	32.3	1.202	1.679	0.760	"	"
"	"	"	"	"	810	93	30.1	0.3838	0.4219	0.764	"	"
"	"	"	"	"	810	92	31.2	0.3965	0.4369	0.777	"	"
"	"	"	"	"	1373	94	29.0	0.1977	0.2348	0.754	"	"
"	"	"	"	"	1373	94	29.0	0.1924	0.2348	0.740	"	"
"	"	"	"	"	1971	102	22.0	0.1105	0.1239	0.720	"	"
"	"	"	"	"	1971	102	22.0	0.1070	0.1239	0.695	"	"
222-140	3	2	122.5	245	300	90	33.4	1.247	1.441	0.767	2	16
"	"	"	"	"	300	92	31.2	1.027	1.343	0.751	"	"
"	"	"	"	"	600	92	31.2	0.5558	0.5922	0.779	"	"
"	"	"	"	"	600	91	32.2	0.5443	0.6134	0.774	"	"

Table XXI - Continued

Notebook and Page No.	Liquid Used	Roll Radius In.	Slow Roll rpm	Fast Roll rpm	Roll Force lb/ft	Film Temp °F	Viscosity Poise	Nip Flow Rate cu ft/ft-sec x 10^{-3} Observed	Nip Flow Rate cu ft/ft-sec x 10^{-3} Theoretical	Transfer Fraction f	Speed Ratio	Run No.
222-140	3	2	122.5	245	1500	96	27.1	0.1718	0.2002	0.703	2	16
"	"	"	"	"	1500	96	27.1	0.1665	0.2002	0.719	"	"
"	"	"	"	"	2400	96	27.1	0.1060	0.1249	0.707	"	"
"	"	"	"	"	2400	96	27.1	0.1177	0.1249	0.731	"	"
222-108	12	2	122.5	245	810	96	36.4	0.5125	0.5147	0.772	2	17
"	"	"	"	"	810	94	38.6	0.5740	0.5464	0.723	"	"
"	"	"	"	"	1373	98	34.4	0.2819	0.2789	0.757	"	"
"	"	"	"	"	1373	98	34.4	0.2745	0.2789	0.752	"	"
"	"	"	"	"	2280	100	32.4	0.1638	0.1574	0.743	"	"
"	"	"	"	"	2280	99	33.4	0.1615	0.1621	0.735	"	"
222-146	10	2	122.5	245	300	102	55.7	1.961	2.76	0.783	2	28
"	"	"	"	"	300	102	55.7	1.971	2.76	0.784	"	"
"	"	"	"	"	900	110	41.4	0.6167	0.5295	0.793	"	"
"	"	"	"	"	900	110	41.4	0.6371	0.5295	0.801	"	"
"	"	"	"	"	1500	113	37.1	0.2201	0.2774	0.742	"	"
"	"	"	"	"	1500	114	35.8	0.2320	0.2675	0.768	"	"
"	"	"	"	"	2400	114	35.8	0.1102	0.1648	0.749	"	"
"	"	"	"	"	2400	114	35.8	0.1201	0.1648	0.796	"	"
222-118	1	2	245	245	255	88	16.45	1.293	1.397	0.499	1	18
"	"	"	"	"	255	88	16.45	1.281	1.397	0.484	"	"
"	"	"	"	"	525	90	15.3	0.5684	0.5888	0.448	"	"
"	"	"	"	"	525	90	15.3	0.5714	0.5888	0.429	"	"
"	"	"	"	"	1373	95	12.85	0.1953	0.1842	0.444	"	"
"	"	"	"	"	1373	96	12.4	0.1889	0.1778	0.458	"	"
"	"	"	"	"	2280	97	12.0	0.1172	0.0879	0.463	"	"
"	"	"	"	"	2280	97	12.0	0.1242	0.0879	0.449	"	"

Table XXI - Continued

Notebook and Page No.	Liquid Used	Roll Radius In.	Slow Roll rpm	Fast Roll rpm	Roll Force lb/ft	Film Temp °F	Viscosity Poise	Nip Flow Rate cu ft/ft-sec × 10^{-3} Observed	Theoretical	Transfer Fraction f	Speed Ratio r	Run No.
222-120	3	2	245	245	255	92	31.2	2.013	3.15	0.495	1	19
"	"	"	"	"	255	92	31.2	1.775	3.15	0.485	"	"
"	"	"	"	"	525	92	31.2	1.022	1.273	0.433	"	"
"	"	"	"	"	525	92	31.2	1.071	1.273	0.437	"	"
"	"	"	"	"	1373	96	27.1	0.3683	0.3927	0.490	"	"
"	"	"	"	"	1373	98	25.3	0.2815	0.3665	0.383	"	"
"	"	"	"	"	2280	103	21.4	0.1603	0.1829	0.456	"	"
"	"	"	"	"	2280	103	21.4	0.1496	0.1829	0.406	"	"
222-122	12	2	245	245	810	96	36.4	0.8531	0.9402	0.454	1	20
"	"	"	"	"	810	96	36.4	0.8325	0.9402	0.467	"	"
"	"	"	"	"	1373	98	34.3	0.4829	0.5036	0.453	"	"
"	"	"	"	"	1373	98	34.3	0.4863	0.5036	0.441	"	"
"	"	"	"	"	2280	100	32.4	0.2676	0.2799	0.429	"	"
"	"	"	"	"	2280	100	32.4	0.2752	0.2799	0.445	"	"
228-6	10	2	245	245	300	97	67.3	3.804	5.40	0.482	1	29
"	"	"	"	"	300	100	60.0	2.865	5.70	0.509	"	"
"	"	"	"	"	900	107	46.1	0.8218	1.081	0.427	"	"
"	"	"	"	"	900	107	46.1	0.7183	1.081	0.444	"	"
"	"	"	"	"	1500	119	29.9	0.4032	0.4027	0.431	"	"
"	"	"	"	"	1500	120	28.8	0.3369	0.3887	0.440	"	"
"	"	"	"	"	2400	122	26.9	0.1871	0.2202	0.385	"	"
"	"	"	"	"	2400	122	26.9	0.1934	0.2202	0.428	"	"
228-28	1	3	66	198	960	72	29.8	0.8422	0.61	0.877	3	38
"	"	"	"	"	1440	70	32.2	0.6612	0.432	0.867	"	"
"	"	"	"	"	2400	77	24.7	0.2687	0.195	0.844	"	"

Table XXI - Continued

Notebook and Page No.	Liquid Used	Roll Radius In.	Slow Roll rpm	Fast Roll rpm	Roll Force lb/ft	Film Temp °F	Viscosity Poise	Nip Flow Rate cu ft/ft-sec x 10^{-3} Observed	Nip Flow Rate cu ft/ft-sec x 10^{-3} Theoretical	Transfer Fraction f	Speed Ratio r	Run No.
228-28	1	3	66	198	3360	71	26.2	0.2147	0.175	0.825	3	38
"	"	"	"	"	4320	76	25.7	0.1472	0.112	0.834	"	"
228-30	5	3	66	198	960	83.5	121	3.036	3.37	0.931	3	37
"	"	"	"	"	1440	80	137	1.770	2.16	0.935	"	"
"	"	"	"	"	2400	82	128	0.917	1.10	0.895	"	"
"	"	"	"	"	3360	80	137	0.572	0.824	0.860	"	"
"	"	"	"	"	4320	80	137	0.409	0.62	0.865	"	"
228-32	6	3	66	198	960	94	226	5.347	10.70	0.951	3	39
"	"	"	"	"	1440	94	226	1.913	4.65	0.913	"	"
"	"	"	"	"	2400	93.5	229	1.172	2.18	0.904	"	"
"	"	"	"	"	3360	92.5	237	0.777	1.50	0.874	"	"
"	"	"	"	"	4320	91.5	240	0.485	1.14	0.848	"	"
231-30	11	3	72	215	1440	130	107	10.686	2.20	0.945	3	72
"	"	"	"	"	1920	126	148.5	7.700	2.06	0.960	"	"
"	"	"	"	"	2400	125	161	5.372	1.69	0.966	"	"
"	"	"	"	"	2880	127	137	4.338	1.155	0.977	"	"
"	"	"	"	"	3360	124	175	3.697	1.24	0.969	"	"
"	"	"	"	"	4320	120	244	2.190	1.32	0.939	"	"
228-102	1	3	99	198	960	80	22.1	0.630	0.572	0.781	2	50
"	"	"	"	"	1440	80	22.1	0.378	0.376	0.769	"	"
"	"	"	"	"	2400	78	24.8	0.290	0.237	0.741	"	"
"	"	"	"	"	3360	80	22.1	0.254	0.156	0.745	"	"
"	"	"	"	"	4320	79	22.9	0.175	0.125	0.747	"	"

Table XXI - Continued

Notebook and Page No.	Liquid Used	Roll Radius In.	Slow Roll rpm	Fast Roll rpm	Roll Force lb/ft	Film Temp °F	Viscosity Poise	Nip Flow Rate cu ft/ft-sec x 10^{-3} Observed	Nip Flow Rate cu ft/ft-sec x 10^{-3} Theoretical	Transfer Fraction f	Speed Ratio r	Run No.
228-34	1	3	99	198	960	78	24.8	0.892	0.625	0.800	2	40
"	"	"	"	"	1440	71	31.0	0.757	0.530	0.789	"	"
"	"	"	"	"	2400	72	29.8	0.402	0.303	0.748	"	"
"	"	"	"	"	3360	70	32.2	0.266	0.234	0.768	"	"
"	"	"	"	"	4320	74	27.6	0.177	0.154	0.718	"	"
228-108	7	3	99	198	960	82.5	28.1	1.257	0.74	0.796	2	53
"	"	"	"	"	1440	82	28.6	0.804	0.495	0.787	"	"
"	"	"	"	"	2400	81	29.5	0.413	0.299	0.763	"	"
"	"	"	"	"	3360	82	28.6	0.311	0.207	0.770	"	"
"	"	"	"	"	4320	81	29.5	0.226	0.165	0.759	"	"
228-104	3	3	99	198	960	82	44.5	0.996	1.20	0.771	2	51
"	"	"	"	"	1440	82	44.5	0.689	0.77	0.780	"	"
"	"	"	"	"	2400	83	43.0	0.386	0.44	0.750	"	"
"	"	"	"	"	3360	83	43.0	0.318	0.313	0.784	"	"
"	"	"	"	"	4320	82	44.5	0.196	0.245	0.783	"	"
228-110	4	3	99	198	960	84	69	2.201	2.01	0.821	2	54
"	"	"	"	"	1440	84	69	1.361	1.26	0.812	"	"
"	"	"	"	"	2400	84	69	0.683	0.715	0.788	"	"
"	"	"	"	"	3360	86	64.7	0.412	0.471	0.763	"	"
"	"	"	"	"	4320	83	71.4	0.320	0.387	0.741	"	"
228-36	5	3	99	198	960	83	123	3.723	4.35	0.879	2	41
"	"	"	"	"	1440	85	114	2.116	2.32	0.888	"	"
"	"	"	"	"	2400	86	107.8	1.128	1.17	0.872	"	"
"	"	"	"	"	3360	81	132.9	0.717	1.00	0.794	"	"
"	"	"	"	"	4320	80	138	0.458	0.785	0.772	"	"

Table XXI - Continued

Notebook and Page No.	Liquid Used	Roll Radius In.	Slow Roll rpm	Fast Roll rpm	Roll Force lb/ft	Film Temp °F	Viscosity Poise	Nip Flow Rate cu ft/ft-sec x 10^{-3} Observed	Nip Flow Rate cu ft/ft-sec x 10^{-3} Theoretical	Transfer Fraction f	Speed Ratio r	Run No.
231-32	11	3	107	215	1440	132	91	9.340	2.20	0.844	2	73
"	"	"	"	"	1920	131	98.7	6.677	1.66	0.933	"	"
"	"	"	"	"	2400	130	107	3.670	1.36	0.958	"	"
"	"	"	"	"	2880	128	126	4.805	1.32	0.953	"	"
"	"	"	"	"	3360	126	148.5	3.014	1.34	0.969	"	"
"	"	"	"	"	4230	125	161	1.318	1.08	0.971	"	"
228-112	8	3	99	198	960	98.5	131	6.759	4.90	0.806	2	55
"	"	"	"	"	1440	100	121.5	4.281	2.49	0.814	"	"
"	"	"	"	"	2400	98.5	131	2.201	1.43	0.789	"	"
"	"	"	"	"	3360	97	141	1.338	1.07	0.776	"	"
"	"	"	"	"	4320	95	155.5	1.161	0.74	0.761	"	"
228-106	6	3	99	198	960	103	169	3.482	8.90	0.881	2	52
"	"	"	"	"	1440	101	180	2.042	4.44	0.872	"	"
"	"	"	"	"	2400	100	186	0.890	2.15	0.838	"	"
"	"	"	"	"	3360	97	204	0.552	1.62	0.820	"	"
"	"	"	"	"	4230	96	212	0.406	1.25	0.827	"	"
228-38	6	3	99	198	960	97.5	202	6.007	13.10	0.904	2	42
"	"	"	"	"	1440	98	198	3.401	5.90	0.905	"	"
"	"	"	"	"	2400	94	226	1.584	2.79	0.886	"	"
"	"	"	"	"	3360	90	257	0.982	2.08	0.852	"	"
"	"	"	"	"	4320	88	274	0.597	1.66	0.780	"	"
228-44	1	3	198	198	960	81	21.2	1.616	0.979	0.509	1	45
"	"	"	"	"	1440	84	19.0	0.903	0.572	0.506	"	"
"	"	"	"	"	2400	85	18.4	0.485	0.323	0.491	"	"

Table XXI - Continued

Notebook and Page No.	Liquid Used	Roll Radius In.	Slow Roll rpm	Fast Roll rpm	Roll Force lb/ft	Film Temp °F	Viscosity Poise	Nip Flow Rate cu ft/ft-sec x 10^{-3} Observed	Nip Flow Rate cu ft/ft-sec x 10^{-3} Theoretical	Transfer Fraction f	Speed Ratio r	Run No.
228-44	1	3	198	198	3360	84	19.0	0.329	0.242	0.470	1	45
"	"	"	"	"	4320	84	19.0	0.250	0.184	0.494	"	"
228-42	5	3	198	198	960	94	81.7	4.221	5.26	0.527	1	44
"	"	"	"	"	1440	88	102.0	3.085	3.64	0.667	"	"
"	"	"	"	"	2400	93	84.9	1.522	1.62	0.607	"	"
"	"	"	"	"	3360	90	94.6	1.001	1.26	0.546	"	"
"	"	"	"	"	4320	90	94.6	0.728	0.96	0.518	"	"
228-40	6	3	198	198	960	100	184	8.261	19.20	0.474	1	43
"	"	"	"	"	1440	107	149	4.733	6.84	0.511	"	"
"	"	"	"	"	2400	110	136	2.762	2.88	0.590	"	"
"	"	"	"	"	3360	108	145	1.721	2.04	0.498	"	"
"	"	"	"	"	4320	108	145	1.138	1.54	0.491	"	"
228-22	1	3	100	300	960	80	22.1	1.480	1.035	0.728	3	34
"	"	"	"	"	1440	78	23.8	1.057	0.744	0.696	"	"
"	"	"	"	"	2400	80	22.1	0.511	0.406	0.651	"	"
"	"	"	"	"	2360	80	22.1	0.302	0.291	0.632	"	"
"	"	"	"	"	4320	80	22.1	0.233	0.222	0.664	"	"
228-144	1	3	103	310	1440	84	19.0	0.821	0.624	0.857	3	62
"	"	"	"	"	1920	84	19.0	0.604	0.460	0.853	"	"
"	"	"	"	"	2400	86	17.7	0.396	0.340	0.848	"	"
"	"	"	"	"	2880	87	17.1	0.343	0.274	0.844	"	"
"	"	"	"	"	3360	87	17.1	0.278	0.238	0.829	"	"
"	"	"	"	"	4320	88	16.5	0.264	0.175	0.823	"	"

Table XXI - Continued

Notebook and Page No.	Liquid Used	Roll Radius In.	Slow Roll rpm	Fast Roll rpm	Roll Force lb/ft	Film Temp °F	Viscosity Poise	Nip Flow Rate cu ft/ft-sec x 10^{-3} Observed	Nip Flow Rate cu ft/ft-sec x 10^{-3} Theoretical	Transfer Fraction f	Speed Ratio r	Run No.
228-74	1	3	100	300	960	82	20.5	1.230	0.97	0.872	3	46
"	"	"	"	"	1440	80	22.1	0.843	0.685	0.863	"	"
"	"	"	"	"	2400	80	22.1	0.386	0.406	0.830	"	"
"	"	"	"	"	3360	80	22.1	0.296	0.291	0.809	"	"
"	"	"	"	"	4320	78	24.8	0.227	0.246	0.842	"	"
228-76	3	3	100	300	960	80	48	2.661	2.48	0.881	3	47
"	"	"	"	"	1440	84	41.5	1.356	1.35	0.878	"	"
"	"	"	"	"	2400	81	46.3	0.822	0.87	0.863	"	"
"	"	"	"	"	3360	79	50	0.535	0.663	0.836	"	"
"	"	"	"	"	4320	78	51.7	0.339	0.524	0.813	"	"
228-146	4	3	103	310	1440	89	58.6	1.067	2.10	0.829	3	63
"	"	"	"	"	1920	88	60.6	1.106	1.56	0.871	"	"
"	"	"	"	"	2400	88	60.6	0.885	1.20	0.877	"	"
"	"	"	"	"	2880	88	60.6	0.478	0.995	0.820	"	"
"	"	"	"	"	3360	90	56.9	0.501	0.80	0.864	"	"
"	"	"	"	"	4320	90	56.9	0.324	0.615	0.818	"	"
228-26	5	3	100	300	960	92	88	3.804	5.45	0.922	3	36
"	"	"	"	"	1440	92.5	86.5	2.740	3.04	0.927	"	"
"	"	"	"	"	2400	94	81.7	1.130	1.58	0.886	"	"
"	"	"	"	"	3360	94	81.7	0.763	1.11	0.868	"	"
"	"	"	"	"	4320	94	81.7	0.518	0.836	0.864	"	"
228-24	6	3	100	300	960	104	164	7.147	18.60	0.925	3	35
"	"	"	"	"	1440	105	159	5.143	7.70	0.938	"	"
"	"	"	"	"	2400	105	159	1.654	3.45	0.908	"	"

Table XXI - Continued

Notebook and Page No.	Liquid Used	Roll Radius In.	Slow Roll rpm	Fast Roll rpm	Roll Force lb/ft	Film Temp °F	Viscosity Poise	Nip Flow Rate cu ft/ft-sec x 10^{-3} Observed	Nip Flow Rate cu ft/ft-sec x 10^{-3} Theoretical	Transfer Fraction f	Speed Ratio r	Run No.
228-24	6	3	100	300	3360	105	159	0.932	2.28	0.867	3	35
"	"	"	"	"	4320	106	153.7	0.590	1.66	0.865	"	"
228-148	6	3	103	310	1440	109	140	3.540	7.22	0.936	3	64
"	"	"	"	"	1920	106	154	2.323	4.86	0.918	"	"
"	"	"	"	"	2400	106	154	1.526	3.43	0.888	"	"
"	"	"	"	"	2880	103	169	1.152	3.06	0.860	"	"
"	"	"	"	"	3360	102	174.5	0.840	2.65	0.836	"	"
"	"	"	"	"	4320	102	174.5	0.608	1.97	0.843	"	"
228-78	1	3	150	300	960	82	20.4	1.487	1.22	0.804	2	48
"	"	"	"	"	1440	80	22.0	1.077	0.86	0.795	"	"
"	"	"	"	"	2400	82	20.4	0.594	0.475	0.762	"	"
"	"	"	"	"	3360	82	20.4	0.311	0.34	0.710	"	"
"	"	"	"	"	4320	82	20.4	0.234	0.26	0.713	"	"
228-18	1	3	150	300	960	76	25.6	2.047	1.565	0.811	2	32
"	"	"	"	"	1440	76	25.6	1.273	1.020	0.805	"	"
"	"	"	"	"	2400	77	24.7	0.642	0.572	0.760	"	"
"	"	"	"	"	3360	78	23.8	0.400	0.397	0.736	"	"
"	"	"	"	"	4320	78	23.8	0.345	0.315	0.775	"	"
228-80	3	3	150	300	960	84	41.5	2.782	2.68	0.826	2	49
"	"	"	"	"	1440	84	41.5	1.744	1.70	0.842	"	"
"	"	"	"	"	2400	84	41.5	0.855	0.98	0.765	"	"
"	"	"	"	"	3360	86	38.6	0.522	0.66	0.764	"	"
"	"	"	"	"	4320	84	41.5	0.411	0.546	0.710	"	"

Table XXI - Continued

Notebook and Page No.	Liquid Used	Roll Radius In.	Slow Roll rpm	Fast Roll rpm	Roll Force lb/ft	Film Temp °F	Viscosity Poise	Nip Flow Rate cu ft/ft-sec x 10^{-3} Observed	Nip Flow Rate cu ft/ft-sec x 10^{-3} Theoretical	Transfer Fraction f	Speed Ratio r	Run No.
228-20	6	3	150	300	960	108	144.8	9.791	20.20	0.864	2	33
"	"	"	"	"	1440	110.5	134	4.852	7.96	0.864	"	"
"	"	"	"	"	2400	110.5	134	2.160	3.74	0.888	"	"
"	"	"	"	"	3360	110.5	134	1.183	2.46	0.828	"	"
"	"	"	"	"	4320	110	136	0.780	1.86	0.820	"	"
228-14	1	3	300	300	960	74	23.8	3.520	3.04	0.517	1	30
"	"	"	"	"	1440	78	23.8	1.898	1.68	0.515	"	"
"	"	"	"	"	2400	80	22	1.178	0.93	0.520	"	"
"	"	"	"	"	3360	80	22	0.719	0.65	0.491	"	"
"	"	"	"	"	4320	84	19	0.528	0.432	0.511	"	"
228-16	6	3	300	300	960	112	128	16.587	31.20	0.480	1	31
"	"	"	"	"	1440	118	106.8	8.540	11.31	0.534	"	"
"	"	"	"	"	2400	122	92.7	4.862	4.64	0.542	"	"
"	"	"	"	"	3360	123	92.1	2.543	3.04	0.548	"	"
"	"	"	"	"	4320	122	92.7	1.566	2.22	0.522	"	"

APPENDIX VII

RESULTS OF GLASS BEAD EXPERIMENTS

Table XXII

Results of Glass Bead Experiments

Notebook and Page No.	Liquid Used	Roll Radius In.	Slow Roll rpm	Fast Roll rpm	Roll Force lb/ft	Film Temp °F	Viscosity Poise	Nip Flow Rate cu-ft/ft-sec x 10^{-3} Observed	Nip Flow Rate cu-ft/ft-sec x 10^{-3} Theoretical	Bead Diameter microns	h_o Theory microns	Transfer Fraction f	Wt % Glass Passed
228-122	1	3	99	198	4320	76	27	0.183	0.148	16	9.45	0.7514	0.09
"	"	"	"	"	3360	80	23	0.190	0.160	17	10.5	0.7713	0.30
"	"	"	"	"	2880	78	25	0.234	0.209	17	13.4	0.7462	0.87
"	"	"	"	"	2400	78	25	0.303	0.250	22	16.1	0.7516	1.78
"	"	"	"	"	1920	78	25	0.376	0.312	29	20.2	0.7469	2.95
"	"	"	"	"	1440	78	25	0.548	0.424	41	26.8	0.7883	5.13
228-138	1	3	99	198	4320	78	25	0.255	0.137	—	8.8	0.8507	0.42
"	"	"	"	"	3360	80	23	0.192	0.160	17	10.5	0.7406	0.27
"	"	"	"	"	2880	80	23	0.244	0.194	18	12.5	0.7958	0.65
"	"	"	"	"	2400	78	25	0.312	0.250	20	16.1	0.7686	1.17
"	"	"	"	"	1920	78	25	0.372	0.312	23	20.2	0.7474	2.75
"	"	"	"	"	1440	78	25	0.604	0.424	67	26.8	0.7931	7.03
228-124	8	3	99	198	4320	106	95.5	0.985	0.53	57	33.8	0.82	6.96
"	"	"	"	"	3360	110	79	1.37	0.576	64	37.3	0.858	6.77
"	"	"	"	"	2880	108	86.7	2.04	0.755	100	47.8	0.864	9.68
"	"	"	"	"	2400	108	86.7	2.71	0.905	90	58.4	0.944	10.33
"	"	"	"	"	1920	106	95.5	3.80	1.27	119	82	0.884	7.08
"	"	"	"	"	1440	106	95.5	4.90	1.75	165	114	0.891	4.55
231-16	1	3	105	315	4320	90	16.1	0.238	0.177	15	8	0.7874	0.33
"	"	"	"	"	3360	90	16.1	0.238	0.228	13	10.3	0.8191	0.79
"	"	"	"	"	2880	88	17.3	0.338	0.288	27	13.1	0.8431	1.77
"	"	"	"	"	2400	88	17.3	0.452	0.348	24	15.7	0.8712	3.52

Table XXII - Continued

Notebook and Page No.	Liquid Used	Roll Radius In.	Slow Roll rpm	Fast Roll rpm	Roll Force lb/ft	Film Temp °F	Viscosity Poise	Nip Flow Rate cu-ft/ft-sec x 10^{-3} Observed	Nip Flow Rate cu-ft/ft-sec x 10^{-3} Theoretical	Bead Diameter microns	h_o Theory microns	Transfer Fraction f	Wt % Glass Passed
231-16	1	3	105	315	1920	89	16.7	0.607	0.425	50	19	0.8670	4.58
"	"	"	"	"	1440	89	16.7	0.929	0.567	39	25.6	0.8885	8.25
231-20	6	3	105	315	4320	104	155	0.546	1.41	28	84	0.8356	----
"	"	"	"	"	3360	108	152	0.886	2.42	45	110	0.8548	1.10
"	"	"	"	"	2880	108	152	1.045	2.90	45	132	0.8452	2.89
"	"	"	"	"	2400	109	147	1.402	3.56	68	163	0.8540	6.43
"	"	"	"	"	1920	108	152	2.14	5.13	78	228	0.9037	8.36
"	"	"	"	"	1440	108	152	3.34	8.40	140	363	0.9263	6.08
231-22	1	3	198	198	4320	82	21.5	0.294	0.21	20	10	0.5090	0.46
"	"	"	"	"	3360	79	24.1	0.381	0.304	21	14.6	0.4705	1.34
"	"	"	"	"	2880	79	24.1	0.451	0.356	25	17.2	0.4909	2.11
"	"	"	"	"	2400	80	23.2	0.614	0.415	30	20	0.5138	3.50
"	"	"	"	"	1920	80	23.2	0.801	0.525	35	25	0.5085	5.54
"	"	"	"	"	1440	80	23.2	1.01	0.699	49	33.4	0.5204	7.76
231-24	6	3	198	198	4320	110	143	2.24	1.38	53	68.4	0.5806	6.78
"	"	"	"	"	3360	114	126	2.84	1.65	70	81.4	0.6606	10.23
"	"	"	"	"	2880	114	126	4.74	2.00	90	98.4	0.6365	8.69
"	"	"	"	"	2400	114	126	6.86	2.50	99	122.5	0.5922	6.96
"	"	"	"	"	1920	120	106	10.50	2.80	92	137	0.5709	7.27

APPENDIX VIII

VITA

James Howard Taylor, Jr. was born on October 9, 1928, in Winchester, Virginia, the son of James H. and Margaret F. Taylor. He attended public schools in Winchester, graduating from John Handley High in 1946. In that year, he entered Virginia Polytechnic Institute, from which he graduated with honors in June, 1950, with a Bachelor of Science degree in Chemical Engineering.

Mr. Taylor entered Lehigh University for graduate work in 1950, and received a Master of Science degree in Chemical Engineering from Lehigh in June, 1952. The title of his Masters degree thesis was, "An Investigation of the Variables Affecting Power Consumption and Production Rate of a Three-Roll Printing Ink Mill". He entered the U. S. Air Force as a 2nd Lt. in the spring of 1952, and was honorably discharged in 1954, having attained the rank of 1st Lt. During his military service, Lt. Taylor was attached to the Engineering Agency of the Army Chemical Corps, at Army Chemical Center, Edgewood, Maryland.

In 1954, Mr. Taylor was employed by the Polychemicals Department of E. I. duPont de Nemours, Inc. and worked in polymer process development at the Experimental Station in Wilmington, Delaware. In November, 1954, he returned to Lehigh University as Supervisor of Dispersion Research in the Lehigh Institute of Research project sponsored by the National Printing Ink Research Institute.

Mr. Taylor was co-author of the following publications:

"Correlation of Floating-Roll Mill Variables"; I and E Chem, 47, 696, April, 1955.

(with A. C. Zettlemoyer and Louis Maus, Jr.)

"Heat Transfer from A Rotating Disk in Turbulent Flow": ASME Paper No 56-A-146, 1956. (with Frank Kreith).

"Production Rate in Three-Roll Mills": Paint Manufacture, 27 No 8, p299, August, 1957. (with A. C. Zettlemoyer).

"Heat and Mass Transfer From A Rotating Disk": Reprint 20, AICHE-ASME Heat Transfer Conference, August, 1958. Trans. ASME, J. Heat Transfer, 81c, No. 2, p. 95, 1959(with F. Kreith, J. Chong).

"Hypothesis on the Mechanism of Ink Splitting During Printing": TAPPI, 41 No 12, p749, December, 1958. (with A. C. Zettlemoyer).

"Heat Transfer in Flow Through Rotating Ducts" Accepted for 1959 AICHE-ASME Heat Transfer Conference. (with C. Y. Kao, H. T. Ida, F. Kreith).

In November, 1953, Mr. Taylor married Eleanor J. Pope. He is the father of three children, James H, III, Robert E., and Lizabeth A. Taylor.